Regulated Surface Water: How Much and Where is it Flowing?

Pritam Das

A dissertation

Submitted in partial fulfillment of the

Requirements for the degree of

Doctor of Philosophy

University of Washington

2025

Reading Committee:

Faisal Hossain, Chair

Erkan Istanbulluoglu

Bart Nijssen

Nicoleta Cristea

Program Authorized to Offer Degree:

Civil and Environmental Engineering

University of Washington

Abstract

Regulated Surface Water: How Much and Where is it Flowing?

Pritam Das

Chair of Supervisory Committee:

Faisal Hossain

Civil and Environmental Engineering

Humans are storing surface water in reservoirs for consumption, irrigation, energy generation and many other uses at an unprecedented scale. While it is crucial to support the needs of human civilization, operation of reservoirs has many undesired impacts, such as water quality degradation and reduced sediment transport, among many. The operation of reservoirs and the effects remain largely un-studied at global scale due to a lack of observational data from ground measurements. With the recent launch of the Surface Water and Ocean Topography (SWOT) satellite mission dedicated for tracking surface water combined with the existing fleet of Earth observing satellites, we can now fill this gap in observational record using the vantage of space. This study is therefore driven by the overarching research question 'Regulated Surface Water: How much and where is it flowing?'

To answer this question, the study first builds the computational modeling framework to track reservoir state in a manner that is globally scalable, leveraging multiple satellite observations. The Reservoir Assessment Tool version 2.0, based on a multi-sensor reservoir storage estimation technique, is developed as a scalable tool to track the operations of reservoirs at a sub-weekly

frequency. Next, an algorithm is developed to estimate reservoir inflow that is regulated by a cascade of upstream and networked dams. The Reservoir Operations driven River Regulation (ResORR) algorithm is developed to account for inflow regulation by upstream dams. Next, the temporal domain of the RAT framework is extended to the near short-term future by forecasting the inflow and the operation of reservoirs based on likely operating scenarios. Finally, the efficacy of the recently launched SWOT satellite in estimating reservoir water storage dynamics is assessed as a global altimeter. Overall, this study paves the way for research and societal applications around the world using satellite remote sensing where understanding and prediction of regulated surface water are critical for responsible stewardship of water resources.

Table of Contents

List of Figures

List of Tables

Acknowledgements

First and foremost, I would like to express my deepest gratitude to my advisor, Prof. Faisal Hossain for his guidance, encouragement, and patience. Being the first ever in my extended family to ever pursue an advanced degree, he has shown me the grace, support, kindness, and nurturing that was essential to achieve the goal of a doctorate degree. Thank you for teaching me to strive for excellence without being hindered by perfection, for believing in me throughout the journey, and for challenging me with unwavering support that have fostered my growth beyond just academics. I would also like to thank my supervisory committee, especially professors Erkan Istanbulluoglu, Bart Nijssen, and Nicoleta Cristea for their valuable feedback, instruction, and support.

I express my gratitude to the Department of Civil and Environmental Engineering for providing the resources, access to expertise, and a vibrant community of students that made this journey both possible and enjoyable. I am also grateful to the University of Washington for offering the support and resources that helped me navigate the challenges of graduate school. A special thanks to the University library system for its extensive collection of resources and beautiful workspaces.

Of course, it goes without saying, I could not have accomplished this feat without the love, compassion, and unwavering encouragement of my parents. I left home by telling my mother that I am going on a *Tapasya*. All I wanted to do was become a person who can perform his duties towards others while also taking care of himself. I would call myself now successful in that front. I have looked up to my father all my life. His sense of doing one's duty with all their heart, giving back to his community, and leaving no one behind has been deeply inspirational for me and I strive every day to emulate his path. Conversations I had with him during my roughest of times have given me the lifelong strength to keep moving forward despite challenges. I am eternally grateful to the both of you.

This work would not be possible without the support, camaraderie, and shared values of selfless service of the SASWE Lab members. From burning midnight's oil on intense work projects to cooking meals together to competing in mario-kart, not only did I get the privilege to work with some of the smartest colleagues, but also gain life-long friends. Shahzaib, you have been the brother to me that I thought I never had. You have given me the support and crucial advice

during lows of graduate school that was essential for me to finishing the work. Sanchit, your friendship and your infectious passion for their work have made my stay in Seattle both enjoyable and enriching. I appreciate your constant willingness to lend a helping hand with a smile. George, every interaction we had brought immense joy to my day. Your unwavering integrity in your work and beliefs was truly inspiring. Your profound and thought-provoking questions made me delve deeper into the essence of my work, going beyond its surface-level aspects. Sarath, your composed and calm demeanor never failed to instill the same in me every time we talked.

I am thankful to the friends I made along the way for their constant support. Shashank da, you have been a constant throughout my graduate school journey. From welcoming me to Seattle, sharing delicious home cooked meals, to providing care and mentorship, you have been instrumental in my stay here. Eric, your friendship has been invaluable for me and making my stay here full of fun and excitement. Thank you for being there through thick and thin. Thank you to the people of fishbowl and treehouse for being wonderful colleagues to share the office space with. Thank you to all my friends for making Seattle feel like a second home, Bareerah, Carina, Liz, Miguel, Bridger, Manjaree, Harry, Aesha, Alaina, Aritra da, Rohan, Tiernan, Alex and Mihir.

This acknowledgment is incomplete without mentioning my family, who have consistently shared their love and compassion, despite the 7000 miles separating us. Tara, Bhai, Boudi, Mou, Kakku, Kakimoni, Shoumya, Borda, Boro Boudi, Hrisha, Turjoy, Ghunghur, Ayush, Dadu, Dida, Thamma and all my mashi, mesho, mama, mami, kakku, kaki, pishi, pishu—your unconditional love, presence, and blessings have continued to bring me immense happiness throughout my graduate school journey.

At the time of writing, Chapter 2 and 3 have been published in the *Environmental Modeling and Software* journal. Chapter 4 has been published in the *Journal of Hydrologic Engineering*. Chapter 5 has been submitted to the special edition, *Science from the Surface Water and Ocean Topography Satellite Mission*, of *Earth and Space Science*. These articles are:

Chapter 2:

Pritam Das, Faisal Hossain, Shahzaib Khan, Nishan Kumar Biswas, Lee, H., Piman, T., Meechaiya, C., Ghimire, U., and Hosen, K. (2022). Reservoir Assessment Tool 2.0: Stakeholder driven improvements to satellite remote sensing-based reservoir monitoring. *Environmental Modelling and Software*, *157*(105533). https://doi.org/10.1016/j.envsoft.2022.105533

Chapter 3:

Das, P., Hossain, F., Minocha, S., Suresh, S., Darkwah, G. K., Lee, H., Andreadis, K., Laverde-Barajas, M., and Oddo, P. (2024). ResORR: A globally scalable and satellite data-driven algorithm for river flow regulation due to reservoir operations. *Environmental Modelling and Software*, *176*, 106026. https://doi.org/10.1016/j.envsoft.2024.106026

Chapter 4:

Das, P., Suresh, S., Hossain, F., Balakrishnan, V., Jainet, P. J., Lee, H., Laverde, M., Hosen, K., Meechaiya, C., and Towashiraporn, P. (2025). Forecast-Informed Reservoir Operations within a Satellite-Based Framework for Mountainous and High-Precipitation Regions: Case of the 2018 Kerala Floods. *Journal of Hydrologic Engineering*, *30*(2), 05025003. https://doi.org/10.1061/JHYEFF.HEENG-6276.

Chapter 5:

Das, P., and Hossain, F. (2025). Multi-satellite Tracking of Surface Water Storage Change in the Era of Surface Water and Ocean Topography (SWOT) Satellite Mission. *Earth and Space Science: Science from the Surface Water and Ocean Topography Mission*.

Dedication

To Maa and Babu,

Mrs. Dulu Deb Das and Mr. Manik Lal Das

Chapter 1. Introduction

1.1 Background Information

1.1.1 The regulation of rivers by dams and reservoirs and its impacts

Rivers around the globe are increasingly regulated by dams. Rivers that flow uninterrupted to their terminus have become the rarity instead of the norm. In 2005, less than 50% of rivers were estimated to flow uninterrupted to the ocean (Nilsson et al., 2005). This number has come down to 23% more recently (Grill et al., 2019). Such interruption of rivers invariably changes the natural flow patterns of rivers, affecting the streamflow timing, intensity, and connectivity. For instance, the discharge in European rivers during summer has decreased by 10% while the discharge during winter has increased by 8% (Biemans et al., 2011). Similarly, the wet-season flow of the Mekong River has reduced by 31% and dry-season flow has increased by 35% (Bonnema and Hossain, 2017; Mekong River Commission, 2019, 2021). Such changes in streamflow timing and intensity can have cumulative negative effects on freshwater ecosystems.

Dams act as physical barriers that reduce fish access to their upstream spawning grounds (Reid et al., 2019). Additionally, altered streamflow regimes can also cause loss of nursery habitats in downstream floodplain (Freeman et al., 2022). Not only is such regulation bad for the environment, but it also makes managing water in a regulated river basin more difficult. With a change in streamflow timing and intensity, downstream water managers, stakeholders, and the public must take upstream dam operations (interchangeably used with “reservoir operations” within the text) into account for decision making. It is most obvious during times of floods, when upstream release of water can make flood events worse.

In 2018, the Indian state of Kerala experienced a 42% increase in precipitation compared to the expected levels during the initial three months of the monsoon season, commencing in June. Notably, June and July witnessed 15% and 18% higher precipitation, respectively, than normal. However, the situation escalated dramatically within the first two weeks of August, when Kerala experienced an unprecedented 164% increase in rainfall, equivalent to a 200-year event (Central Water Commission, 2018; Mishra et al., 2018). This surge in precipitation led to extensive flooding within the state, causing significant damage to life, property, and infrastructure. The already unprecedented flood event was exacerbated by the uncontrolled release of water from upstream

dams due to inadequate preparedness for the overwhelming volume of incoming water during the flood. The Mullaperiyar (upstream) and Idukki (downstream) dams were the focal points of attention following the flood, as the upstream dam is operated by the neighboring state of Tamil Nadu, which faced accusations of releasing water during the peak of the flood. To comprehend the role of reservoirs in such critical river-basin-scale processes, it is essential to model the impact of reservoir operations on river flow. However, integrating dam operations into hydrological modeling frameworks presents a significant challenge, as dam operations are entirely driven by human decisions.

1.1.2 Representation of dams and reservoirs within hydrological models

Dams are largely operated based on rule curves that specify the target storage of a reservoir in a within-year period. The dam operator then releases water from the reservoir to attain those storage targets. A reservoir optimized for hydropower production, for instance, would be kept near its full storage capacity to maximize energy production, while a flood control reservoir would be kept at a low storage to maximize the volume of water that can be attenuated during a flood .

Existing studies have used the primary use of dams and historical operating patterns to model dam operations to integrate within hydrological models (Dong et al., 2023; Hanasaki et al., 2006), land-water management schemes, and demand based parameterizations (Alcamo et al., 2003; Biemans et al., 2011; Haddeland et al., 2006; Vanderkelen et al., 2022). However, often these techniques are highly parameterized which fail to represent the actual dam operations. In reality, how a dam is operated depends on a myriad of factors, such as year-over-year changes in total precipitation or drought conditions, competing targets in multi-purpose dams, and dynamically operated forecast-informed dam-operation strategies. The most accurate way of integrating reservoirs within a hydrological model would be to use actual storage changes of reservoirs instead of simulated operations. However, availability of reservoir operations data is a major limitation to this pursuit.

1.1.3 Lack of in-situ reservoir operations data

Publicly available datasets on reservoir operations are rare and often limited to developed regions of the world. ResOpsUS (Steyaert et al., 2022) compiles reservoir operations data (inflow, outflow, and storage change) of 679 major reservoirs within the United States. The Bureau of

Reclamation maintains the Reclamation Information Sharing Environment (RISE) platform. It gives access to various reservoir-specific data, including operations, for reservoirs managed by the Bureau in the Western United States (Bureau of Reclamation, n.d.). Similar access is provided by the Royal Irrigation Department, Thailand (RID, 2024) and Central Water Commission, India (*India-WRIS*, n.d.), although the latter limits access to the water-surface area and elevation of reservoirs rather than storage change. Additionally, reservoir-operations data from South Africa and Spain are compiled by Donchyts et al. (2022). Barring these few countries, reservoir-operations data are largely not made publicly available across the rest of the world due to concerns of national security, a lack of incentive to share data, and the high cost of maintaining a platform for data access.

The Global Reservoir Storage (GRS) data product by (Y. Li et al., 2023) estimate reservoir operations globally at a monthly frequency for 7245 reservoirs globally. Similarly, Yao et al., (2023) estimate the storage for at a monthly frequency for 921 large reservoirs, taking a parameterized approach to estimating the area-elevation-volume (AEV) relationship. Cooley et al., (2021) use the water surface elevation estimated by satellite laser altimetry to estimate the storage variations of 8964 reservoirs. Although these remote sensing-based datasets have filled a gap in in-situ data availability, there exist significant limitations. These existing methods estimate the storage at a monthly frequency and lower, even though reservoirs are usually operated at a much higher frequency, typically sub-weekly. This is a major limitation as any sub-weekly operations of reservoirs will not be captured by these methods. Yao et al., (2023) also limit their study to only the largest reservoirs to a greater challenge in estimating storage of smaller reservoirs due to the fidelity of remote sensing datasets used. While these datasets fill an important gap in data availability on reservoir operations, the lack of a comprehensive framework for monitoring reservoirs leaves much at the table that can be addressed using the full constellation of Earth Observing satellites.

1.1.4 The need for a comprehensive reservoir monitoring framework

None of the studies discussed in the previous section provide a framework for obtaining the reservoir operations independently. This limits the availability of reservoir operations information to the subset of reservoirs chosen by the respective authors, instead of being scalable and applicable to reservoirs globally. Furthermore, the ability to continuously monitor reservoirs

at a near-real time timeliness is crucial for operational monitoring of reservoirs which is not possible without a framework and tools that are available publicly. It is especially important for stakeholders who manage water within transboundary river basins, in which case downstream reservoir operators must manage reservoirs that receive regulated water from upstream reservoirs, often with gaps in communication between the parties. Not only the hindcast/nowcast operations of reservoirs but forecasting how upstream reservoirs might release water in the short-term future is also crucial especially in cases of flooding, such as the 2018 flood in Kerala discussed in the previous section.

1.1.5 The Surface Water and Ocean Topography (SWOT) mission

The SWOT satellite was launched in 2022 and is a first of its kind satellite designed entirely with a focus on terrestrial hydrology applications. It is equipped with a Ka-band Radar Interferometer (KaRIN) sensor that can measure both the water surface elevation and area simultaneously in all weather conditions. The SWOT satellite is set to drastically improve the fidelity with which volume, area and elevation dynamics of water bodies would be possible to estimate globally. The RAT framework is positioned ideally for leveraging the observations by SWOT to improve the accuracy of estimating reservoir dynamics. However, with a little less than two years of data and algorithms for detecting water that are still at their infancy. The actual improvement brought forth by SWOT observations in estimating reservoir dynamics is yet to be established. The performance of SWOT in estimating reservoir storage change is hence assessed by pursuing the development of a multi-satellite algorithm for reservoir storage change estimation centered around SWOT.

1.2 Research Objectives

The objective of this dissertation is to develop the toolset to empower stakeholders to obtain reservoir operations and river regulation information in both the past and future using open-source tools, publicly accessible data, and models. It is especially timely, considering the recently launched SWOT satellite and the opportunity that it provides to track reservoir operations holistically due to its unique observation capabilities. The specific research objectives are as follows:

(1) To develop a satellite-based reservoir operations estimation framework leveraging observations from multiple satellite sensors.
(2) To develop a River regulation module for estimation of streamflow regulated by reservoir operations.
(3) To develop a module for forecasting the inflow and releases from reservoirs under various operating scenarios.
(4) To assess the skill of the SWOT satellite in estimation of reservoir dynamics globally.

In the long term, this research aims to lay the foundation for a comprehensive satellite-based reservoir operations monitoring framework that empowers users by making a level playing field for stakeholders especially in transboundary river basins.

1.3 APPROACH

The dissertation is organized as follows. First, Chapter 2 lays the foundation of the Reservoir Assessment Tool (RAT) by implementing several upgrades to the first version of RAT developed by Biswas et al., (2021) based on stakeholder feedback. Next, in Chapter 3 a scalable river regulation module – the Reservoir Operations driven River Regulation (ResORR) – is developed. In Chapter 4, the RAT framework is extended to forecast the inflow and the outflow from reservoirs under different operating scenarios. Finally, in Chapter 5, the skill of the recently launched Surface Water and Ocean Topography (SWOT) satellite is assessed in estimating the reservoir storage change, both independently and within a multi-satellite framework.

Chapter 2. Reservoir Assessment Tool 2.0: Stakeholder driven improvements to satellite remote sensing-based reservoir monitoring

Note: *This chapter has been published mostly in its current form in the Environmental Modeling and Software journal (Das et al., 2022). Used with permission from Elsevier.*

Pritam Das, Faisal Hossain, Shahzaib Khan, Nishan Kumar Biswas, Lee, H., Piman, T., Meechaiya, C., Ghimire, U., and Hosen, K. (2022). Reservoir Assessment Tool 2.0: Stakeholder driven improvements to satellite remote sensing-based reservoir monitoring. *Environmental Modelling and Software*, *157*(105533). https://doi.org/10.1016/j.envsoft.2022.105533

Key Points:

- The Reservoir Assessment Tool (RAT) framework, which utilizes hydrological modeling and satellite observations to estimate reservoir dynamics, is enhanced based on feedback from stakeholders.
- A novel multi-sensor reservoir area mapping technique called Tiered Multi-Tier – Optical and SAR (TMS-OS) is developed. The effectiveness of TMS-OS and radar altimetry-based storage change estimation is evaluated in the Mekong river basin.
- Functionality for visualizing forecasted outflow is added to the RAT framework.

ABSTRACT: In light of the rapidly increasing regulation of rivers due to planned and constructed reservoirs, monitoring reservoir operations has become very crucial. The Reservoir Assessment Tool (RAT) framework was developed to monitor reservoir operations globally, using hydrological modeling and satellite observations. With feedback from stakeholders, improvements in the RAT framework are demonstrated in this study using the Mekong River Basin as an example. A novel multi-sensor reservoir area mapping technique was developed using complementary strengths of optical and SAR sensors at a 1-5 day temporal resolution, allowing the quantification of sub-weekly reservoir operations. Additionally, the skill of radar altimeters in the RAT framework was tested using the Jason-3 altimeter. Using in-situ data from three Thai reservoirs in the Mekong Basin, consistent improvements were observed as compared to the original RAT framework. A functionality for visualizing forecasted outflow was also

added using historically inferred reservoir operations or stakeholder-driven target storage expectations.

2.1 INTRODUCTION

Humans have significantly changed how the world's rivers flow by building dams and reservoirs at an unprecedented rate in the past couple of decades. Estimates suggest that about 1/6th of the total annual river flow is stored in reservoirs (Hanasaki et al., 2006; Mulligan et al., 2020). These reservoirs account for 57% of the Earth's total surface water storage variability (Cooley et al., 2021) that also have a characteristically different storage change pattern as compared to natural lakes (Ryan et al., 2020). These dams have significantly changed the seasonal streamflow characteristics of major rivers around the world (Cooley et al., 2021; Lehner et al., 2011; T. Zhou et al., 2016). For instance, due to regulation by existing reservoirs, the wet-season flow of the Mekong River is estimated to have reduced by 31%, while the dry-season flow has increased by 35% (Bonnema and Hossain, 2017; Mekong River Commission, 2019, 2021).

At a global scale, 48% of freshwater in rivers are impacted by anthropogenic regulation due to reservoirs, which is projected to increase to about 93% in the future (Grill et al., 2015). The effects of this regulation are very apparent in the basin-wide disturbance to biodiversity (Barbarossa et al., 2020), sediment and nutrient flux to the oceans (S. Li et al., 2021), channel morphology and land-use-land-cover (Fernandes et al., 2020). Information on reservoir operations is therefore crucial to understand how streamflow regulation Drives human alteration of the natural aquatic environment and water resources. Developing this understanding requires prediction of the dynamic condition of the reservoir, such as inflow, outflow, active storage, storage change, water level and evaporative losses. Such data are usually measured and collected at the specific dam sites. However, barring a few exceptions, most data are not made publicly accessible or available, especially in developing nations, due to confidentiality requirements on grounds of national security (Plengsaeng et al., 2014) or lack of in-situ measurement infrastructure (Bernauer and Böhmelt, 2020; Bonnema and Hossain, 2017). Thus, the overwhelmingly opaque nature of dam operations at most locations worldwide poses a significant challenge to tracking the dynamic nature of human alteration of flow by dams. Consequently, this hampers building a more complete understanding of the dam's impact on the natural-socioeconomic systems that are dependent on

the river basins. This also hinders our ability to improve existing resource management tools in an increasingly dammed and human-impacted river basin in the future.

In dammed river basins, an increasing amount of a river's downstream streamflow is affected by upstream regulation. It is therefore crucial for these downstream reservoir operators to understand how the upstream reservoirs are operated, so that improved operating strategies can be adapted for irrigation, hydropower, and flood/drought management, while also maintaining environmental flow requirements (Bonnema et al., 2016). This naturally calls for cooperation and a need for open data-sharing among all dam operating and stakeholder agencies in a basin. However, this is difficult to establish and maintain in transboundary river basins (Bakker, 2009). Effective data sharing between countries requires a combination of various favorable factors, both technological and political (Balthrop and Hossain, 2010; Eldardiry and Hossain, 2021). These include, but are not limited to, streamlined data-sharing mechanisms, transboundary water treaties for data sharing that facilitate reservoir operations and a willingness for all riparian countries to adopt a shared vision of development. Even in basins that are within a single country, such cooperation and data sharing can be a challenge. A prime example of which is the Cauvery basin dispute between the Indian states of Karnataka and Tamil Nadu (Khandekar and Srinivasan, 2021).

In this increasingly regulated and impounded river basin scenario of the near future, satellite remote sensing-based approaches can help fill the current gaps in data-availability and data access on reservoir operations and streamflow regulation. For instance, Global Reservoirs and Lakes Monitor (G-REALM; https://ipad.fas.usda.gov/cropexplorer/global_reservoir/) is one such satellite observation enabled product that reports the water level of select lakes and reservoirs based on satellite radar altimetry (Birkett et al., 2018). While such information on the water level of lakes and reservoirs can help understand the state of these water storage systems, additional information such as storage change, outflow from reservoirs, and reservoir operation patterns that are critical to understanding the human impact, are not derived. A similar and more regionalized system for monitoring reservoirs is the recent Mekong Dam Monitor created by the Stimson Center (https://www.stimson.org/project/mekong-dam-monitor/). While the breadth of information provided by Mekong Dam Monitor is extensive, to the best of our knowledge, the system is not open-source where all the source code and inputs are made publicly available to ensure reproducibility and scalability to other regions of the world.

In response to current limitations of the existing state of the art on reservoir monitoring systems, Biswas et al., (2021) introduced an open-source and reproducible tool based on satellite observations and hydrological modeling-based called the Reservoir Assessment Tool (RAT; https://depts.washington.edu/saswe/rat_beta/). At the moment of writing, it was operational for a total of 1598 reservoirs around the world with scripts and data processing methodologies made fully public. Since it is the first version (1.0) of such a global and reproducible tool, we refer to it as RAT 1.0 in the rest of the manuscript. RAT 1.0 reports the daily modeled reservoir inflow, monthly surface area variation, storage change and outflow, and the inferred rule curve for South America, Africa, South and Southeast Asia. The open-source nature of the project encourages stakeholders to freely use the framework and add features needed by stakeholders. For example, RAT 1.0 framework has been successfully used to develop a RAT for simultaneous management of water quantity and water quality (RAT-WQ^2) by several stakeholder agencies, such as by the Center for Water Resources Development and Management (CWRDM) of Kerala (India) (http://depts.washington.edu/saswe/kerala/), and for the Nile River Basin (NiBRAS; https://depts.washington.edu/saswe/nibras/; Eldardiry and Hossain, 2019, and Eldardiry and Hossain 2021).

In this paper, we propose the second version (2.0) of the RAT framework, with various improvements in accuracy and functionality, based on continuous feedback received from stakeholders of the Mekong basin. This second iteration of improvement of the RAT framework is hereafter referred to as RAT 2.0 in the manuscript. Our motivation for developing RAT 2.0 is driven by the need for continuous improvement based on the increasing availability of satellite remote sensing data from multiple sensors, hydrologic model improvements and innovations in information technology (IT). Another goal for the development of RAT 2.0 is the need to improve the accuracy of prediction of reservoir's dynamic state to a level that triggers more actionable decision making for stakeholder agencies such as the Member Countries of the Mekong River Commission (MRC), including Cambodia, Lao PDR, Thailand and Viet Nam. Continuous feedback was obtained via close deliberations with the MRC during a year-long period spanning March 2021-May 2022. These deliberations were based on the global version of RAT 1.0. Based on this year-long feedback from the MRC and the need for continuous improvement, the design goals of RAT 2.0 that drove the current study were as follows:

- Improve the temporal resolution of the reservoir's dynamic state prediction from monthly, to weekly to sub-weekly allowing a more granular tracking of upstream reservoir operations.
- Improve accuracy of reservoir storage change and outflow in RAT 2.0, by leveraging advanced water classification methods and a larger suite of satellite remote sensing data.
- Provide outflow forecasting functionality in RAT 2.0 based on user-provided operating scenarios to allow stakeholders more lead time in responding to likely impacts of upstream dam operation.

The key research question we aim to address in this paper is – how skillfully can a reservoir's dynamic state, specifically, the surface area change, storage change, and outflow, be predicted using a more comprehensive suite of satellite sensors, methodological advances, and an improved information technology framework? Our hope with the continued improvement of the RAT from RAT 1.0 to RAT 2.0, is to empower stakeholder agencies with information on reservoir operations using publicly available satellite observations that can improve decision-making for water resources management, while honoring the goals of open-access, reproducibility, and scalability. The paper is organized as follows: Section 2.2 provides a short description of the study region of the Mekong River Basin over which where RAT 2.0 was developed and tested. Section 2.3 describes the data, models and methods used in RAT 2.0 that comprise key improvements to RAT 1.0. Section 2.4 discusses results, showcasing the overall skill of prediction of reservoirs' dynamic state. Finally, Section 2.5 summarizes the key finding, limitations, and recommendations for further work.

2.2 Study Region: The Mekong River Basin

Situated in South East Asia, the Mekong River is one of Asia's longest transboundary river systems, with a length of 4,763 km. It passes through a total of six countries – China, Myanmar, Thailand, Lao PDR, Cambodia and Viet Nam, draining about 810,000 km^2 (Mekong River Commission, 2021). The seasonal cycle of the basin is driven by a tropical monsoonal climatic system, with the basin receiving most of the precipitation during the period of May to October (Hossain et al., 2017).

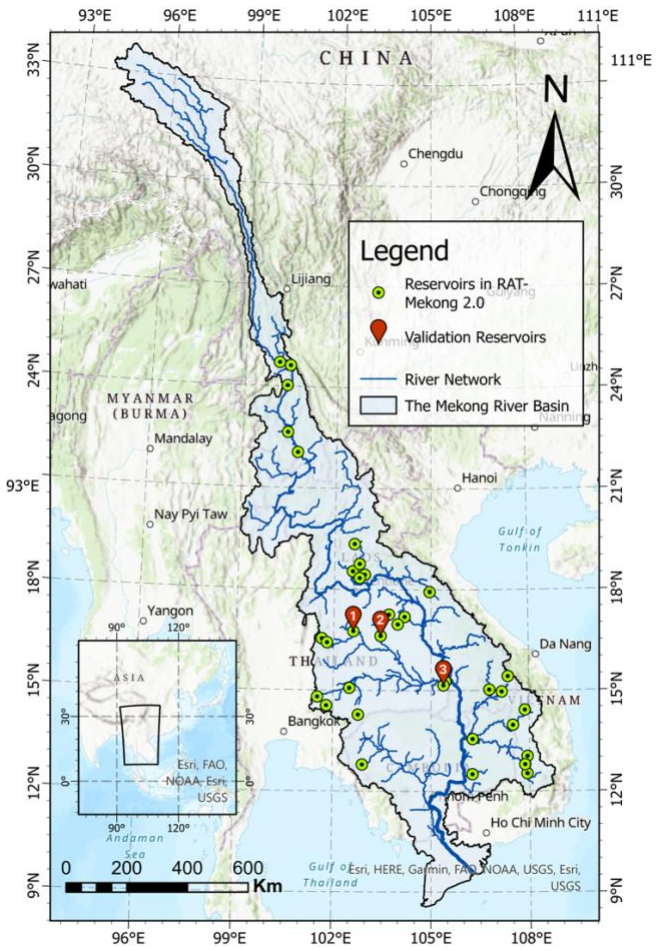

Figure 2.1 Map of the study area, depicting the Mekong River and the reservoirs monitored in RAT 2.0. The validation reservoirs are as follows – 1: Lam Pao, 2: Ubol Ratana, 3: Sirindhorn.

The Mekong River has been subject to increasing flow regulation in the recent past by the construction of reservoirs, especially due to an increasing demand for food, energy, and water for sustaining the rapidly growing economies of the region. The effects of this increased regulation are also very apparent in its current flow conditions, characterized by reduced flow during wet seasons and higher flows during dry seasons (Mekong River Commission, 2019 and Mekong River Commission 2021), and a decreased sediment load (Kondolf et al., 2018; Mekong River Commission, 2019). The Mekong River Basin also houses the Tonle Sap Lake (TSL) system, which experiences one-of-its-kind hydrodynamic phenomenon of annual flow reversal due to the monsoonal flood pulse. In addition to providing significant economic, cultural and nutritional value to the inhabitants of the TSL region, it also supports a unique ecosystem and fisheries (Arias et al., 2012). Further dampening of the flood pulse due to upstream flow regulation can lead to

cessation of the flow reversal phenomenon, leading to significant disruption to the ecosystem that it supports (Pokhrel et al., 2018).

The biodiversity supported by the Mekong River is currently categorized as relatively high (Dac Tran et al., 2020), with an estimated total of 924 species of fish, of which 219 are considered endemic to the basin (Valbo-Jørgensen et al., 2009). This biodiversity and the livelihood of a major portion of the population that depends on it are under direct threat by current and planned reservoirs (Ziv et al., 2012). These issues are not unique to the Mekong River Basin, as major river basins all over the developing world are facing similar problems due to increasing regulation through reservoirs. The Mekong River Basin may therefore be considered a microcosm of what is already happening or likely to happen to relatively undammed river basins of the developing world. Hence, lessons learned for the Mekong River Basin on reservoir operations monitoring using satellite data are expected to be relevant to other regions of the world. While the RAT 2.0 is developed using Mekong as an example, the usefulness and scalability of the new framework is therefore global.

The portion of the Mekong River's basin lying in the 4 downstream countries – Thailand, Lao PDR, Cambodia and Viet Nam – constitute the Lower Mekong Basin (LMB), while the upstream sub-basin in China and Myanmar is referred to as the Upper Mekong Basin (UMB). Established in 1995 by the LMB countries based on the principles of Integrated Water Resources Management (IWRM), the MRC is an intergovernmental organization that provides a platform for basin-wide dialogue and cooperation among the riparian countries of the Mekong River, especially the LMB. Apart from providing an advocacy platform for the riparian countries, MRC also provides technical assistance and strategic advice to the member countries on sustainable development of the food, energy and water nexus. The MRC has been instrumental in providing feedback on the problems faced by downstream stakeholders and the solutions necessary for addressing them.

A total of 36 reservoirs of the Mekong River Basin are currently monitored in RAT 2.0. These reservoirs were initially selected from the Global Reservoir and Dam (GranD) database (Lehner et al., 2011). Three additional reservoirs were added for monitoring that were not in the GranD database based on the feedback obtained from the stakeholder agency. Location of all of the reservoirs is denoted in green in figure 2.1. Three Thai reservoirs out of these 36 reservoirs, Sirindhorn, Ubol Ratana and Lam Pao were selected for validation of the RAT 2.0 framework.

2.3 DATA AND METHODS

2.3.1 Datasets

Publicly available data from a large array of currently operational remote sensing satellites, such as Landsat 8, Sentinel 1 and 2 make it possible to measure the reservoir surface area changes at a high temporal frequency. Highly accurate water level measurements at a 10-day temporal resolution can be made using Jason-3. RAT 2.0 improves both accuracy and temporal resolution of water area/level estimates using an ensemble of satellite sensors – Synthetic Aperture Radar (SAR) based Sentinel-1, Multispectral imaging-based Landsat-8 and Sentinel-2 A/B, and Radar altimetry-based JASON-3. A detailed discussion on the surface area estimation can be found in section 2.3.5. The reservoir surface area and water level elevation were estimated using an ensemble of sensors summarized in table 2.1.

Table 2.1 Summary of satellite sensors used in RAT 2.0

Sensor	Spatial Resolution	Temporal Resolution (revisit period)	Sensor Type
Landsat-8 MSI (Surface Area)	30 m	16 Days	Optical
Sentinel-2 A/B MSI (Surface Area)	10-20 m	10 Days for a single satellite (~5 Days for two satellites)	Optical
Sentinel-1 C-band SAR (Surface Area)	10 m	10 Days	Synthetic Aperture Radar (SAR)
JASON-3 (Water Level)	~300 m	10 Days	Radar Altimetry

The in-situ area-elevation curve was also obtained from the Electricity Generating Authority of Thailand (EGAT, 2019). In-situ data on water fluxes – inflow, active storage, and outflow were obtained from the Royal Irrigation Department, Thailand (http://app.rid.go.th:88/reservoir/; RID, 2022). The data was obtained for three reservoirs in North-Eastern Thailand – Sirindhorn, Lam Pao and Ubol Ratana – for validation of the estimated fluxes.

Forecasted meteorological conditions were also obtained from the Global Forecasting System (GFS) (National Centers For Environmental Prediction/National Weather Service/NOAA/U.S. Department Of Commerce, 2015) dataset to force the hydrological model to generate forecasted inflow in the reservoirs. The forecasted inflow was then used in conjunction with the inferred reservoir rule curve from Biswas et al., (2021) to estimate the forecasted outflow.

A detailed discussion on the outflow forecasting component is provided in section 2.4.7. The outflow forecasting component of RAT has been further developed in chapter 4.

2.3.2 RAT 2.0 model setup

The underlying core assumptions and design of the RAT 2.0 framework is similar to the original RAT 1.0 described in Biswas et al., (2021). The RAT framework comprises two main modules – (i) the hydrological modeling component, which provides the modeled inflow to reservoirs, and (ii) the satellite remote-sensing based reservoir observation component, which provides information on the changing reservoir state. The modular design of the framework allows RAT 2.0 to be model agnostic, and input data for any part of the components can be replaced easily with alternate options as necessary.

The dynamic state of the reservoir is modelled using the modeled fluxes to the reservoir and observed change in reservoir. At each reservoir, an assumption of conservation of mass is made –

$$O = I - E - \Delta S \tag{1}$$

Where, O is the outflow from the reservoir, I is the inflow to the reservoir, E is the evaporation from the reservoir, and ΔS is the storage change of the reservoir (figure 2.2 *(a)*). Ground seepage and precipitation on the reservoir are assumed to be negligible components of the reservoir mass balance. The Inflow is modeled using the Variable Infiltration Capacity – 5 (VIC 5) model (J. J. Hamman et al., 2018), but it can be swapped with any other hydrologic model. It must be noted here that the reported outflow from the reservoir in equation 1 is a combination of released water from the reservoir and all the other losses, such as lateral diversions, groundwater seepage losses and consumptive uses. Even though it would be much more meaningful for stakeholders to model the actual downstream releases from the dam via the spillway and penstocks, due to the current limitations of data sources, partitioning the outflow into its constituent fluxes such as lateral outflow, spilled flow and penstock flow, is not trivial. This limitation of a mass balance-based reservoir modeling schema has to be considered by stakeholders when using the outflow estimated by the RAT framework.

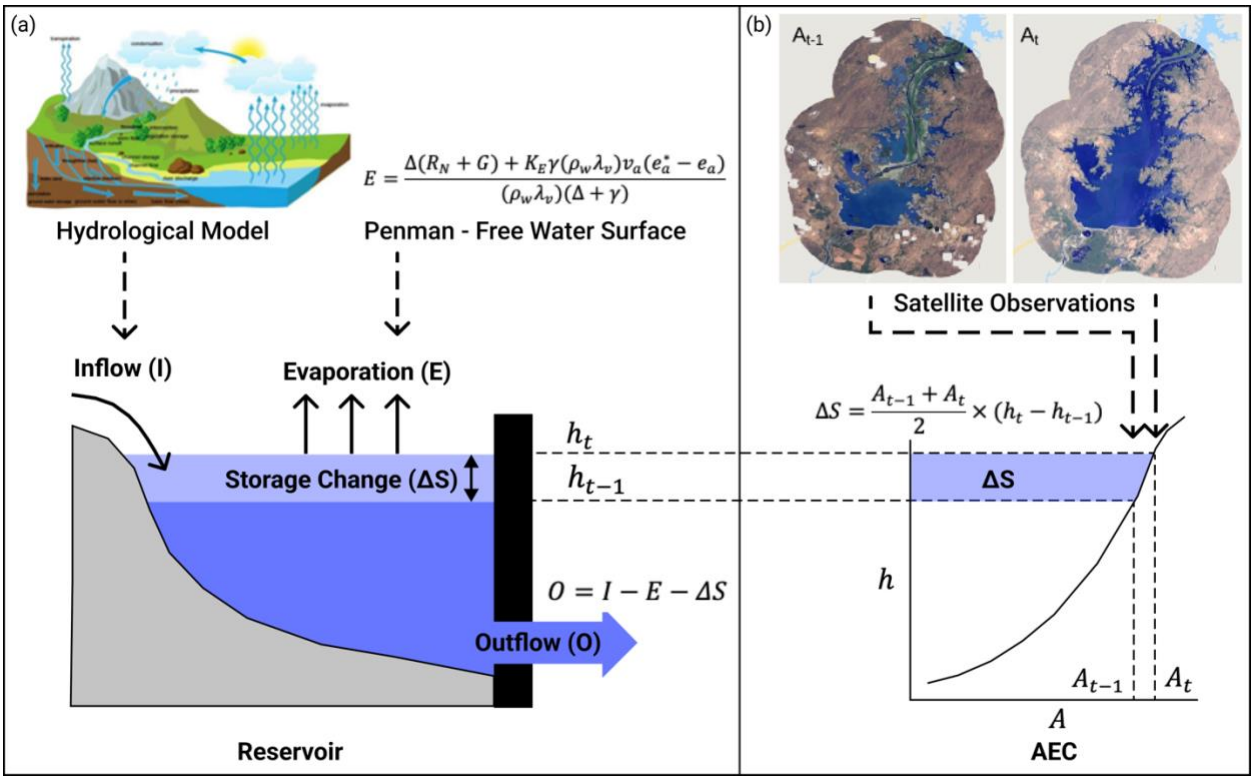

Figure 2.2 (a) Conceptual model of the RAT 2.0 framework; (b) Illustration depicting the storage change estimation using satellite observations of surface area and the Area Elevation Curve (AEC).

The storage change (ΔS) of the reservoir is estimated by assuming a trapezoidal bathymetry of the reservoir.

$$\Delta S = \frac{A_{t-1} + A_t}{2} \times (h_t - h_{t-1}) \quad (2)$$

Here, ΔS refers to the total volumetric storage change, A_t and A_{t-1} refer to the observed surface areas from satellite remote sensing. The h_t and h_{t-1} are the water levels associated with the surface areas for time t and $t-1$ (figure 2.2 *(b)*). The h and A values, estimated from satellite data, are related to each other through the Area Elevation Curve (AEC) relationship. This allows for storage change estimations using either two successive satellite-based surface area observations, or two successive satellite altimeter-based water level elevation estimates.

The AEC relationship of each reservoir was calculated using the SRTM 1-Arc Second (30 m resolution) Global Digital Elevation Model (DEM) (Earth Resources Observation And Science (EROS) Center, 2017). The SRTM DEM was generated using SAR technology, which is limited in its ability to penetrate water surfaces to obtain the bathymetric elevation information. This

means that the directly observable bathymetry is limited to above the water elevation that existed during SRTM overpass. To address the issue of missing bathymetry below the water level, we generated the AEC by a combination of additional observations from other satellite sensors and extrapolation. The AEC generation methodology is further described in (Biswas et al., 2021), which extrapolates the AEC below the water surface using a fitted power law curve. Given the modular nature of RAT 2.0, topographical survey-based AEC was also used when available to understand the impact of AEC quality on the prediction of reservoir outflow.

2.3.3 Hydrological Modeling: VIC-5 and MetSim

The RAT 2.0 framework is designed to be hydrological model agnostic, and hence users can use their preferred hydrologic model if needed. The current hydrological model used in RAT 2.0 during development is VIC 5 (J. Hamman et al., 2021). This model has a number of improvements compared to VIC 4.2.d (J. Hamman and Nijssen, 2016) which was used in RAT 1.0. A discussion on the improvements can be found in (J. J. Hamman et al., 2018).

The meteorological simulation and forcing disaggregation are decoupled from the hydrological modeling routines in VIC 5, and are packaged as a separate model – MetSim model (Bennett et al., 2020). MetSim was used to perform the meteorological simulation at a 6-hour timestep using (i) the daily minimum and maximum temperatures, (ii) daily precipitation, and (iii) wind speed, as inputs. These meteorological forcings are then disaggregated to – (i) average air temperature, (ii) total precipitation, (iii) pressure, (iv) incoming shortwave radiation, (v) incoming longwave radiation, (vi) vapor pressure, and (vii) wind speed.

Using the disaggregated forcings obtained from MetSim, VIC 5 was run at 0.0625° grid resolution for the Mekong River Basin. The model is run in parallel computing mode, exploiting the native support for the Message Passing Interface (MPI) standard, resulting in drastic improvements to performance. The VIC Routing model (Lohmann et al., 1998) was used to perform streamflow routing for the basin. Dominant River Tracing (DRT) based flow directions at 0.0625° spatial resolution by (Wu et al., 2011) were used in the routing model.

In the current scheme of RAT 2.0, an explicit representation of inflow regulation by upstream reservoir was not performed. The inflow regulation was omitted in the current scheme for two reasons – (a) most of the reservoirs (21 out of 36) studied in this study are situated in

separate tributaries of the Mekong river and lack upstream reservoirs; (b) even in the few cases (15 out of 36) when upstream reservoirs are present on the same stream, they are situated several hundreds of kilometers away. Due to these reasons, we believe inflow regulation by upstream reservoirs will have a negligible effect on the downstream reservoirs in the currently modeled reservoirs of the Mekong. The overall higher performance metrics for the three validation reservoirs of RAT 2.0 over RAT 1.0 also underscore that inflow regulation has a negligible effect in these reservoirs, and RAT 2.0 is still able to produce more accurate predictions. However, we recognize that to improve the global utility of RAT 2.0, upstream regulation will have to be actively modeled, which we hope to carry out in a future iteration of improvement of the RAT framework.

2.3.4 Evaporation – Penman Equation

In contrast to RAT 1.0, where the modeled Evaporation from the VIC hydrological model was used, the evaporation in RAT 2.0 is modeled explicitly using the Penman Equation. Also known as the combination equation, the Penman equation for free water surface (Penman, 1948; Van Bavel, 1966) is defined as follows –

$$E = \frac{\Delta(R_N + G) + K_E \gamma (\rho_w \lambda_v) v_a (e_a^* - e_a)}{(\rho_w \lambda_v)(\Delta + \gamma)} \quad (3)$$

Where, E is the evaporation; Δ is the slope of the saturation vapor pressure – temperature relation; R_N is the net incoming radiation; G is the ground heat flux, which can be assumed to be 0 for daily calculations; K_E is the mass transfer coefficient, see (Dingman, 2015, p. 259; Harbeck, 1962), γ is the psychrometric constant; ρ_w is the water density; λ_v is the latent heat of vaporization; v_a is the wind speed; e_a^* and e_a are the saturation and actual vapor pressure for the air temperature. This volumetric evaporative loss $[L^3\ T^{-1}]$ was estimated by multiplying the evaporation $[L\ T^{-1}]$ with the latest observed surface area of the reservoir.

2.3.5 High-frequency Surface Area estimation – A Tiered Multi-Sensor (TMS) approach

High temporal resolution of the storage change and outflow estimates is crucial for stakeholders to understand weekly to sub-weekly reservoir operations of upstream reservoirs. RAT 1.0 quantified the reservoir surface area at a monthly resolution by mosaicking Landsat scenes. The advantage of this approach is that mosaicking of multiple Landsat scenes helps address the

effect of cloud cover that can cause a loss of accuracy in the reservoir surface area estimation. The disadvantage of this approach, however, is the inability to quantify any sub-monthly reservoir operations.

Hence, to address the need for modeling sub-monthly reservoir operations, a novel multi-sensor surface area estimation algorithm with a tiered self-correction process was developed. This method takes advantage of the strengths of both optical and SAR sensors in a teamwork fashion. Optical sensors can very accurately estimate the water area (Cordeiro et al., 2021), but they can be highly limited by the presence of clouds. They also can be uncertain around dendritic reservoir shorelines if the perimeter is significantly larger than the nominal surface area (Biswas et al., 2021). On the other hand, SAR can penetrate clouds and is hence not affected by the presence of clouds. However, SAR backscatter threshold-based water extent estimation methods are highly sensitive to the choice of the chosen threshold, and have a tendency to underestimate the surface areas in inundated vegetation (Ahmad, Hossain, Pavelsky, et al., 2020). This method combines the high accuracy of optical sensors with the cloud penetrating property of SAR sensors. This method is referred to as TMS-OS (**T**iered **M**ulti-**S**ensor approach – **O**ptical, **S**AR, pronounced as *Teams-OS*) in the rest of the manuscript.

The first module processes Sentinel-2 and Landsat-8 scenes in GEE to obtain the reservoir surface area using recommendations and findings from (Cordeiro et al., 2021). The Region of Interest (ROI) was first delineated by taking a buffer around the reservoir boundary. The buffer distance was taken as 500 m by default, but is user configurable. The Sentinel-2 L2A – Surface Reflectance overlapping the ROI was scaled, and clouds were masked using the Scenes Classification Map (SCM) band in the preprocessing stage. Landsat-8 L2 Collection 2, Tier 1 – Surface Reflectance scenes overlapping the ROI were also identified, and clouds were masked using its pixel quality bitmask band (QA_PIXEL). The scenes with more than 90% cloud cover over the ROI were filtered out due to extreme cloud cover conditions, and no further processing was performed.

The cascade simple k-means clustering algorithm (Google, 2022) was used to perform unsupervised classification on a subset of pixels sampled from cloud-masked scenes. The best value for k was chosen based on the Calinski and Harabasz, (1974) criterion. The cluster with the highest Multiband Water Index (MBWI) (X. Wang et al., 2018) was then classified as the cluster

of water pixels. This cascade k-means model was then used to classify the entire scene into water and non-water pixels. The Normalized Difference Water Index (NDWI) and B12 ($2.185 - 2.202\ \mu m$) bands were selected for Sentinel-2, and the NDWI, Modified Normalized Difference Water Index (MNDWI) and B7 ($2.107 - 2.294\ \mu m$) bands were selected for Landsat-8 as features for training the clustering model. These features were chosen after assessing the relative performance of a combination of various features (Cordeiro et al., 2021).

After classifying the unmasked pixels as water or non-water, the Zhao and Gao, (2018) method of classifying masked pixels as water/non-water based on historical water probability (Pekel et al., 2016) was employed. The water classification and cloud mask correction components were both implemented in GEE, resulting in minimal on-premise computing requirements. The resulting reservoir water area time-series of 16 and 5-day temporal resolutions from Landsat-8 and Sentinel-2, respectively, were combined to obtain a time-series of 1–5-day frequency ($A^{Optical}$).

Even after employing skillful unsupervised clustering method for classifying water and correcting for cloud-cover related artifacts, the time-series can still have unrealistic drop or gain in surface area estimates. This can happen for several reasons, especially owing to complete automation of the processing pipeline – such as sub-optimal choice of K by the Calinski and Harabasz, (1974) criterion, or inability of the Zhao and Gao, (2018) algorithm to completely filter out cloud related artifacts. Since SAR can penetrate clouds, a reasonable assumption was made that Sentinel-1 will be able to accurately quantify the trends of reservoir surface area correctly as increasing or decreasing even if there is quantitative mis-match from ground observations. Hence, further filtering and a novel trend-based correction using Sentinel-1 (SAR) was applied to the optically derived surface area time-series.

In the first tier of filtering, the areas reported by optical sensors are compared against Sentinel-1 after applying a bias-correction step. The reservoir surface area time-series (A^{SAR}) was first obtained by applying backscatter thresholding method described in (Ahmad, Hossain, Eldardiry, et al., 2020) on Sentinel-1 SAR GRD: C-band data in GEE. The A^{SAR} was linearly interpolated to the frequency of $A^{Optical}$, referred to as A_*^{SAR} in the manuscript. The $deviations$ between the time-series were defined as the difference in reported areas by both the sensors - $deviations = A^{Optical} - A_*^{SAR}$, obtaining a distribution of the deviations. The apparent bias between both the time-series can be obtained by taking the median of the distribution of deviations,

if there were no outliers. However, since the $A^{Optical}$ time-series can contain outlier values due to challenging scenarios as described above which can skew the estimated median, a further filtering step was performed using a standard deviation (σ) threshold. Using a trial-and-error method, a threshold value of $\pm 2\sigma$ was found to be skillful in filtering out these outliers, by discarding deviation values outside the $\pm 2\sigma$ range. Finally, the apparent bias ($bias$) was calculated as the median deviation of this filtered distribution. This filtration step and calculation of $bias$ is illustrated pictorially in figure 2.3 using dummy data.

The normalized deviations were then calculated as: $norm.deviations = deviations - bias$. Data points were filtered if the normalized deviation was greater than a defined threshold value. Using a trial-and-error method, a threshold value of ~5% of the nominal surface area of the reservoir was found to be skillful at filtering out physically unrealistic surface areas. The effect of the choice of various threshold values for filtering based on deviations in area are presented in appendix A.

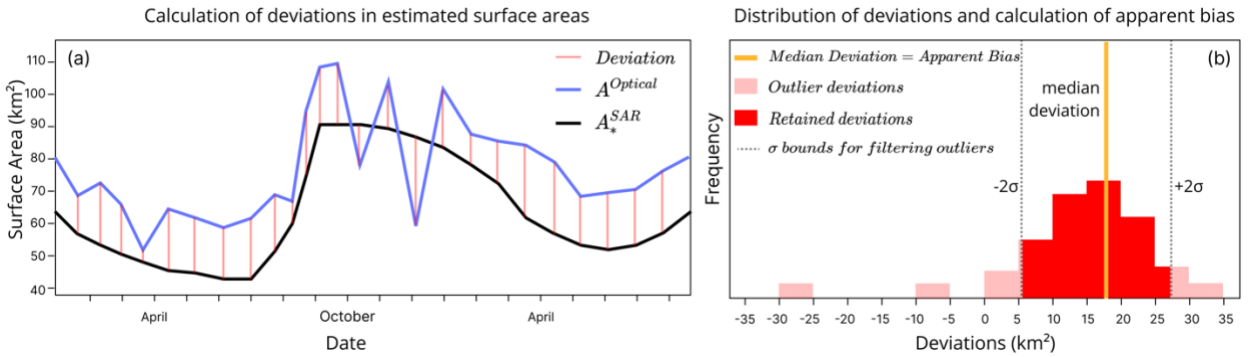

Figure 2.3 Illustration depicting calculation of apparent bias using dummy data. (a) Depiction of calculation of deviation between $A^{Optical}$ and A_*^{SAR}. The deviation between these time-series were used to estimate the apparent bias of A_*^{SAR}. (b) The distribution of the deviations between the two time-series (dummy data, for illustrative purposes). Since the reported surface areas can have unusually high deviations during challenging conditions (outliers) – seen at the tail ends of the distribution, a standard deviation threshold-based filtering was performed to discard these outliers. The median of the retained deviation values was then calculated, which was defined as the apparent bias.

The normalized deviations were then calculated as: $norm.deviations = deviations - bias$. Data points were filtered if the normalized deviation was greater than a defined threshold value. Using a trial-and-error method, a threshold value of ~5% of the nominal surface area of the reservoir was found to be skillful at filtering out physically unrealistic surface areas.

A second tier of filtering was applied to the dataset by comparing the reservoir water area change trends estimated by optical and SAR sensors. Data points were filtered out if the difference in trends was greater than a defined threshold value. Using a trial-and-error method, a threshold value of ~5% of the nominal surface area of the reservoir was found to work well as the threshold value in weeding out unrealistic drops in $A^{Optical}$. The trend is defined as follows:

$$trend^{SAR} = \frac{A^{SAR}_{*\,(t2)} - A^{SAR}_{*(t1)}}{t2 - t1} \tag{4}$$

Where, $t1$ and $t2$ are dates of observation of optical sensors (1–5-day resolution) and $A^{SAR}_{*(t1)}$ and $A^{SAR}_{*(t2)}$ are the interpolated areas on the respective dates by the SAR Sentinel-1 sensor. Similarly, the trends in $A^{Optical}$ were also obtained.

Finally, a trend-based correction step was applied to fill in the filtered data points using the apparent trend in surface area change estimated by the SAR sensor, $trend^{SAR}$. This step assumes that, even if A^{SAR} are biased, the bias term will get cancelled out while calculating $trend^{SAR}$. For each point that was filtered out in the tiered filtering steps, the data was filled by estimating the area using $trend^{SAR}$ as follows –

$$A'_{(t2)} = A_{(t1)} + (trend^{SAR} \times (t2 - t1)) \tag{5}$$

Where, $t2$ is the date of observation of a data point that was filtered out, and $t1$ is the previous date of observation. $A'_{(t2)}$ is the area estimated by the trend correction step, and $A_{(t2)}$ is the area observed on $t1$. This calculation was performed iteratively for all the filtered data points to obtain the final 1-5 day trend-corrected reservoir surface area time-series.

This 1-5 day frequency reservoir surface area time-series obtained using TMS-OS was then used to obtain the storage change using equation 2. Using this storage change estimate, along with the inflow from the hydrological model and the evaporation using the penman equation, the outflow was estimated using equation 1.

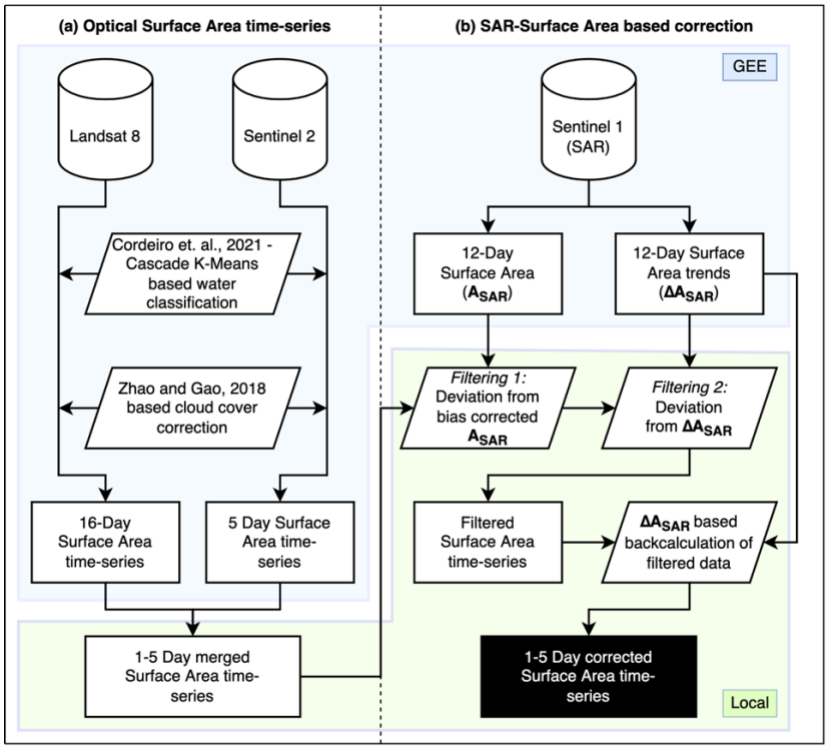

Figure 2.4 Flow chart describing the TMS-OS algorithm. (a) Reservoir surface area estimation using unsupervised clustering (Cordeiro et al., 2021) and cloud-cover correction (Zhao and Gao, 2018); (b) SAR trend based filtering and correction of reservoir surface area time series. The blue and green shaded regions indicate if the processing is done in the GEE cloud or locally, respectively.

2.3.6 Water Level – Altimetry

The reservoir water level was also mapped using the Jason-3 radar altimeter, in addition to estimating the reservoir surface area using optical and SAR sensors. Radar altimetry-based water level estimates are highly accurate, however, their applicability in regional to global reservoir mapping is limited due to poor spatial coverage and temporal resolution of the sensors. Due to the sparse spatial coverage of the Jason-3 altimeter, we validated the use of altimeter data over two reservoirs as a proof of concept to show how RAT 2.0 can benefit from altimeter-type data on reservoir elevation when available.

The water level (h) of reservoirs were estimated using the Okeowo et al., (2017), an automated clustering based method for obtaining in-land water surface elevations from Jason-3 observations. Although the Okeowo et al., (2017) method is quite robust for most cases as it uses a k-means clustering technique, there will always be challenging cases that warrant a final

statistical sanity check and adjustment. For example, when the altimeter ground track has a short length over the reservoir or is near the shoreline, the reported height may be erroneous, especially if the reservoir shoreline contracts substantially due to reservoir drawdown or during a drought. These outliers appear as sudden jumps in the estimated reservoir water level, and were filtered using a standard deviation threshold-based method.

For an observation, the standard deviation was calculated in a rolling window of 4 preceding (left standard deviation - σ_l) and 4 following (right standard deviation - σ_r) observations. A filtration condition was then defined, such that, if *both* the left and right standard deviations were higher than 2 standard deviations, then the data points were filtered out. The threshold value of 2 standard deviations was chosen based on a trial-and-error basis such that most of the outliers were filtered out, and the authors recommend selecting a threshold value specific to each reservoir based on the intersection of the ground track with the reservoir. The rationale of the filtration step is as follows – if a data point is more than 2 standard deviations as compared to both previous and next observations, then it is very likely that the data point does not reflect an actual rise or decrease in the water level, and hence can be filtered out, and *vice versa*. The filtered out points were then filled by linearly interpolating the neighboring observations. The AEC was then used to obtain the corresponding surface area of the reservoir and the storage change was then estimated using equation (2).

2.3.7 Outflow Forecasting

In addition to providing nowcast and historical (hindcast) estimates of outflow, the functionality to forecast outflow for a 15-day lead time was also added to RAT 2.0. The forecasted meteorological conditions – minimum and maximum temperature, u- and v-components of wind speed, and precipitation – obtained from the GFS dataset were used to force the VIC hydrological model to estimate the forecasted inflow to the reservoirs. The forecasted evaporation was also estimated using equation (3) with forecasted meteorological conditions obtained from the GFS dataset.

The RAT 2.0 forecasting framework provides two options of rule-curved based estimation of outflow for a 15-day lead time – (1) satellite derived rule curve from RAT 1.0, (2) user defined rule curve or time-varying target storage. The rule curve in RAT 1.0 is derived based on averaging

the historical storage change patterns over a multi-year period for each month, and then inferring the most likely storage target (S) that the reservoir has tried to achieve, as a fraction of the maximum storage (S_{max}). The rule curves are then interpolated to a 5-day frequency using linear interpolation. The interpolation is performed to stay consistent with the pentad frequency of hindcasted ΔS using the TMS-OS approach. The expected storage change is then estimated from the interpolated derived rule curve as follows –

$$\Delta S_T = (S_0/S_{max} - S_T/S_{max}) \times S_{max} \quad (6)$$

Where ΔS_T is the expected storage change as a percentage of maximum storage based on rule curve for lead time, T. S_T/S_{max} corresponds to the storage as a fraction of maximum storage at lead time T, and S_0/S_{max} corresponds to the storage as a fraction of S_{max} for the current time-step. The S_T can be obtained either from the inferred rule curve (option 1) or from a user-defined target storage at T. The S_{max} can be obtained either from in-situ data, or from dam metadata repositories, such as the GRanD database (Lehner et al., 2011). This expected storage change was used in the mass balance equation 1 to estimate the forecasted outflow.

$$O_T = I_T - \Delta S_T \quad (7)$$

Where O_T, I_T and ΔS_T are the outflow, inflow and storage change at a future time T. The evaporation was ignored due to the low contribution of the evaporation in dictating the outflow for the Mekong region. A discussion on the importance of evaporation for the Mekong basin is provided in section 4.1.

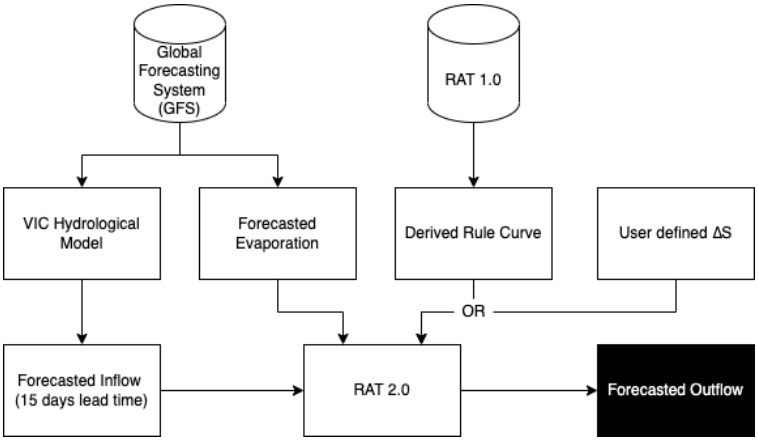

Figure 2.5 Flowchart illustrating outflow forecasting functionality of RAT 2.0.

Since reservoir operations can highly depend on the on-site decisions made by the dam operator, antecedent conditions, and the need to meet storage and distribution targets, RAT 2.0 also provides the functionality to directly input the expected storage change for a given lead time and visualize the expected outflow for the same lead time.

2.3.8 Computational Configuration of RAT 2.0

The RAT 2.0 was developed and tested in a CentOS 7 Linux environment, setup on a high-performance server. The server is configured with 2× 8 core Intel Xeon Gold processors, each having 2 threads per code, equating to a total of 32 computing units. MetSim and the VIC hydrological model were both configured to make use of the 32 computing units for parallel computation. The main memory of the system totals to 192 GB, allowing for a high ceiling of in-core processing.

A data-processing module for pre-processing raw satellite data-products and transforming them into model inputs was developed. This module makes use of the high memory ceiling for performing data transformations as in-core operations to significantly improve the performance. While this implementation has high memory requirements, the implementation can be easily changed to an out-of-core processing schema according to constraints.

In its current implementation, the RAT-Mekong model takes about 3 hours to run for the Mekong basin. Due to high computational requirements, MetSim is run only for the newly acquired data with a spin-up time of 3 months. The VIC model is then run for the entire time period of 2000-*current* at a daily time-step to obtain basin-wide modeled runoff and baseflow. The VIC routing model is then used to route the modeled runoff and baseflow to obtain daily modeled streamflow (inflow) at the reservoirs. For generation of the modeled streamflow by the routing model, the station locations have to be defined as the coordinates in terms of indices of the grid array. A python script was created to perform the conversion from latitude-longitude values of stations to their respective array-index representation in the model grid.

The remote sensing module offloads the processing to Google Earth Engine's (GEE) cloud computing infrastructure, and hence has minimal local processing requirements. Currently, the RAT model is set up to run daily at a 3-day lag, to offset any data provider side delays and their inherent latency. For example, many satellite datasets have a 1-2 day latency, sometimes even

longer with data outages. If there were no delays or latency associated with input data, then RAT 2.0 can theoretically produce outputs within 24 hours of the most recent satellite observation. We anticipate such a scenario to be a reality as IT capabilities improve and latency decreases for satellite missions and data providers.

Compared to RAT 1.0, the web interface of RAT 2.0 is virtually unchanged, with only a new tab to show altimetry data for reservoirs that have JASON-3 overpasses. The new backend is available as an open-source project under the GNU General Public License v3.0 (GNU GPLv3) license on GitHub at - https://github.com/pritamd47/rat_v2. The improvements in RAT 2.0 over RAT 1.0 are summarized in Table 2 below.

Table 2.2 Summary of improvements introduced in RAT 2.0 as compared to RAT 1.0.

	RAT 1.0	**RAT 2.0**
Hydrological model	VIC 4.2.d (sequential computing)	MetSim + VIC 5 (parallel computing)
Evaporation	Obtained from VIC 4.2.d	Explicitly modeled using Penman Combination method
Satellite Sensors used to estimate Surface Area	Landsat 7, Landsat 8	Sentinel 1, Sentinel 2, Landsat 8 (TMS-OS algorithm), Jason-3 (Altimeter)
Surface Area, ΔS and Outflow temporal frequency	30 days	1-5 days
Area-Elevation Curve	SRTM derived	In-situ if available, otherwise SRTM derived
Outflow Forecasting	Not performed	Performed using GFS and historical/expected ΔS

2.4 RESULTS AND DISCUSSION

2.4.1 Reservoir Evaporation

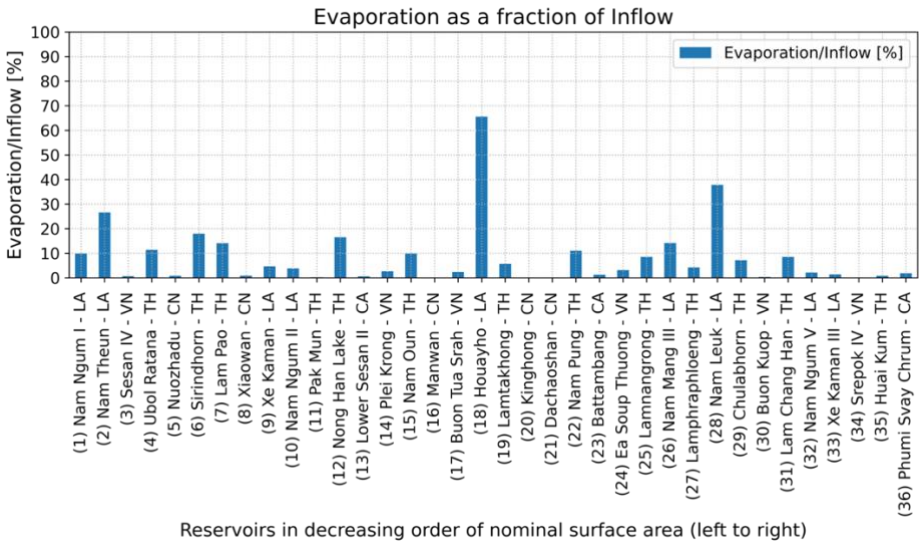

Figure 2.6 Average monthly evaporative losses compared to average monthly inflow at selected reservoirs in the Mekong River Basin. The suffixes denote the country where the reservoirs are located – CA: Cambodia, CN: China, LA: Lao PDR, TH: Thailand, and VN: Viet Nam.

The evaporative losses were found to be very nominal for the South East Asian reservoirs, with flux magnitudes less than 10% of inflow for 30 out of 36 assessed reservoirs. The catchment areas of the remaining 6 reservoirs are relatively small, which generate low inflow volumes. Moreover, out of 6 other reservoirs, 5 are primarily used for hydroelectricity. Operators usually keep the reservoir close to full to maximize hydroelectricity production, which explains the higher evaporation compared to the natural inflow.

In general, the evaporation does not seem to be a major control on the water balance of the reservoirs of South East Asian River basins, which is consistent with previous study of (Bonnema et al., 2016). However, in other river systems across the globe, evaporative losses may be significant for relatively drier river systems, such as in the Nile (Eldardiry and Hossain, 2019) and the Tigris-Euphrates. Since the RAT 2.0 framework is designed for global applications, the evaporative losses are still taken into account for the hindcast and nowcast of the outflow from reservoirs, even though the evaporative losses do not play a major role in the currently studied Mekong Region.

2.4.2 High-frequency Surface Area estimation – TMS-OS

The surface areas using TMS-OS were obtained for the period of 2019-2021 (3 years) due to the overlap of data between all the datasets – Sentinel-2, Landsat-8 and Sentinel-1. Figure 2.7 *(a)* shows the 1-5 day surface area time-series obtained using the optical sensors employing the methodology described in figure 2.4 *(a)*. At this step, rapid drops and rises in the estimated surface areas can be noted. These drops in surface areas do not reflect actual changes in reservoir surface area, rather, they are artifacts of the Cascade k-means clustering algorithm and limitations of the optical sensor to discriminate water from land. Since the (Calinski and Harabasz, 1974) criterion is used to select the number of clusters, a sub-optimal value for k can be selected by the criterion in case of challenging scenes. Such challenging scenes include, but are not limited to, cloud pixels that do not get identified accurately by the cloud masking algorithms, presence of high sediment load or algal conditions, or issues such as shadows in the scene due to terrain or clouds. In such cases, the clustering algorithm can select a higher value of k, that, even though has the lowest Calinski-Harabasz index value, the chosen cluster of water pixels may not represent all the water pixels in the scene. Choosing a sub-optimal value of k is a disadvantage of automatic selection of the number of clusters. However, these errors get identified, filtered and corrected in the next steps of the algorithm (see figure 2.7).

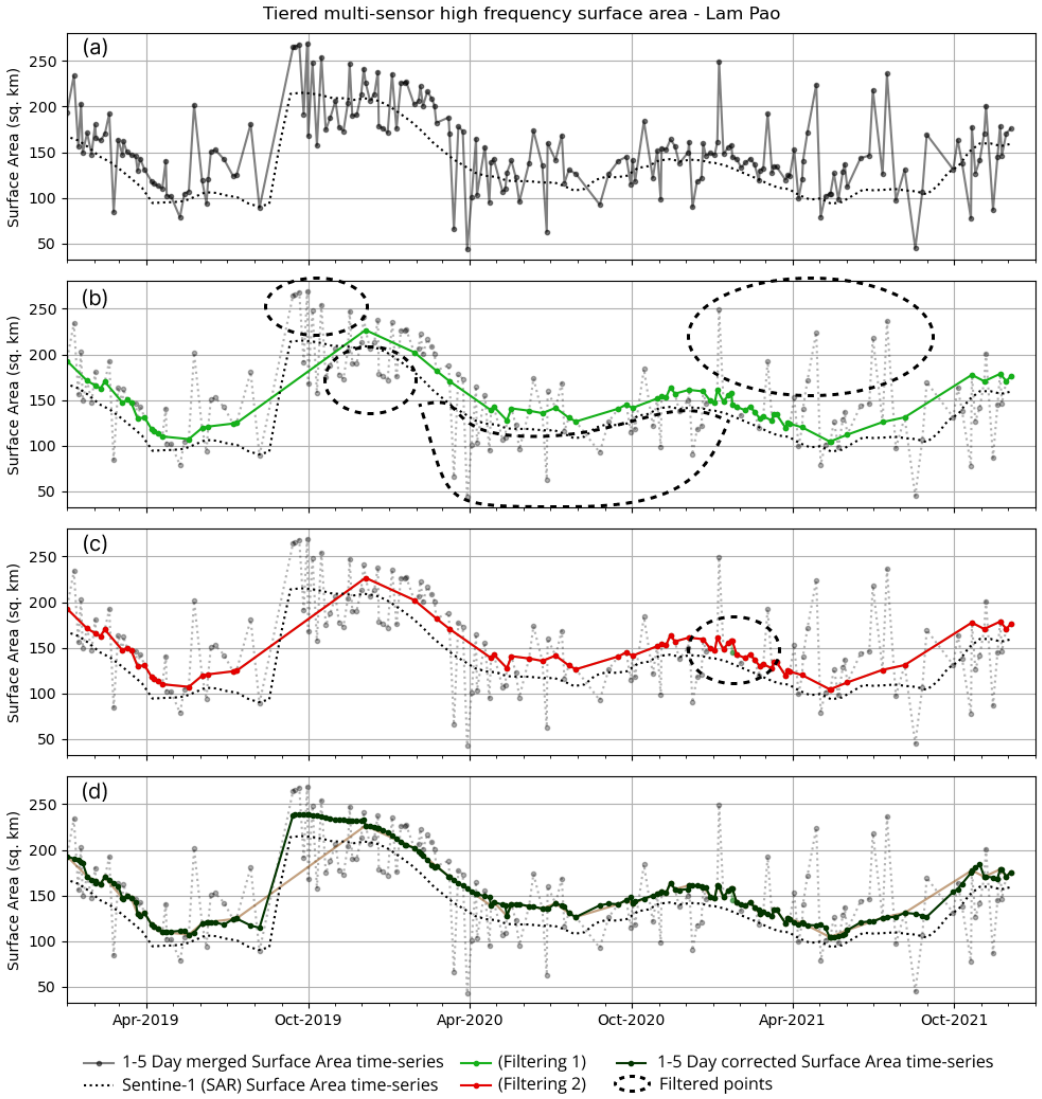

Figure 2.7 Illustration of progressive tiers of filtering and correction in TMS-OS for the Lam Pao reservoir, Thailand. (a) 1-5 Day optically derived reservoir surface area time-series using clustering based classification and Zhao and Gao, (2018) cloud-correction. (b) Filtering 1: Filtering based on deviation from bias corrected SAR surface areas. (c) Filtering 2: Filtering based on deviation from SAR surface area trends. (d) 1-5 Day corrected surface area time-series obtained by back-calculation of filtered data points using SAR surface area trends.

Figure 2.7 *(b)* and *(c)* illustrate the surface area time-series after applying filtering-1 and filtering-2, respectively (see figure 2.4 for filtering methodology). At this stage, the filtered-out data points were replaced by no-data values. The number of points that get filtered out in each step highly depends on the choice of the threshold values. Using a trial-and-error method, a threshold value of ~5% of the nominal surface area of the reservoir for both the filtering steps was found to be a good balance between filtering out unphysical data points while retaining surface area values

that could not be confidently identified as erroneous. These steps combined provide an automatic way of filtering out data points based on the agreement between surface area estimates from two different sensors with complementary strengths.

Finally, figure 2.7 *(d)* shows the 1-5 day corrected surface area time-series, obtained by filling the previously filtered data points using trends from SAR derived surface area time-series. The resulting time-series is free of unphysical changes in reservoir surface areas. The accuracy of the estimated surface areas was tested by comparing the modeled storage change (ΔS_{RAT}) with observed storage change (ΔS_{Obs}) in section 4.3.

2.4.3 Storage Change

The modeled storage changes derived from RAT 2.0-TMS-OS, RAT 2.0-Altimetry and RAT 1.0 were compared against in-situ observed storage change. The in-situ storage change was defined as follows –

$$\Delta S_{Obs} = S_{(t2)} - S_{(t1)} \tag{7}$$

Where $t1$ and $t2$ are dates of consecutive satellite observation, and, $S_{(t1)}$ and $S_{(t2)}$ are the corresponding in-situ storages. The ΔS, hence has a unit of $[L^3]$, representing the amount of storage change between consecutive satellite observations. The comparison metrics are summarized in table 2.

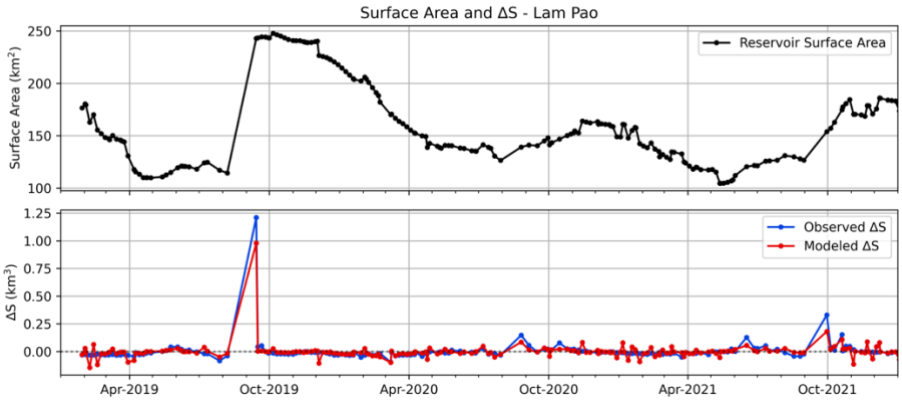

Figure 2.8 Comparison of modeled storage change using surface area observations obtained using the TMS-OS methodology with observed storage change for Lam Pao, Thailand.

The estimated storage change values using Jason 3 altimeter elevation data that were further corrected based on methodology described in section 2.3.5, were compared against the

observed in-situ storage change. The comparison metrics are summarized in table 3. Figure 2.9 shows the derived water level after filtering out outliers, and the estimated storage change values overlaid on the observed in-situ storage change. With the highest correlation, the altimeter-based technique was found to be the most skillful in modeling the storage change, albeit at a 10-day frequency.

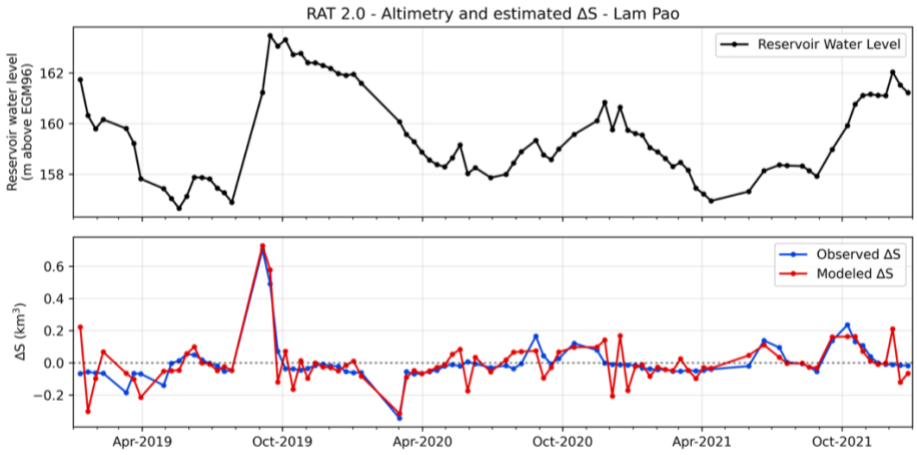

Figure 2.9 Comparison of modeled storage change using altimeter measurements of reservoir water level with observed storage change for Lam Pao, Thailand.

Since the comparisons were performed at the temporal resolution of the respective models, the statistics corresponding to RAT 2.0-TMS-OS quantify the performance at a 1-5 day frequency, RAT 2.0-Altimetry at a 10 day frequency, and RAT 1.0 at a 30 day frequency. This underlines the inherent improvement brought forth by RAT 2.0, that is, observing the reservoir dynamics at a pentad frequency or less using optical and SAR, and at 10-days using altimetry, as opposed to the monthly frequency of RAT 1.0. Even at this frequency, RAT 2.0 performs better for every metric. Overall, the Kling-Gupta Efficiency (KGE) (Gupta et al., 2009) of the RAT 2.0 represent an improvement over the RAT 1.0 estimates in most of the cases. For the TMS-OS based estimations, the average correlation increased from 0.59 to 0.77, the average normalized RMSE decreased from 15.3 % to 7.1 %, and the average normalized MAE decreased from 9.6 % to 4.0 %. The RAT 2.0-Altimetry based estimates perform the best, with an average correlation of 0.82, normalized RMSE of 7.3 %, and a normalized MAE of 5.3 %. However, the sparse spatial coverage of the altimetry method limits the number of mappable reservoirs.

Table 2.3 Statistics comparing storage change modeled by RAT 2.0-TMS-OS (1-5 days), RAT 2.0-Altimeter (10 days), and RAT 1.0 (monthly) with observed storage change for the time period 2019-2021. Acronyms of performance metrics used - KGE: Kling-Gupta Efficiency (Gupta et al., 2009); RMSE: Root Mean Squared Error; MAE: Mean Absolute Error.

	Metric	RAT 2.0 (TMS-OS)	RAT 2.0 (Altimetry)	RAT 1.0
Sirindhorn	Correlation	0.61	0.85	0.33
	KGE	0.41	0.68	-2.4
	Normalized RMSE	8.3 %	6.5 %	15.8 %
	Normalized MAE	5.1 %	5.0 %	9.7 %
Lam Pao	Correlation	0.91	0.80	0.71
	KGE	0.58	-0.03	-0.63
	Normalized RMSE	3.4 %	8.2 %	13.8 %
	Normalized MAE	2.1 %	5.6 %	8.6 %
Ubol Ratana	Correlation	0.78	-	0.74
	KGE	-0.27	-	0.12
	Normalized RMSE	9.8 %	-	16.4 %
	Normalized MAE	4.9 %	-	10.6 %

2.4.4 Outflow

The outflow estimates obtained using equation (1) were compared with the observed outflows for the three validation reservoirs. Additionally, the outflow estimated by RAT 2.0 using the TMS-OS approach was compared against the outflows estimated by RAT 1.0 which are summarized in table 4. The metrics were obtained for 1-5 day temporal resolution for RAT 2.0, and at a monthly frequency for RAT 1.0. Even at this higher temporal frequency, RAT 2.0 is able to improve the flux estimations as compared to RAT 1.0.

Table 2.4 Statistics comparing outflow modeled by RAT 2.0-TMS-OS (1-5 days), RAT 2.0-Altimeter (10 days), and RAT 1.0 (monthly) with observed outflow for the time period 2019-2021. Acronyms of performance metrics used - KGE: Kling-Gupta Efficiency (Gupta et al., 2009); RMSE: Root Mean Squared Error; MAE: Mean Absolute Error.

	Metric	RAT 2.0 (TMS-OS)	RAT 2.0 (Altimetry)	RAT 1.0
Sirindhorn	Correlation	0.55	0.47	0.11 (p-val > 0.05)
	KGE	-0.08	-0.02	-0.51
	Normalized RMSE	11.3 %	23.8 %	28.6 %
	Normalized MAE	6.0 %	17.6 %	19.4 %
Lam Pao	Correlation	0.38	0.27	-0.17 (p-val > 0.05)
	KGE	-0.3	-0.29	-0.63
	Normalized RMSE	8.1 %	16.4 %	45.9 %
	Normalized MAE	2.7 %	9.5 %	33.7 %
Ubol Ratana	Correlation	0.13 (p-val > 0.05)	-	-0.07 (p-val > 0.05)
	KGE	-0.3	-	-0.72
	Normalized RMSE	10.5 %	-	34.4 %
	Normalized MAE	4.4 %	-	24.2 %

Since the outflow is estimated by assuming water mass balance at the reservoirs, the errors in the constituent fluxes can add up, propagating forward into the estimated outflow. For this reason, even though RAT 1.0 was able to quantify the constituent fluxes, *i.e.*, inflow and storage change with reasonable accuracy, the estimated outflow deviated significantly from the observed outflow. However, the improvements in the accuracy of modeled constituent fluxes by RAT 2.0 using a multi-sensor and approach for improving data quality, now allows for quantifiably better outflow estimation. The KGE values for RAT 2.0 are higher as compared to RAT 1.0 across the board (table 4). All the KGE values for RAT 2.0 are also better than -0.41, which is equivalent to the model performing as good as using the mean value of observations as a predictor (Knoben et al., 2019). The correlation of estimated outflow with the observed outflow at two out of three tested reservoirs increased from statistically insignificant correlation in RAT 1.0 to 0.38 and 0.59 for Lam Pao and Sirindhorn respectively. The normalized RMSE decreased from an average of 36.3% to 10.6%, while the normalized MAE decreased from an average of 25.8% to 4.6%.

2.4.5 Outflow Forecasting

Figure 2.10 *(a)* shows the idea behind the outflow forecasting of RAT 2.0 for the Lam Pao reservoir. To demonstrate the functionality of the outflow forecasting module, an example date of 28th March 2022 was chosen as the "current" observation. The forecasted ΔS was then derived using the rule curve for Lam Pao for a 15-day lead time at a 5-day temporal resolution to mimic the observations that can be obtained in that time-period. Using the simulated ΔS, in conjunction with the forecasted inflow for the time-period, the forecasted outflow was visualized. The "res" drop-down can be used to choose the reservoir of interest. In the front-end of RAT 2.0, the user has the option to select the reservoir of their choice using the "res" drop down menu, as demonstrated in figure 2.10 *(a)*. The three validation reservoirs were used for demonstration purposes for this manuscript.

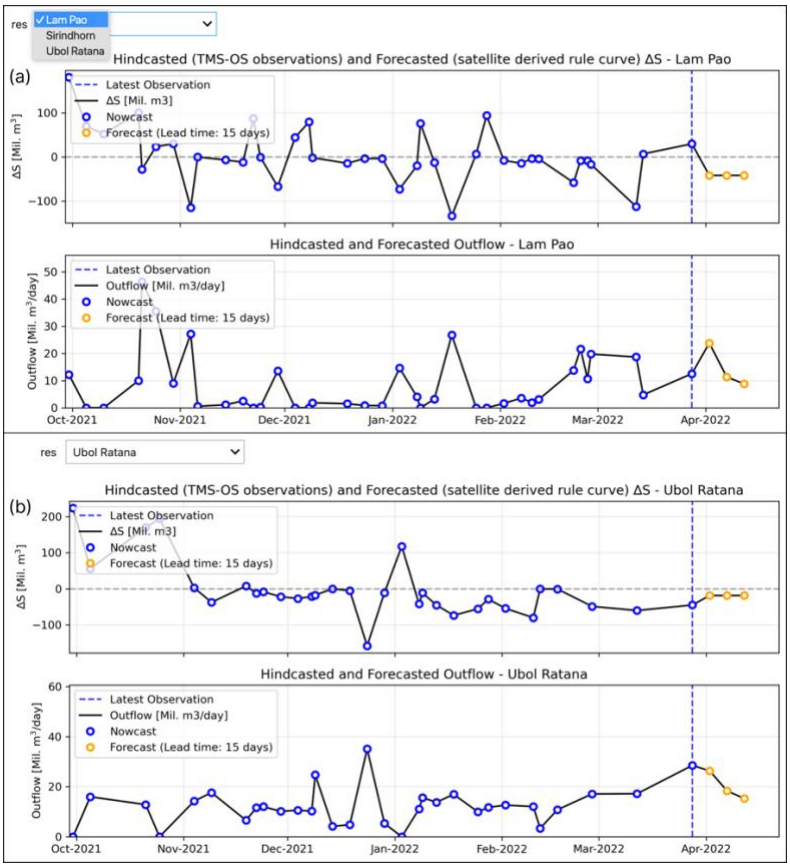

Figure 2.10 Forecasted outflow using historical satellite observations derived rule curve. (a) Conceptually, the reservoir of interest can be selected using the drop-down menu, with Lam Pao reservoir selected for visualization in the current case. (b) Selecting Ubol Ratana from the drop-down list updates the graphic to reflect forecasted outflow for the reservoir.

Additionally, the second method of outflow forecasting, using ΔS defined by the stakeholders, is presented in figure 2.11. The user has to first select the reservoir of interest using the "res" drop-down menu. Once chosen, the user is presented with a table showing the "nowcast" estimates for inflow, ΔS, outflow and a column describing if the estimate is a "nowcast" or "forecast". The user is also presented with three rows of inputs, corresponding to the next 3 anticipated satellite observation dates, where the expected storage change as a percentage of the maximum storage of the reservoir can be passed. The plot showing the ΔS and outflow will then update, based on the choice of ΔS, with the forecasted outflows highlighted as orange circles.

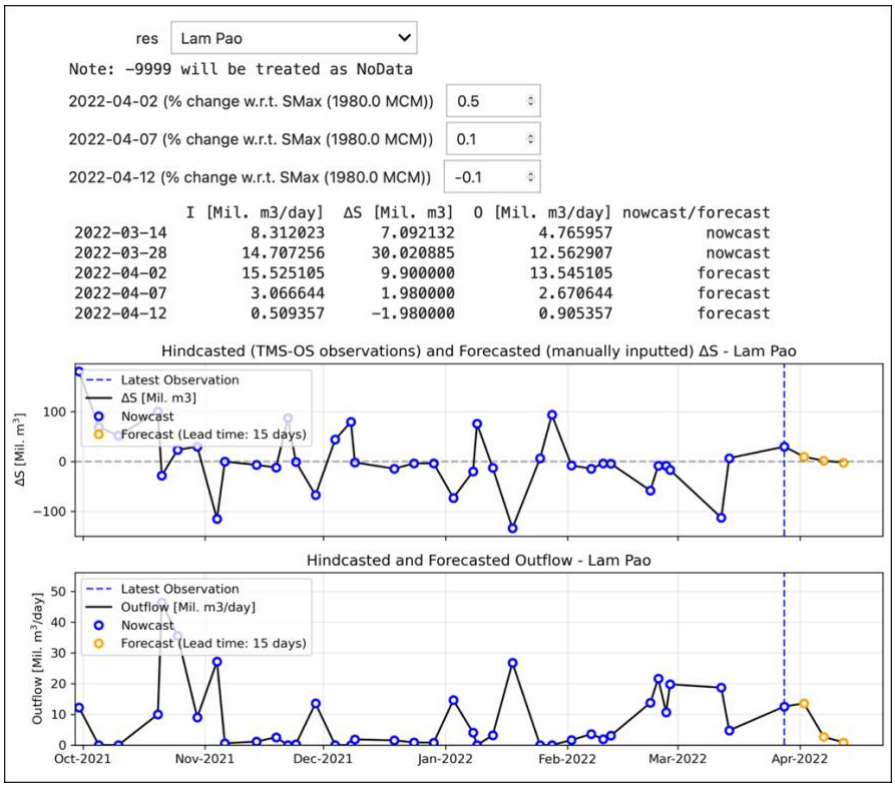

Figure 2.11 Forecasted outflow using user-defined ΔS, as a percentage of maximum Storage of the reservoir.

2.5 CONCLUSION

Regulation of rivers, and the issues associated with it, such as environmental degradation, conflicts among nations, and change in the river geomorphology are negatively affecting an increasing portion of the world. With a near-global coverage, publicly accessible methods and open-source code, and a record of reservoir operation dynamics, RAT 1.0 (Biswas et al., 2021)

provided information on reservoir operation dynamics for understanding these increasingly regulated river systems.

Building on RAT 1.0, we made several improvements, based on stakeholder feedback, to develop a more skillful version 2.0 of the RAT framework. While these improvements were demonstrated using the Mekong River basin as an example, the newly developed framework can apply anywhere where reservoirs need to be monitored routinely. Using techniques such as, advanced unsupervised classification-based water area estimation, an ensemble of sensors with complementing strengths, and a tiered filtering and correction approach, we were able to estimate changes in the reservoir dynamics with higher accuracies than RAT 1.0. This method, called the TMS-OS, was found to be highly skillful in quantifying the storage change, with a higher average correlation, and lower RMSE and MAE values as compared to RAT 1.0. This bodes well for the Surface Water and Ocean Topography (SWOT) mission (https://swot.jpl.nasa.gov/) which is planned for launch in 2022. The SWOT satellite mission is a joint mission of the National Aeronautics and Space Administration (NASA) and Centre National d'Etudes Spatiales (CNES), with contributions from the Canada Space Agency and the United Kingdom Space Agency (Biancamaria et al., 2016). SWOT is expected to monitor reservoir elevation and extent at a global scale using its wide-swath capability (Lee et al., 2010) and thereby complement altimeters that have limited but accurate spatial sampling. The SWOT mission is therefore expected to further improve our ability to predict the dynamic state of reservoirs.

In general, RAT 2.0, with its use of multiple sensors and tiered methodologies, performed better than RAT 1.0 in characterizing the outflow from reservoirs. The ability of visualize the forecasted outflow, based on forecasted inflow and forecasted storage change, either from historical reservoir operation patterns, or expectation of dam operators based on human understanding, was also introduced in RAT 2.0.

Even though significant strides were made in quantification of the reservoir operation dynamics, there is always room for improvement. The effect of upstream reservoir operations on the downstream reservoirs remains to be taken into account and studied at the basin level. This problem is addressed in Chapter 3. The RAT framework developed in this chapter to estimate reservoir operations is taken a step further to model the combined effect of regulation by reservoirs within a basin.

Chapter 3. ResORR: A Globally Scalable and Satellite Data-driven Algorithm for River Flow Regulation due to Reservoir Operations

***Note**: This chapter has been published mostly in its current form in the Environmental Modelling and Software journal (Das et al., 2024). Used with permission from Elsevier.*

Das, P., Hossain, F., Minocha, S., Suresh, S., Darkwah, G. K., Lee, H., Andreadis, K., Laverde-Barajas, M., and Oddo, P. (2024). ResORR: A globally scalable and satellite data-driven algorithm for river flow regulation due to reservoir operations. *Environmental Modelling and Software, 176,* 106026. https://doi.org/10.1016/j.envsoft.2024.106026

Key Points:

- A novel algorithm for estimating river regulation due to reservoirs upstream reservoirs– ResORR – is developed and tested over a heavily regulated river basin.
- The algorithm is designed to utilize satellite observations and simulated streamflow under ideal conditions. It is developed through a series of experiments conducted using in-situ data, gradually introducing more uncertainty.
- The model improved regulated river flow simulation for over 50% of all reservoirs tested as compared to a hydrologic model without a regulation module.

Abstract: We propose a globally scalable algorithm, ResORR (Reservoir Operations driven River Regulation), to predict regulated river flow and tested it over the heavily regulated basin of the Cumberland River in the US. ResORR was found able to model regulated river flow due to upstream reservoir operations of the Cumberland River. Over a mountainous basin dominated by high rainfall, ResORR was effective in capturing extreme flooding modified by upstream hydropower dam operations. On average, ResORR improved regulation river flow simulation for more than 50% of the cases across all performance metrics when compared to a hydrologic model without a regulation module. ResORR is a timely software algorithm for understanding human regulation of surface water as satellite-estimated reservoir state is expected to improve globally with the recently launched Surface Water and Ocean Topography (SWOT) mission.

3.1 INTRODUCTION

In the previous chapter, a satellite remote sensing and hydrological modeling-based framework was developed for estimating how reservoirs are operated. Although this framework provides the toolset required to estimate how rivers are regulated by individual reservoirs, most rivers are regulated by a network of several reservoirs. For example, the main stem of the Mekong River is regulated by a series of ten dams of capacity greater than 0.1 km^3 and many more smaller dams. More examples include the Columbia river basin which has more than 250 reservoirs (*Columbia River Basin Dams*, n.d.) and the Ganga river basin that has nearly 800 reservoirs (*Dams in Ganga Basin - INDIA WRIS WIKI*, 2021). In this chapter, we extend the framework from the last chapter to model how a series of reservoirs regulate the streamflow of a heavily regulated river.

Rivers have provided humans with food, water and energy security since human civilization first started to take shape in ancient valleys of Tigris-Euphrates, Indus and Nile rivers. This has only been made possible by means of control structures such as dams and reservoirs, which allow storage and release of water from the river according to human needs. Usually, water from the river is stored in reservoirs when the river naturally has higher flows, resulting in a net reduction in the downstream flow of the river. This storage is driven by human needs such as flood control or to meet future freshwater demand when natural availability may be insufficient. The converse happens during naturally occurring periods of low flows, when release of water from reservoirs artificially increases the downstream flow rate during the dry season to meet demand for water. This regulation of surface water, in the form of alteration of the streamflow from its natural pattern of discharge under pristine conditions, can be termed as river regulation.

River regulation can change how the basin responds to a hydro-meteorological event in the form of precipitation or snowmelt, affecting its natural variability and streamflow timing. For instance, Wisser and Fekete (2009) found that the average residence time has increased by 42 days globally over the past century due to construction of reservoirs. Such disruption and alteration of natural conditions is even more profound at a regional scale, for instance, Bonnema and Hossain, (2017) note about 11-30% streamflow alteration in the Mekong basin, with the residence time of reservoirs varying from 0.09 to 4.04 years. Vu et al., (2021) estimate that reservoirs in the Mekong

hold 50% of its dry season flow and 83% of its wet season flow. As a result, the high flows of the Mekong-river have reduced by 31%, while the low-flows have increased by 35%.

River regulation can also have serious ecological repercussions. For instance, the unique annual flow reversal of the Tonle Sap River (TSR) leading to filling up the Tonle Sap Lake (TSL) during the wet season and draining it during dry season may cease to exist if the flood pulse of the Mekong River dampens by 50% and is delayed by a month (Pokhrel et al., 2018). The absence of this unique flow reversal may have a negative impact on aquatic biodiversity, particularly for fisheries and paddy planting (Marcaida et al., 2021). Similarly, in European rivers, high-flows appear to be down by 10% while low-flows are up by 8% (Biemans et al., 2011). Negative consequences are not limited to only ecological aspects but can also influence the regional demand-and-supply of resources, with the potential to escalate pre-existing water conflicts. The construction and filling up of the Grand Ethiopian Renaissance Dam (GERD) on the Nile River has been a source of contention between Ethiopia and the other riparian countries – Egypt and Sudan. Eldardiry and Hossain, (2021) estimate that if unprepared, the High Aswan Dam (HAD) – a dam of existential importance to Egypt for its water-food-energy security – may take anywhere from 2 years to 7 years to fully recover following the filling-up of the GERD. Although, they also optimistically estimate that with cooperation and planning between the riparian countries, the recovery period can be limited to immediate 2 years.

Apart from the direct alteration of streamflow timing of rivers, regulation due to dam and reservoir operations can have an indirect effect on other components of the eco-system. For instance, river regulation disturbs the natural sediment flow, resulting in a net reduction in sediment deposition along shorelines of rivers, estuaries and oceans (F. E. Dunn et al., 2019; S. Li et al., 2021). River water temperature anomalies owing to thermal stratification in reservoirs have also been widely recognized (Ahmad et al., 2021; Cheng et al., 2020). Considering the sensitivity of aquatic life to the water temperature changes (Caissie, 2006), river regulation can negatively affect the environmental suitability for aquatic organisms (Cheng et al., 2022). Such negative environmental consequences are a direct result of human decisions – which many consider necessary to support the demands of a rapidly growing population. A better understanding of human regulation of river flow, exacerbated by a changing climate and increasing freshwater demand, is urgently required to ensure a sustainable future.

The coupled nature of human-water resources has led to developments in explicitly modeling reservoir operations in Large-Scale Hydrological Models (LHMs) and Global Circulation Models (GCMs) (Hanasaki et al., 2018; Wada et al., 2017). Existing methods to represent human activities in hydrological models rely on modeling the optimal reservoir release based on operating parameters such as the design role of the reservoir (Hanasaki et al., 2006), land-water management schemes, downstream demand for water and energy (Alcamo et al., 2003; Biemans et al., 2011; Haddeland et al., 2006; Vanderkelen et al., 2022). Many of these human activities are often assumed or 'parameterized' due to lack of sufficient observational data on reservoir operations. Using such a parameterized approach, Zhou et al. (2016) found that in highly regulated basins, such as the Yellow and the Yangtze rivers, the seasonal reservoir storage variations can contribute up to 72% of the variability of the basin's total storage. While such key insights can be obtained using generic schemes of reservoir operations, the underlying assumption of optimal reservoir operations may not always hold true. Stakeholders and reservoir managers must often deviate from optimal operating conditions based on a variety of reasons, such as adapting to regional water and energy demands, new hydro-political reality, environmental regulations, and changing weather and climate patterns that result in river flow to exceed the bounds of pre-dam historical flow records.

In the past, modeling human decisions of reservoir operations using parameterizations or criteria-based assumptions has been the primary way for characterizing river-regulation due to a lack of publicly available observations on dam operations. However, to better understand river regulation, which is representative of the intricacies of operation of individual reservoirs, we need to characterize and quantify river regulation grounded in observations of reservoir operations (Biswas et al., 2021; Das et al., 2022; T. Zhou et al., 2016). Earth observing satellites, with their vantage of space and a multi-decadal record of observations on reservoir operations now provide an opportunity to fill this data availability gap by inferring reservoir operations from space (Bonnema and Hossain, 2017).

Studies have used satellite remote sensing-based reservoir operations monitoring techniques to model the resulting regulation of streamflow. Reservoir releases are obtained by typically assuming water mass balance at the reservoirs, by modeling the inflow and storage change of the reservoirs. For instance, Yoon and Beighley, (2015) and Yoon et al., (2016) model the inflow at reservoirs in the Cumberland basin due to surface runoff and upstream releases using

the Hillslope River Routing (HRR) model. The storage change is estimated using historical record of reservoir operations by Yoon and Beighley, (2015) and by simulating SWOT-like storage change estimates by Yoon et al., (2016). The performance of the simulated discharges in both cases improves with the inclusion of reservoirs. Han et al., (2020) also take the approach of simulating reservoir operations by deriving the operating curve of reservoirs using satellite observations. Reservoir releases from upstream reservoirs were added to the inflow of downstream reservoirs in a cascade reservoir system in the Mekong River basin. However, in this case the inclusion of upstream releases did not improve the performance of regulated streamflow estimates drastically. Dong et al., (2023) use historical satellite observations of reservoir water level to calibrate parameters of a reservoir operation scheme. The reservoir releases are routed downstream using the Coupled Land Surface and Hydrologic Model System (CLHMS). All the existing studies rely on specific hydrological routing models to route the runoff and releases downstream. There doesn't exist a method to leverage existing hydrological model setups, that are usually calibrated using data that is only accessible to local stakeholders. Furthermore, the availability of high frequency satellite observations near-real time provides an opportunity to move away from parameterization and simulation driven estimation of reservoir operations to a direct observation-based approach for modeling reservoir releases. Rather than relying on parameterized or criteria-based assumptions of reservoir operations, we can now use actual observation-based reservoir operations to quantify the regulation of flow in physical models. Because satellite observations today can track the dynamic state of reservoirs comprising surface area, water surface elevation, evapotranspiration losses, storage change and even outflow (Cooley et al., 2021; Hossain et al., 2017; Lee et al., 2010; Okeowo et al., 2017; Zhao et al., 2022), there is now a stronger argument to move away from assumptions and parameterizations in representing human flow regulation in physical hydrologic models.

Satellites such as the Landsat, Sentinel, and Jason series have been extensively monitoring hydrologically relevant aspects of the Earth's surface, such as surface reflectance and elevation, at the global scale. For instance, Gao et al., (2012) were able to recreate storage variations of large reservoirs using observations from the Moderate Resolution Imaging Spectroradiometer (MODIS) satellite platform. Cooley et al., (2021) used NASA's ICESat-2 satellite observations of water level height to estimate that about $3/5^{th}$ of the Earth's surface water storage variability takes place due to reservoirs. Moreover, the recently launched terrestrial hydrology-focused Surface Water and

Ocean Topography (SWOT) satellite is now expected to improve the monitoring of surface water resources at an unprecedented scale and accuracy (Biancamaria et al., 2016). Together, these Earth-observing satellites provide an opportunity to independently track various aspects of the hydrological cycle, including reservoir operations (Bonnema and Hossain, 2017; Hossain et al., 2017). Using multi-sensor satellite data on surface water, we can now build comprehensive, distributed, and scalable modeling platforms to simulate reservoir-river systems. The Reservoir Assessment Tool (RAT) is one such modeling platform that can estimate reservoir fluxes, comprising inflow to the reservoir, storage change, evaporative losses and outflow, solely using satellite data and hydrological modeling (Biswas et al., 2021; Das et al., 2022). More recent developments have made it easier to monitor reservoirs using RAT, further democratizing the availability of surface water data at the granular level for regulated river systems (Minocha et al., 2023). This has allowed for both global and regional scale studies of the anthropogenic impact on terrestrial water storage (Biswas and Hossain, 2022) and floods (Suresh et al., 2024), especially in the regions of the world that lack a robust data collection and sharing infrastructure.

Considering the importance and urgency of an observations-driven understanding of river regulation, there is now a need to develop methods to quantify river regulation due to reservoir operations that can be scaled globally based on publicly and globally available satellite observables. The wide availability of satellite-based reservoir operations data will only keep increasing with the recent launch of the SWOT mission that is optimized for surface water tracking, particularly for lakes and reservoirs. Here, the multi-satellite observations used by RAT to estimate storage change (Das et al., 2022) can be directly used as observations to quantify river regulation, obviating the need to separately model reservoir operations based on parameterizations or operating assumptions, which can be both difficult and unrepresentative of actual reservoir operations. Given the availability of multi-decadal satellite observations of surface water that are now made widely accessible due to advancements in information technology, we are now uniquely positioned to predict regulated flow at a level of granularity that was not possible before. Estimation of river regulation grounded in observational data inherently represents the actual or likely decisions made by reservoir operators. The primary research question that this paper addresses is – *How can river regulation due to operation of reservoirs be formulated in a globally scalable format using primarily satellite observations?* The objectives of the paper are as follows:

- To develop a globally scalable river-regulation algorithm based on satellite observables or satellite derived reservoir data for predicting the human regulation of surface water.
- To investigate incorporation of the river-regulation algorithm in the RAT modeling platform for regulated rivers, and quantify its skill in capturing river flow regulation at a basin scale.

3.2 Study area and Data

3.2.1 The Cumberland River in Tennessee, US

The Cumberland River is highly regulated by a system of 10 major dams and reservoirs with varying primary use cases, making it one of the most heavily regulated basins. The United States Army Corps of Engineers (USACE) Nashville District, own and operate 10 such multi-purpose dam/reservoir projects on the Cumberland River, with the first dams being built in 1950s. These dams are used for hydropower generation, flood control, recreation, commercial navigation, public water supply, and fisheries and wildlife management – bringing in immense economic benefits to the region (Robinson, 2019). Figure 3.1 compares the daily discharge in the Cumberland River for two time-periods corresponding to unregulated conditions (1916-1920) and regulated conditions (2016-2020). The effect of regulation can be clearly seen in the figure, in the form of reduced range and variability in the discharge hydrograph. Studies suggest that such regulation has caused a sharp decline in the population and species variety of Mussels in the basin, which were plentiful when the river was unregulated (Neel and Allen, 1964; Tippit et al., 1995; Wilson and Clark, 1914). In addition to the highly regulated status of the basin, the availability of long periods of in-situ observational data from the operating agencies makes this basin an ideal test bed for investigating anthropogenic river regulation (Bonnet et al., 2015).

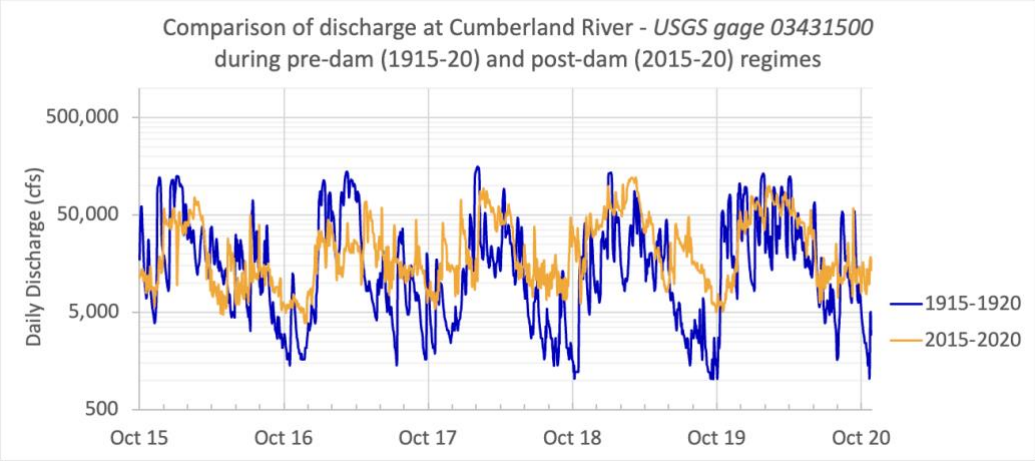

Figure 3.1 Comparison of 5 years of daily discharge during (a) unregulated conditions, prior to construction and operation of major dams (1916-1920), and (b) regulated conditions, as observed in the Cumberland River near Nashville, TN. The flow rate in a regulated regime has a markedly attenuated peak-trough range – with low flows rarely dropping below 5000 cfs as compared to the unregulated regime when flow rates naturally used to drop to 1000 cfs. Source: United States Geological Survey (USGS).

Originating in the Appalachian Mountains, the Cumberland River flows westwards through the states of Kentucky and Tennessee in the United States, draining a region of about 18,000 sq. miles (~45,000 sq. km), before merging into the Ohio River. Ten dams – Martins Fork, Laurel, Wolf Creek, Dale Hollow, Cordell Hull, Center Hill, Old Hickory, J. Percy Priest, Cheatham, and Barkley dams – are operated by USACE, with some additional dams operated by the Tennessee Valley Authority (TVA) (Robinson, 2019). Limited by the availability of in-situ reservoir operations data, 8 of the USACE owned dams were included in this study. Based on the conclusions of the study, the authors believe that the results are not affected by the exclusion of the 2 USACE dams owing to their relatively insignificant (Martin's Fork dam) to no storage (Cheatham dam). The region generally has a temperate, warm, and humid climate, with most of the precipitation occurring from December through May.

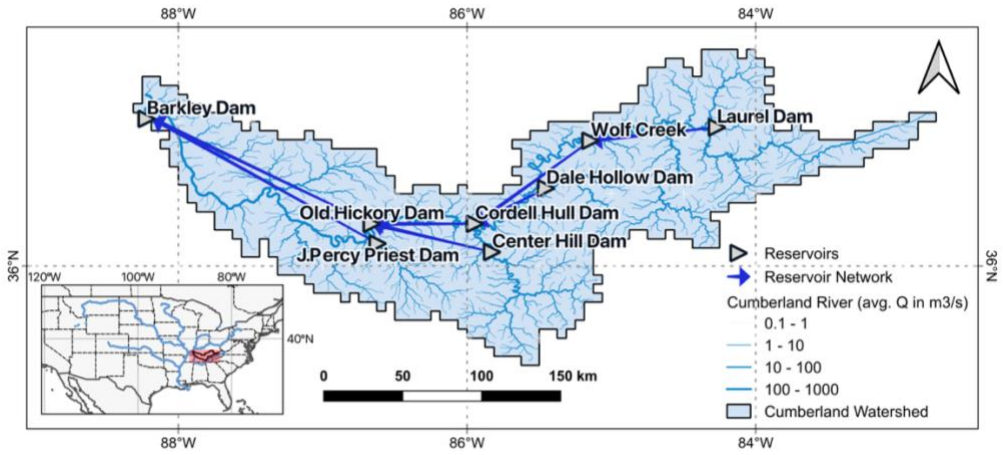

Figure 3.2 Map of the Cumberland basin, showing locations of the reservoirs, the reservoir network and the location of the Cumberland basin in the US.

3.2.2 In-situ and satellite observations of reservoir dynamics

To develop, test and validate the river-regulation algorithm, observed in-situ data pertaining to reservoir operations – inflow, outflow, and storage – were used, which were obtained from the ResOpsUS (Steyaert et al., 2022) dataset. This dataset is a compilation of in-situ reservoir operations data for 679 major dams in the US, including 8 of the USACE dams in the Cumberland basin and one dam operated by the TVA, until November 2019. Daily storage change was calculated using the storage values in the dataset for all but 2 dams – Old Hickory and J. Percy Priest – which had missing storage data from July 2015 onwards. The storage change for these reservoirs were obtained by subtracting the reported Outflow from the Inflow ($\Delta S = I - O$). Readers are referred to section 3.3.1 for more discussion on this data preparation step. The in-situ data was also used to force the river-regulation model in a series of experiments to compare the sensitivity of the river-regulation model to the accuracy of input data – a detailed discussion is provided in section 3.4. Additionally, the in-situ Area-Elevation Curve (AEC) of all the USACE reservoirs were also obtained from the Access to Water Resources Data – Corps Water Management System (CWMS) Data Dissemination tool (USACE, n.d.).

The latest version of Reservoir Assessment Tool (RAT 3.0) was used to obtain the storage change and river flow under pristine (naturalized) conditions (assuming no upstream reservoirs). Originally developed by Biswas et al., (2021), the RAT framework is designed to improve access to information on reservoir dynamics, especially with recent developments leading to both a higher performance and accessibility (Minocha et al., 2023; Das et al., 2022). Using the default

hydrological model of RAT, Variable Infiltration Capacity (VIC) (Liang et al., 1994), rainfall-runoff modeling was performed at a 0.0625° spatial resolution. The inflow to each reservoir's location under natural conditions was estimated using the VIC-Routing model (Lohmann et al., 1998), which uses the linearized Saint-Venant equation to route streamflow within the watershed. The default VIC parameters, and sources of temperature and wind data used in RAT 3.0 were used to force the hydrological model. The precipitation was obtained from the ERA-5 reanalysis dataset (Hersbach et al., 2020). It must be noted here that the VIC-based reservoir inflow in RAT 3.0 does not take upstream reservoir operations into account, and hence the need to develop a model that can supplement the RAT framework by taking upstream regulation into consideration. A detailed discussion on how the hydrological model's estimated inflow in pristine conditions is used in the river regulation model can be found in section 3.3.3.1. Since the in-situ AEC of the TVA-owned reservoir was not available, the default AEC option in RAT 3.0 was applied based on the Shuttle Radar Topography Mission Digital Elevation Model (SRTM DEM) (Earth Resources Observation And Science (EROS) Center, 2017).

3.3 METHODS

3.3.1 Reservoir Operations driven River Regulation (ResORR) – Conceptual algorithm

The core assumption of the ResORR algorithm is that the volume of water entering the reservoir, Inflow (I), is composed of two components – natural and regulated. The Natural Runoff (NR) is defined as the component of surface runoff that flows naturally into the reservoir without passing through any upstream reservoirs. Similarly, the Regulated Runoff (RR) is the component of surface runoff that first gets intercepted by an upstream reservoir before being released based on the reservoir's operations policy. The partitioning of the inflow to a reservoir is defined by the following equation,

$$I = NR + RR \tag{1}$$

Essentially, the problem of estimating the inflow at any reservoir is decomposed into the two parts of estimating the natural and regulated components of the incoming streamflow. A detailed discussion on estimating these sub-components of inflow is provided later in the section. The estimated inflow to a reservoir in this scheme will, hence, be affected by regulation due to upstream reservoir operations.

For example, consider the example of a two-reservoir system (A and B), where reservoir B is downstream of reservoir A, depicted in the schematic in figure 3.3 (a). In this scenario, the inflow at reservoir B would have contributions from the outflow of the upstream reservoir A in the form of RR (i.e., $RR \neq 0$), in addition to the NR. On the other hand, since reservoir A has no upstream reservoirs, the inflow to the reservoir would be fully natural, i.e., $RR = 0$ and $I = NR$.

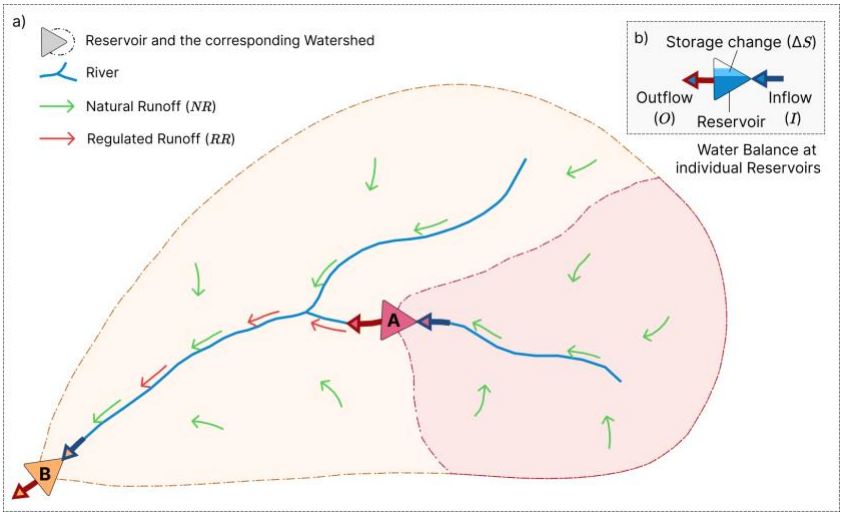

Figure 3.3 Conceptual schematic of the ResORR model. Panel (a) depicts the flow of surface runoff and streamflow, along with the contribution of the natural (green arrows) and regulated (red arrows along the stream) components, referred to in this paper as Natural Runoff (NR) and Regulated Runoff (RR) to the Inflow ($I = NR + RR$) to a reservoir. Panel (b) describes the components of the water balance equation ($O = I - \Delta S$) used at the reservoir to obtain the outflow from the reservoir, which is treated as the regulated component of the downstream streamflow.

As discussed above, the RR is defined as the component of inflow to a reservoir due to upstream reservoir releases. It is estimated as the sum of all Outflow (O) of the upstream reservoirs.

$$RR_i = \sum_{j}^{N} O_j \qquad (2)$$

Where RR_i is the incoming Regulated Runoff to reservoir i; O_j is the Outflow from the j^{th} upstream reservoir; N is the total number of upstream dams for reservoir i.

The NR is defined as the volume of water inflow to the reservoir due to surface runoff unaffected by any upstream reservoir operations., i.e., the generated surface runoff drains directly to the reservoir, without passing through any other reservoir. This surface runoff is generated in the part of the watershed which is not shared by any other upstream dams. For instance, in **Error!**

Reference source not found. 3.3, the orange and red shaded regions of the watershed will generate the NR for reservoirs B and A respectively. The NR for a reservoir can be estimated using the theoretical inflow into a reservoir if there were no upstream dams, which is referred to as the Theoretical Natural Runoff (TNR) in this paper. The Theoretical Natural Runoff (TNR) refers to the inflow to a reservoir if none of the upstream dams existed. The TNR can be calculated using the following equation –

$$TNR_i = NR_i + \sum_{j}^{N} NR_j \quad (3)$$

Where, TNR_i is the Theoretical Natural Runoff of reservoir i; NR_i is the Natural Runoff to reservoir i; and N is the total number of upstream dams of reservoir i along the same river network. For example, in the schematic in figure 3.3, the TNR of reservoir A and B would be NR_A and $NR_B + NR_A$ respectively.

Since the TNR represents streamflow into a reservoir in pristine conditions (without considering upstream reservoirs), it is analogous to the modeled inflow at reservoirs using traditional hydrologic models which do not take reservoir operations into account. The NR of any reservoir can be obtained by rearranging the terms of (3, and calculating the NR for reservoirs by iteratively moving downstream for each time-step. The NR for any reservoir can hence be obtained using the TNR of the reservoir, and the NR of the upstream reservoirs using the following equation –

$$NR_i = TNR_i - \sum_{j}^{N} NR_j \quad (4)$$

Using the estimated NR and RR components, the inflow to a reservoir under regulated conditions is then calculated using (1. Using the storage change of the reservoir, obtained either in-situ or using satellite estimates, the outflow can then be calculated using the water balance equation –

$$O = I - \Delta S \quad (5)$$

Where O, I and ΔS are the outflow, inflow and storage change of a reservoir respectively. In the current form of the mass balance equation of the reservoir fluxes, the evaporative losses are

not considered. For semi-arid to arid parts of the world, such as the Western US, the Middle East, and Australia, evaporation from reservoirs can play an important role in reservoir water balance (Zhao et al., 2022). For the application ResORR over the Cumberland basin, which has a humid subtropical climate and is a relatively wet region. Here, the evaporative losses from reservoirs do not play a major role in the water balance and was hence safely ignored. For instance, the evaporation from the Wolf Creek reservoir is about only 1-2% of the total inflow to the reservoir annually.

These equations were solved for the reservoirs mapped in figure 3.2 by traversing down the network of reservoirs for each time-step. Since the TNR is obtained by routing water through the watershed, the travel time of water between the reservoirs is inherently considered in the subsequent calculations that depend on this routed hydrograph. The proposed methodology is not a routing scheme, rather it operates on precomputed hydrographs obtained by routing water through a watershed using traditional routing algorithms. The proposed algorithm uses observational reservoir operations, either from in-situ or satellite platforms to adjust the streamflow for regulation due to upstream reservoir operations in a post-processing fashion.

To assess the performance of the model, sensitivity to uncertainties in the model inputs, and generally investigate the limitations of the model, various experiments were setup which are discussed in section 3.4.1. To test the theoretical robustness of the proposed river regulation algorithm as a mass conserving scheme, we set up a two inter-connected linear reservoir problem where outflow is proportional to water storage and according to the elevation head available at the outlet. Using this set up we generated regulated inflow that should theoretically happen at the second reservoir (reservoir 2) based on storage and regulation effect of the upstream reservoir (reservoir 1). Consequently, we tested the algorithm's ability to mimic the same regulated inflow to reservoir 2 using storage and upstream unregulated inflow of reservoir 1 that would be available in a globally scalable manner from satellite observations and modeling platforms such as RAT 3.0. Our algorithm demonstrated perfect theoretical consistency as a mass conserving scheme. More details on this theoretical robustness check of the ResORR algorithm are provided in the .

3.3.2 Reservoir network

The reservoir network represents the connectivity of the reservoirs in the model and is represented by a directed tree data structure, with the nodes representing the reservoirs and the links depicting their connectivity, while preserving the order of reservoirs. The model first topologically sorts the reservoir network, to order them such that the water balance computations of upstream reservoirs are performed before the subsequent downstream reservoir. At each time-step, the model iterates over the topologically sorted reservoir network, and solves the series of equations discussed in section 3.3.1.

The reservoir network is generated using the location of reservoirs and the Global Dominant River Tracing (DRT) dataset (Wu et al., 2011). Since the river-regulation model is designed as an add-on to the RAT framework, the script to generate the reservoir network can use the inputs and intermediary outputs of RAT to generate the reservoir network.

3.4 Experiments and Results

3.4.1 River regulation experiment setups using in-situ data

The ResORR algorithm is fully described by equations (1)-(5), which uses estimates of streamflow under pristine conditions from a hydrological model. However, the uncertainties in the estimations of hydrological model may propagate as uncertainty in the river-regulation model. Experiments were performed to isolate the performance of the core of the algorithm, its ability to partition the inflow between the natural and regulated components using in-situ observations in place of hydrological model and satellite estimates. By reducing uncertainties in certain parts of the algorithm, the performance of the individual components could be investigated, shedding light on the sensitivity of the algorithm components to the input data accuracy. Moreover, the observed in-situ ΔS was used in these experiments to gauge the baseline performance of ResORR using best available reservoir operations data, avoiding the higher uncertainties normally associated with satellite estimates of storage change.

To investigate the strengths and weaknesses of ResORR, especially in terms of scalability, the experiment designs were iteratively modified and updated in order from E1 to E4 over the

period of 2015-2019. Details about the experiment designs and the rationale behind the experiments are summarized in **Error! Reference source not found.**.

Table 3.1 Summary of the experiments performed on the river regulation model along with the corresponding symbols used in the performance comparison plot (figure 3.4).

Exp.	In-situ data used	Description	Rationale
E1 ○	ΔS	In-situ ΔS was used in eqn. (5) to estimate O. VIC hydrologic model was not calibrated for estimating natural inflow.	Uncertainties in satellite estimates of ΔS are minimized in this experiment.
E2 □	O	Observed O was used in eqn. (3) to estimate RR.	Uncertainties in otherwise estimated O, due to uncertainties in modeled I are minimized. The RR obtained as such would reflect the "theoretically" best estimate of incoming regulated streamflow.
E3 △	I, ΔS	Observed I was used in eqn. (4) only at the most upstream dam, where NR = TNR = I. In-situ ΔS was used in (5) to estimate O.	For upstream-most reservoirs all the incoming streamflows would be due to natural runoff, hence, by using the observed I, the uncertainties due to modeled I are minimized. The RR in this case would reflect the "theoretical best estimate" of the downstream regulated streamflow.
E4 ✚	ΔS	In-situ ΔS resampled to a 16-day frequency was used in eq (5) to estimate O. The VIC hydrological model, forced with satellite data, was calibrated at upstream most dams of Center Hill Dam, Dale Hollow Dam, and Laurel Dam.	The modeled inflow to the upstream most dams were calibrated using the observed inflow, essentially, minimizing the uncertainties at the upstream boundary of the reservoir network. This represents the ResORR in its globally scalable form under the scenario of perfect ΔS. The resampling to 16-day frequency was done to simulate the observational frequency of the satellite used later in this study.

The regulated inflows obtained at the 4 dams, which have at least one upstream dam were compared against the observed inflow at those same dams. The comparison statistics measuring the performance of the river regulation model against observed inflow data are summarized in figure 3.4. To understand how the river regulation algorithm is performing under various input scenarios and assumptions, one should compare the relative position of the symbols for each dam along the horizontal axis only. The TNR, obtained from the VIC hydrological model are denoted using grey and black circles, corresponding to the streamflow modeled using default parameter

values and calibrated parameters. Formulation of performance metrics are provided in Appendix B.

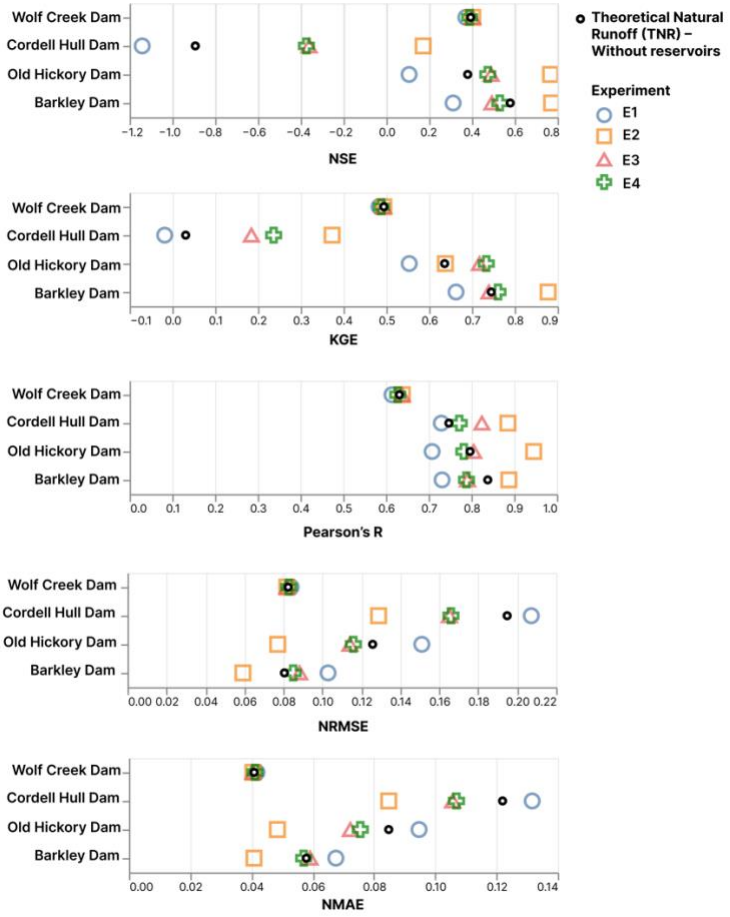

Figure 3.4 River regulation model performance for E experiments using in-situ reservoir dynamics data.*

Compared to the uncalibrated VIC streamflow estimates, the performance of the river regulation model in the E1 experiment in improving the accuracy of regulated inflow seems to be reduced. In other words, ResORR using in-situ ΔS, but with uncalibrated VIC flow at upstream most location does not improve the skill in predicted regulated inflow at downstream dam locations. However, on taking a closer look at the hydrographs comparing modeled inflow, TNR and observed inflow in figure 3.5, it is apparent that the variability in the observed inflow, which is regulated inflow, is more closely replicated by the variability in the modeled inflow than the TNR. This likely suggests that even though the overall performance of ResORR gets reduced as a regulated streamflow predictor, the signature of human regulation is still captured well.

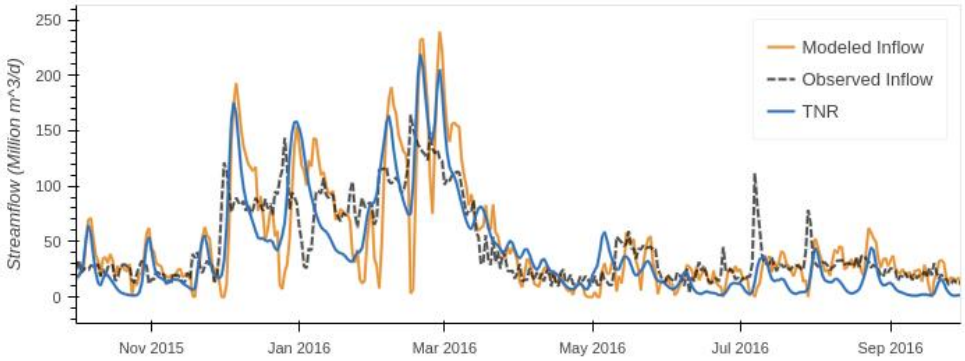

Figure 3.5 Hydrographs comparing the Modeled, Observed and TNR at Old Hickory Dam, which is the second most downstream dam in the network. The observed inflow is regulated inflow.

While analyzing the observed inflow hydrographs of two consecutive dams (Cordell Hull and Old Hickory dams) in figure 3.6, a closer relationship between the downstream inflow and upstream outflow can be noted. It is clear that the upstream outflow plays a dominant role in dictating the downstream and regulated inflow at the next downstream dam as would be normally expected in the event of no lateral flow diversion. This relationship is further explored in the E2 experiment, where the daily in-situ outflow is used to calculate the RR to the downstream dam. Overall, the results improve across the board in the E2 experiment, underlining the role of upstream reservoir releases in predicting the downstream regulated streamflow. The E2 experiment also stresses the importance of having high accuracy estimates of reservoir storage data.

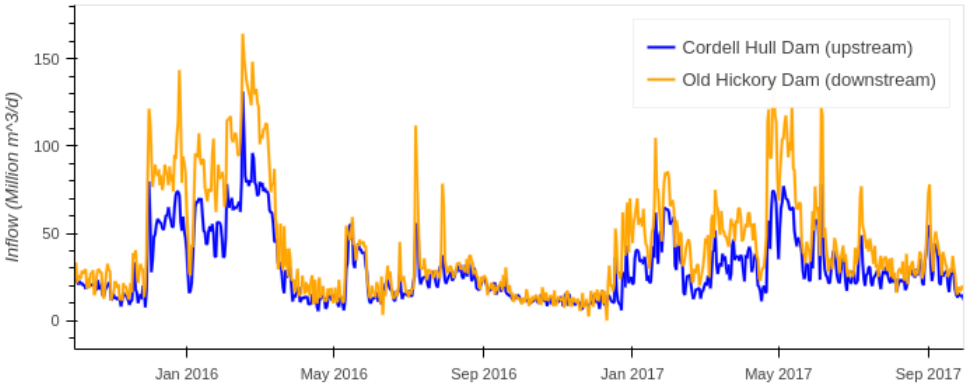

Figure 3.6 Observed inflows at two consecutive dams. The upstream Cordell Hull Dam drains into the downstream Old Hickory Dam, with the effect of upstream reservoir dynamics.

In the E3 experiment, the observed inflow to the upstream most dams was used as the NR. In most cases, the performance of the streamflow predictions still improved when adjusted for upstream regulation, as compared to the TNR. While this experiment suggests that if the accuracy

of inflow estimates at the upstream most boundary conditions are accurate, that can improve the regulated streamflow estimates along that downstream network as well. Following this, the final E4 experiment, representative of the performance of the proposed and scalable river regulation model under accurate ΔS was performed. Here the VIC hydrological model was calibrated using the observed inflow at the upstream most dams. The result of this experiment shows overall improvement for nearly all the reservoirs. These results indicate that using in-situ reservoir dynamics, specifically storage change, and inflow hydrograph modeled without considering reservoirs (TNR) can be used to improve the performance of downstream streamflow estimates.

Moreover, the experiment results also shed light on the relationship between the model performance and the number of upstream dams. For instance, taking the case of the Wolf Creek dam (7.4 km^3 storage capacity), which only has one upstream dam (Laurel Dam, 0.5 km^3 storage capacity), the performance of the model does not improve as significantly as compared to the TNR. On the other hand, Cordell Hull Dam (run-of-the-river) is highly regulated and has two upstream dams, the Dale Hollow dam (2.1 km^3) and the Wolf Creek dam, and the performance of the streamflow estimates improves significantly by almost 50% across all the dams in the basin. Overall, the results show that considering the effect of upstream regulation improves the performance of the streamflow estimates at the downstream dams.

3.4.2 River regulation using satellite estimates of reservoir storage change

Now that E4 results established robustness of the proposed river regulation algorithm, we explore how well ResORR fares with satellite-derived ΔS that will have higher uncertainty. The inundation area of the reservoirs were obtained using the Landsat-8 and Sentinel-1 satellite data from June 2018 to October 2019, using the TMS-OS algorithm described by Das et al., (2022). The storage change of the reservoirs were then obtained using these surface area estimates and in-situ Area-Elevation Curve (AEC), using the following equation –

$$\Delta S_t = \frac{A_t + A_{t-1}}{2} \times (h_t - h_{t-1}) \quad (6)$$

Here the ΔS in equation 6 is the total volumetric storage change, A is the inundation area, and h is the water level height corresponding to the inundation area, obtained using the AEC relationship. The date of satellite observation is denoted by t, with $t-1$ referring to the last satellite observation. For instance, since Landsat-8 has a revisit period of 16 days, the estimated

storage change would refer to the volumetric storage change within those 16 days. These storage change estimates were transformed to daily values by linearly distributing the volumetric change over 16 days. Based on the findings of the previous section, the VIC hydrological model was calibrated at the upstream most dams, like the E4 experiment. The modeled inflow as such and the streamflow estimates from VIC were compared against the observed in-situ inflow. The results are summarized in figure 3.7.

Similar to the results in the previous section, for the Cordell Hull and Old Hickory, both run-of-the-river dams having upstream dams with large storage capacities, ResORR performance increases significantly across all metrics. For the Wolf Creek dam, adjusting for the upstream Laurel Dam's operations, ResORR performance does not increase as drastically, which can be explained due to the relatively smaller size of the upstream Laurel Dam. In contrast, the performance increases the most for the Cordell Hull Dam, which is preceded by two large dams, Wolf Creek Dam and Dale Hollow dam. The improvement in performance gradually reduces downstream with marginal improvement for the downstream most Barkley Dam. This can be explained by the run-of-the-river nature of the upstream dams, the storage change dynamics of which can be difficult to quantify using satellite observations. Overall, the results suggest that river regulation due to dams can be characterized by the proposed ResORR algorithm using satellite estimates of reservoir storage dynamics. Adjusting for flow regulation due to upstream reservoir storage change improves the overall inflow predictions in a regulated basin.

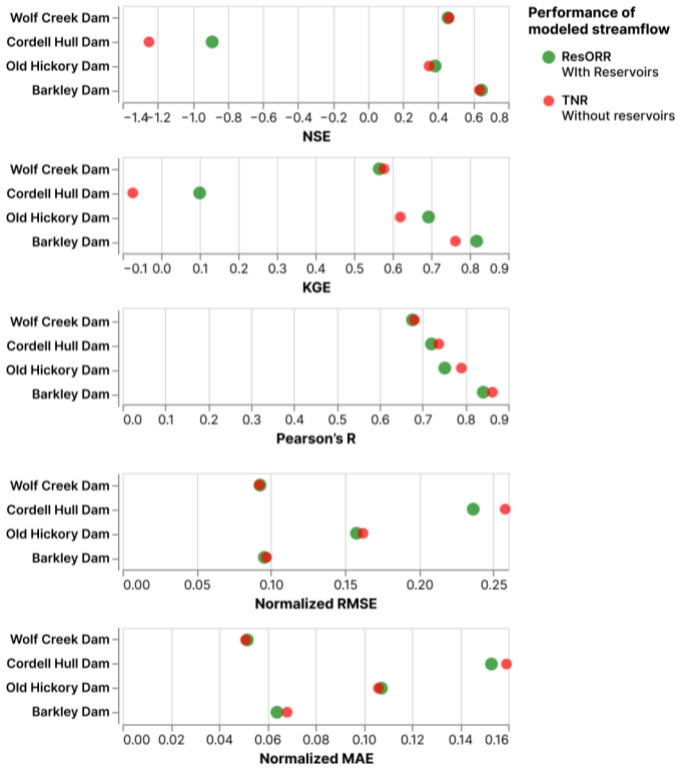

Figure 3.7 ResORR model performance using satellite derived reservoir storage change.

3.5 Conclusions and Discussion

Rivers of the 21st century are marked with numerous reservoirs, which store, and release water based on their primary objectives, playing a vital role in providing food, water, and energy security. However, such reservoir operations can alter the natural streamflow patterns, reducing the water availability downstream by storing water during high flows, and *vice versa*. In this study, we developed and tested a scalable river regulation model, ResORR, to predict the regulation of streamflow due to upstream reservoir operations. Overall, we find that adjusting for upstream reservoir operations via storage change improves the accuracy of downstream streamflow predictions. The theoretical basis of the ResORR model was tested using in-situ data in the heavily regulated Cumberland basin. The results stress the importance of having high accuracy estimates of both the storage change and the hydrological model. Moreover, we find that if the hydrological model can be calibrated for boundary conditions of the reservoir network, *i.e.*, at the upstream most dams, significant improvement can be achieved in predicting regulated inflow at all the downstream dam locations.

Currently, the reservoir network is automatically generated using the dam locations and the DRT flow directions, and hence, any inter- or intra-basin diversions between reservoirs or lateral diversions cannot yet be modeled. The regulation caused by reservoirs is also determined by its storage capacity, and in a case where a small reservoir drains into a larger reservoir, the algorithm adds little value to the streamflow predictions. Moreover, if the storage change of the upstream reservoir is relatively low, the performance improvement of regulated streamflow estimation downstream can be limited. Such a case was experienced in a case-study of the devastating flood due to extreme precipitation in the state of Kerala, India, in 2018. Due to high precipitation leading up to the main extreme precipitation event, the reservoirs were already at full supply level. All the incoming inflow due to the extreme precipitation event had to be released by the upstream reservoir, with little to no storage change. Even with these limitations, the ResORR algorithm can play an important role in quantifying the regulation of river flow due to reservoirs in changing the world's river systems.

With advancements in satellite observations-based reservoir dynamics tracking, especially the RAT 3.0, which has democratized access to reservoir operations information, it is now possible to easily track the operations of reservoirs globally. Building on top of the RAT framework, the proposed river regulation algorithm ResORR would also be able to characterize the regulation of river flow using only satellite-tracked reservoir states at the global scale. The algorithm was developed over the Cumberland basin which is in a humid region. The evaporative losses from the reservoirs therefore play a relatively minor role compared to the inflow into the reservoir due to surface runoff. Hence, the evaporative losses were not considered while calculating the outflow. However, the evaporative losses play an important role in arid region. For application over such regions, the evaporation from the reservoirs can be included in the water mass balance of the reservoirs in eq. (5). The ResORR software architecture is also designed to work seamlessly within the RAT framework, i.e., it can run entirely using the RAT model outputs and intermediary files. With this river regulation tool, the RAT framework will be able to not only infer reservoir dynamics, but also quantify the regulation of streamflow caused by the upstream reservoir operations. We can expect ResORR to soon become a truly scalable algorithm based on the globally available reservoir storage change data of unprecedent accuracy from the Surface Water and Ocean Topography mission.

While RAT and ResORR in chapter 2 and chapter 3 together provides a toolset required to study reservoir driven regulation of rivers in the past, it is imperative for stakeholders to be informed of upstream reservoirs may regulate water in the near-term future. In chapter 4, we further extend the capability of estimating reservoir operations of the RAT framework to the near term future and study its potential on the case of wide scale floods that occurred in Kerala in 2018. Furthermore, in this chapter we find that, among all variables required to estimate river regulation, the accuracy of storage change of reservoirs is key for accurately estimate river regulation. In Chapter 5, the newly launched SWOT satellite's accuracy is tested to determine its ability to estimate storage changes.

Chapter 4. Forecast Informed Reservoir Operations within a Satellite based Framework for Mountainous and High Precipitation Regions: The Case of the 2018 Kerala Floods

***Note**: This chapter has been published mostly in its current form in the Journal of Hydrologic Engineering (Das et al., 2025). Used with permission from ASCE.*

Das, P., Suresh, S., Hossain, F., Balakrishnan, V., Jainet, P. J., Lee, H., Laverde, M., Hosen, K., Meechaiya, C., and Towashiraporn, P. (2025). Forecast-Informed Reservoir Operations within a Satellite-Based Framework for Mountainous and High-Precipitation Regions: Case of the 2018 Kerala Floods. *Journal of Hydrologic Engineering*, *30*(2), 05025003. https://doi.org/10.1061/JHYEFF.HEENG-6276.

Key Points:

- Gauge precipitation-corrected weather forecasts and likely reservoir operating scenarios are utilized to forecast inflow and outflow from reservoirs.
- The potential of forecast informed reservoir operations estimation is investigated by taking the extreme precipitation driven floods of 2018 in Kerala as a Case Study. Forecasting can give reservoir operators a lead time of 2 to 3 days, with high certainty, to predict rising trends, and potentially up to a week in advance.
- The module is designed as a scalable, globally applicable module for the Reservoirs Assesment Tool (RAT) framework. The scalability of the system is demonstrated by its successful application during the floods in Tripura and Southeastern Bangladesh in 2024.

ABSTRACT: River regulation in mountainous and high precipitation regions with hydropower dams often struggles to find the right balance between hydropower generation while ensuring flood protection for downstream inhabitants. The goal of hydropower generation is to keep reservoirs at the maximum pool as often as possible while for flood control, it is to maintain sufficient cushion in available storage to absorb an incoming flood wave. Using weather forecasts to proactively manage reservoir operations for such conflicting goals is now a well-known solution. However, this challenge of applying forecast-informed reservoir operations is magnified in developing regions where there is a paucity of ground data to track reservoir dynamics. In this study, we explore the utility of using publicly available precipitation forecast from the Global Ensemble

Forecasting System (GEFS) with a fully satellite-based reservoir tracking framework called Reservoir Assessment Tool (RAT) to understand the potential of forecast-informed operations in highly mountainous and high precipitation regions that are mostly ungauged. We apply our investigation to the case of damaging floods that took place in 2018 in the Southern Indian state of Kerala where river regulation is carried out with a fleet of hydropower dams. Our results show that the precipitation forecast from GEFS has sufficient skill, if focused on trends and bias adjustment, to predict reservoir inflow peaks up to a week ahead of time where the trend for timing of the peak and rate of rise match well. Using our satellite-based RAT framework, we explore the range of actionable scenarios for dam operators that could potentially minimize downstream flood risk with this forecast-informed reservoir operations scheme.

4.1 INTRODUCTION

In the previous chapters, the RAT and ResORR models were developed to estimate the operations of reservoirs using satellite observations and hydrological modeling and the resulting regulation of rivers due to a series of reservoirs. Both the models operate on historical meteorological conditions and satellite observations to hindcast the model outputs. However, forecasting the near-term operations of reservoirs remains a crucial piece of the puzzle for stakeholders and public alike, especially in cases of extreme events such as floods. In this chapter, we extend the framework built so far to forecast reservoirs operations in the near future under several likely operating scenarios.

Floods affect millions of people resulting in loss of life, livelihoods, and damage to infrastructure each year. An estimated 23% of the world population is directly exposed to catastrophic floods, among which about 90% live in low- to middle-income countries, with limited ability to cope with such disasters (Rentschler et al., 2022). Such floods, especially in mountainous regions with steep slopes can be made more disastrous by extreme precipitation events, such as the devastating floods and landslides in Uttarakhand, India, in 2013; in Kerala, India in 2018, and in South Korea in 2023 (Shin, 2023; Vijaykumar et al., 2021). An increase in the intensity and frequency of such extreme precipitation events has been observed globally, especially in the past decade (Dunn et al., 2020; Sun et al., 2021). Climate models suggest that such extreme precipitation events are very likely to keep increasing in frequency and intensity due to climate

change making such floods more frequent (Fischer et al., 2015; Intergovernmental Panel On Climate Change, 2014; Kharin et al., 2018; C. Li et al., 2021).

Reservoirs play a crucial role in providing a cushion against such floods. However, they are often optimized for multiple purposes, such as flood control and hydropower, for maximizing the benefits of existing infrastructure (Ahmad & Hossain, 2020a). Due to the competing nature of optimization strategies of such reservoirs, floods that are exacerbated due to extreme precipitation events in mountainous regions pose additional risks for reservoir operations. For instance, hydropower dams in Kerala (India) in 2018 were faced with floods due to extreme precipitation, which were almost full for hydropower generation (Vijaykumar et al., 2021). This led to little-to-no storage cushioning to mitigate the impending flood pulse, leading to full-scale devastation of the unattenuated flood pulse downstream. Consequently, the flood event claimed the lives of over 489 people, displaced over 1.4 million people, and caused damages of more than $5 billion (Pramanick et al., 2022; Suresh et al., 2024).

During such extreme flood events, forecasted information about the impending flood could be potentially useful in informing reservoir operators to be proactive. Recent forensic studies on the Kerala 2018 floods present a dichotomy of views. Mishra et al., (2018) report that a week's lead time in forecasting could have potentially mitigated the situation with proactive reservoir operations. On the other hand, a study by Sudheer et al., (2019) claims that no amount of forecasting could have helped given how anomalous and extreme the precipitation patterns were during that time. Regardless of the debate, the value of such forecasted information arguably depends on the flexibility in the operation of reservoirs afforded to the reservoir operators, because reservoirs are operated on predefined rule curves mixed with the dam operator's situational awareness of the evolving situation. However, there is no doubt that if the peak of the catastrophic flood wave was forecasted sufficiently ahead of time and in an actionable manner, dam operators could have acted on the forecasted information early. For example, with a sufficient lead time, forecasted incoming flood can be potentially mitigated of its risk posed by reducing the peak flow rate downstream through early release to make room for flood storage (Saavedra Valeriano et al., 2010).

With longer forecast lead times, the skill of the forecasts gradually degrades (Siqueira et al., 2020). Anghileri et al., (2016) reported that the value of long-term streamflow (seasonal to

inter-annual) forecasting has limited value for designing adaptive reservoir operation strategies. Instead, streamflow forecasting and reservoir optimization at a shorter time scales, with lead times of days to a few weeks, is more suited for preparedness against floods (F. Wang et al., 2012). In addition to flood preparedness, forecasted reservoir inflow can also pave the way for forecast-informed adaptive management for more efficient hydropower production where the dual and conflicting goals of flood control and hydropower can be maintained (Ahmad & Hossain, 2020b; Anghileri et al., 2016).

Operational streamflow forecasting has been a topic of great interest, and decision support systems exist at varying spatial and temporal scales. For instance, the GloFAS system uses short-term daily meteorological forecasts and long-term climatological data to forecast streamflow globally using the Lisflood hydrological model (Van Der Knijff et al., 2010). This system performs well for medium-large sized river basins, with low basin water storage, but the performance decreases with decreasing drainage area, which is the case for most of the mountainous basins in the Southwestern coast of India such as in Kerala. Wu et al., (2012) developed the Global Flood Monitoring System (GFMS) which forecasts streamflow at a quasi-global scale, between 50°N-50°S up to a 5-day lead time driven by the GEOS-5 forecasted precipitation. While this system is generally able to detect floods with a probability of detection (POD) of 0.7, the performance reduces with the presence of river regulation that is not explicitly accounted for.

By the end of the century, climate model projections estimate that dams may help reduce the exposure to floods for about 12.9%-20.6% of the population (Boulange et al., 2021). In spite of the important role played by reservoirs, they are either not considered by hydrological models or their incorporation in modeling is highly parameterized due to a lack of availability of reservoir operations data (Alcamo et al., 2003; Biemans et al., 2011; Haddeland et al., 2006; Hanasaki et al., 2006, 2018). Using publicly available satellite observations covering nearly the entire Earth, reservoir operations, including inflow, storage change, evaporation and outflow from dams, is now being inferred globally from space (Biswas & Hossain, 2022; Kumar et al., 2024; Y. Li et al., 2023).

The Reservoir Assessment Tool (RAT) is one such publicly accessible and globally scalable tool, for both operational monitoring and historical analyses of reservoir operations. RAT leverages observations from multiple satellites to infer reservoir operations (Biswas et al., 2021;

Das et al., 2022; Minocha et al., 2023). RAT has been set up operationally over various basins across the world for near-real time reservoir operations tracking, such as the Columbia, Mekong, Tigris-Euphrates, Kerala, and is used as an operational decision support system by stakeholders, such as the Mekong River Commission (MRC) and Columbia River Inter-tribal Fish Commission (CRITFC). Given the debate surrounding the value of precipitation forecasting for proactive reservoir operations for Kerala 2018 floods and our ability to track reservoirs from space, we believe it is now important to put the satellite-based modeling of reservoir state within the context of exploring forecast-informed operations to investigate the issue further.

For this study, using meteorological forecasts, including gauge corrected precipitation forecasts, and historical reservoir storage change, we have augmented RAT with a forecasting module. We assess the value added by the forecasting module of the RAT system in informing reservoir operators of forecasted streamflow and exploring reservoir outflows based on actionable reservoir operation scenarios. Specifically, we investigate the utility of forecasts at different lead times over the mountainous basin of Kerala using the 2018 flood as our case study. Our choice for this region is representative of the vast regions in the tropical and developing world where rivers are regulated by hydropower dams, are flood prone and yet often lack ground measurement or public sharing of reservoir state information. The overarching research question of our study is, *how effective are gauge-adjusted precipitation forecasts in informing reservoir operations in highly mountainous and high precipitating regions?* In this study, we address the following objectives:

- To test the effectiveness of forecasted inflow for flood preparedness in mountainous and high precipitation regions using forecasted precipitation by the Global Ensemble Forecast System calibrated to in-situ gauge observations in the South Indian region of Kerala.
- To explore the range of actionable scenarios for dam operators that could have potentially minimized downstream flood risk of the Kerala 2018 floods with this forecast-informed reservoir operations scheme of RAT.

4.2 Data and Methods

4.2.1 Study Area

We conducted the investigation over the Greater Periyar basin of Kerala, India. The Periyar river is the longest river in Kerala. Bounded by the Arabian Sea to the West and the Western Ghats mountains to the East, Kerala's topography varies from low-lying coastal areas to highly mountainous with steep slopes (Figure 4.1). Kerala receives most of the annual precipitation due to southwest monsoonal winds during July-September, receiving more than about 3000 mm precipitation annually. The windward slopes of the Western Ghats receive heavy precipitation leading to a high risk of flooding (Simon & Mohankumar, 2004; Thomas & Prasannakumar, 2016). The Kerala 2018 flood was one of the worst floods in recent history due to an extremely high precipitation event in the month of August. Between August 1 to August 19, 2018, Idukki received more than 700mm of rainfall, which is about 164% more than the normal amount of rainfall during this period (Central Water Commission, 2018).

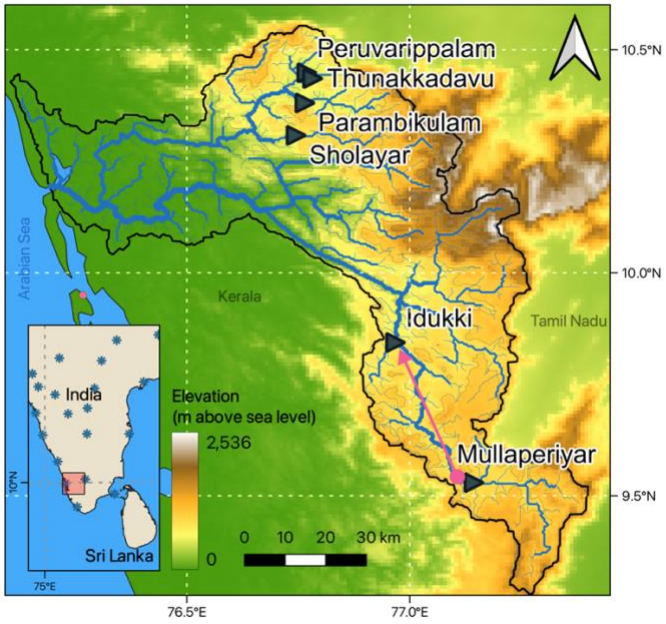

Figure 4.1 Map of the Greater Periyar River Basin showing the location of six study reservoirs. A pink arrow highlights the flow of water from the Mullaperiyar Dam to the Idukki Dam. An inset map to the bottom left shows the location of the Greater Periyar basin in the Indian subcontinent, including the location of precipitation measuring stations used in generation of the GEFS-CHIRPS dataset as blue stars.

The Periyar river is regulated by 13 dams, with the Idukki dam being the largest. The investigation concentrates on 6 major dams out of the 13, due to their availability in public global dam databases such as The Global Reservoir and Dam (GRanD) database (Lehner et al., 2011). The water management in the basin, especially for the Idukki dam is made challenging by the fact that the upstream reservoir, the Mullaperiyar dam, is operated by the neighboring state of Tamil Nadu, which is under a separate operating jurisdiction than Kerala's. This jurisdictional complexity, which is common around the world, is a key justification for a satellite-based framework that provides level-playing, publicly accessible and near real-time state of reservoir for all concerned stakeholder agencies.

All the data, except for the in-situ reservoir inflow data to the Idukki dam, used in this study are publicly accessible. Forecast precipitation as the CHIRPS-GEFS dataset was obtained from the Climate Hazards Center at UC Santa Barbara from https://chc.ucsb.edu/data/chirps-gefs. The minimum, maximum temperatures and the U- and V- components of wind are obtained from the historical archives at the Research Data Archive at the National Center for Atmospheric Research (https://rda.ucar.edu/datasets/ds084.1/dataaccess/). The RAT software can be installed using the conda package manager or from https://github.com/UW-SASWE/RAT. Install instructions and the documentation for RAT are available at http://ratdocs.io. The documentation for RAT-Forecasting module and the data associated with this study can also be accessed at https://rat-satellitedams.readthedocs.io/en/latest/Plugins/Forecasting/. The forecasted data generated for the study is available at https://www.dropbox.com/scl/fo/9hbdmu5wbh5wowd95qdsu/ADejOG0KT2FiSnQ8yJKacXk?rlkey=w3z2mk41kasx2ldx5futuifrs&dl=0

4.2.2 Meteorological forecast datasets

The accuracy of streamflow estimation, especially in monsoon driven regions like Kerala, depends significantly on the accuracy of the precipitation estimates used to drive the hydrological modeling. Here, we used the recently released Climate Hazards Center InfraRed Precipitation with Stations - Global Ensemble Forecasting System (CHIRPS-GEFS) (Harrison et al., 2022) operational precipitation forecast dataset for streamflow forecasting. It is generated by combining the widely used Climate Hazards InfraRed Precipitation with Stations (CHIRPS) product (Funk et al., 2015) with the Global Ensemble Forecast System (GEFS) v12 (X. Zhou et al., 2022). The

GEFS by itself, is a global numerical weather prediction system which operationally forecasts key atmospheric variables at an hourly temporal resolution for the globe. The spatial resolution varies from 0.25° for forecasts up to a 10 days lead time and 0.5° for 11-16 days lead time. Within the state of Kerala, there are three stations used for generating the CHIRPS dataset – Trivandrum, Cochin, and Kozhikode. Although none are within the Periyar basin, the closest station is located 75 kms from the Idukki reservoir. Due to the coastal location of the station, it may not be able to appropriately capture the high intensity rainfall experienced at the upper reaches of the Periyar basin, which underscores the paucity of ground data within the basin and the necessity for more accurate satellite based precipitation estimates. However, such numerical weather predictions based meteorological forecasts can have systemic biases, especially at higher lead times, which can lead to higher uncertainties in streamflow predictions, necessitating post-processing bias correction of the precipitation products (Wood et al. 2004; Yang et al. 2020). Furthermore, the low spatial resolution of the GEFS precipitation forecasts at 0.25-0.5º (~25-50 km) is limited in representing the smaller scale precipitation features that control the rainfall-runoff processes in mountainous basins.

Using a quantile-quantile matching algorithm, the observed historical CHIRPS precipitation dataset is used to remove systemic biases in GEFS precipitation forecast. It is then statistically downscaled to 5km leading to the GEFS-CHIRPS forecast data product (Harrison et al., 2022). The other key meteorological variables for streamflow estimation, such as the minimum and maximum temperature, wind speed and wind direction are derived from the Global Forecasting System (GFS). The core global model of GEFS-CHIRPS, the GFS, is a widely used operational global weather forecast model with a lead time of up to 16 days, producing forecasts at an hourly (for the first 120 hours of forecast) to 3-hourly (for the rest of the duration of forecast) temporal resolution and at a spatial resolution of 0.25°.

4.2.3 Reservoir operations and streamflow datasets

The hindcast streamflow estimates for all the six reservoirs were first estimated using the RAT 3.0 software package, driven by the Variable Infiltration Capacity (VIC) hydrological model (Liang et al., 1994). The model is forced using the GPM-IMERG run (Huffman et al., 2020; Precipitation Processing System (PPS), 2022) precipitation product, and temperature and wind speed data from NOAA CPC Global Temperatures and NCEP-Reanalysis respectively. The

timeliness of the “hindcast” estimates of streamflow are limited by the availability of recorded temperature and wind speed, which are available usually at a lag of 2-3 days. We also “nowcast” the streamflow using GPM-IMERG precipitation, specifically, the IMERG-Late product and forecasted temperature and wind speed from the Global Forecasting System (GFS) when hindcast data is unavailable. Finally, we also “forecast” the incoming streamflow into the reservoir using the CHIRPS-GEFS precipitation forecast and the GFS forecasted meteorology. In-situ streamflow observations were obtained, when available, from the local stakeholder agencies for validation of the streamflow nowcast and forecast.

Earlier, Biswas et al. (2021) used long term satellite observations of reservoir surface areas to infer the likely operation rule curves of the reservoirs. These operation rule curves, relating the storage of the reservoirs for a given month as a fraction of the maximum storage capacity, were used to explore a range of actionable scenarios for dam operators that could have potentially minimized downstream flood risk (described in greater detail in section 4.3.2).

4.3 METHODOLOGY

4.3.1 Integration in RAT 3.0 and Forecasting Inflow and Evaporation

The developed forecasting module is designed for integration in the RAT 3.0 software package with minimal changes to the existing code base. The RAT works on the basis of mass balance at the reservoir where inflow, storage change and evaporative losses are modeled or estimated from satellite data to estimate the likely outflow (Figure 4.2 and 4.3). Here the outflow is an aggregation of reservoir release longitudinally along the river and lateral diversion via irrigation or water supply canals. For more detailed information on the development and theory behind RAT, the reader should refer to Biswas et al. (2021), Das et al. (2022), and Minocha et al. (2023).

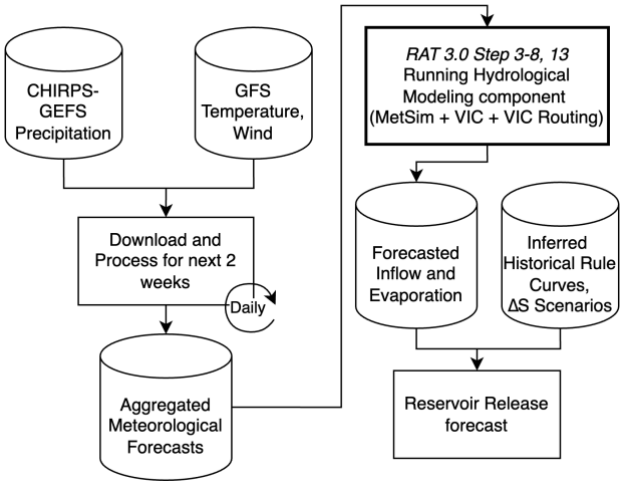

Figure 4.2 Flow chart illustrating the methodology for generation of inflow and reservoir outflow forecast.

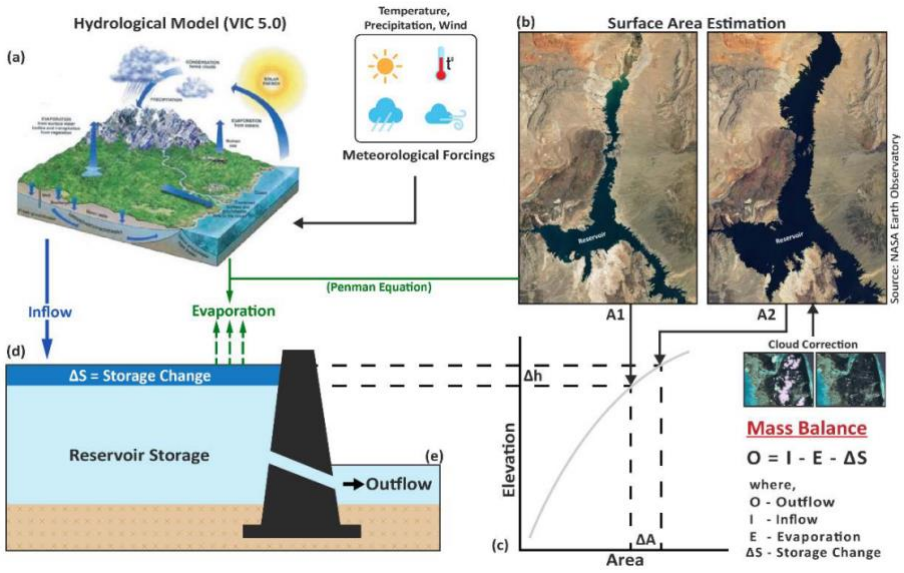

Figure 4.3 Illustration of the conceptual model of RAT 3.0. (a) The Variable Infiltration Capacity (VIC) 5.0 hydrological model is used to model the inflow to the reservoir using satellite observations derived meteorological forcings; (b) Surface area is estimated using the TMS-OS algorithm at a frequency of 1-5 days using observations from multiple satellites – Sentinel-1, Sentinel-2 A/B, Landsat 8 and Landsat 9; (c) Storage change is estimated using observed reservoir surface area and the Area-Elevation relationship of the reservoir; (d) Evaporation is computed using the Penman equation; (e) Using mass balance, outflow is estimation for the reservoirs.

The RAT framework has a total of 14 distinct modular steps that can be run to generate various reservoir operations monitoring datasets (Figure 4.3; see http://www.ratdocs.io for details). Step 1-3 of RAT 3.0 download and process nowcast meteorological observations by satellites – scaling, aligning and clipping to the region of interest in the process, finally generating forcing

inputs for the MetSim (Bennett et al., 2020) meteorological disaggregation model, used in the subsequent steps. The proposed forecasting module replicates these steps in essence, producing the forcing inputs for the MetSim model, but uses forecast meteorological inputs instead of nowcast observations. Using the processed meteorological forecast data, steps 3-8 of RAT 3.0 are run, which uses the MetSim, VIC and the VIC Routing (Lohmann et al., 1996) models to model the streamflow forecast estimates at each reservoir. Step 13 of RAT 3.0 is then used to obtain the forecasted evaporation and the inflow to each reservoir (see Minocha et al., 2023 or https://ratdocs.io). The methodology for obtaining forecasted inflow, evaporation and release under different scenarios is described pictorially in figure 4.2.

The RAT-forecasting module was run for all six dams in the Greater Periyar basin. The VIC model of RAT 3.0 used in this study was calibrated against observed inflow for different basins across Kerala (Suresh et al., 2024). Within the Idukki basin, only the observed inflows to the Idukki reservoir were available. The R^2 and NRMSE (as %) values comparing the observed and nowcast inflows for this reservoir were 0.61 and 40% respectively. While the peak inflow values to the reservoir were underestimated, the trends of the rise and fall of the streamflow rate and the timing of the peak flood were predicted well. The inflow forecasts at different lead times were compared against the satellite-observations based nowcast inflow. This comparison allowed an assessment of skill of forecast against a benchmark of nowcast inflow based on satellite precipitation data. The skill of forecasted inflow was evaluated by calculating the coefficient of determination (R^2) and the Root Mean Squared Error normalized by the range (RMSE-range) at different lead times. The results of this comparison are summarized in figure 4.8.

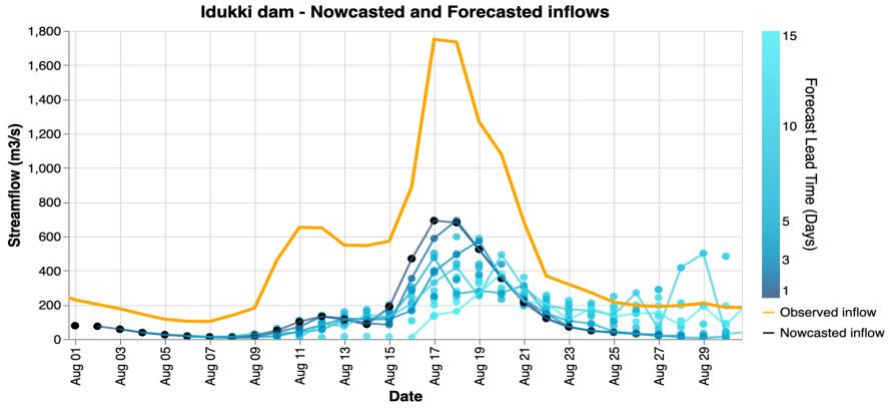

Figure 4.4 Comparison of observed inflow (Orange) with inflow modeled using satellite precipitation data using RAT to the Idukki dam (Black line) overlain with forecasted inflow (Blue circles and lines) during the flood in August 2018. Forecasts for lead times 1, 3, 5, 10 and 15 days are highlighted by joining the blue circles representing the forecast time-series.

To further visualize the timing and intensity of the flood peak, the forecasted inflow is also presented as a 2D grid of nowcast and forecast values in figure 4.5. The x-axis represents the date within the forecast horizon, while the y-axis represents the date of generating forecast. For any given date in the forecast horizon, the forecasted inflow at shorter lead times can be read by moving down the y-axis. For each day of forecast generation, the forecasted inflow at "X days ahead" can be read by moving right along the x-axis. A discussion on the inferences provided in greater detail in section 4.4.2.

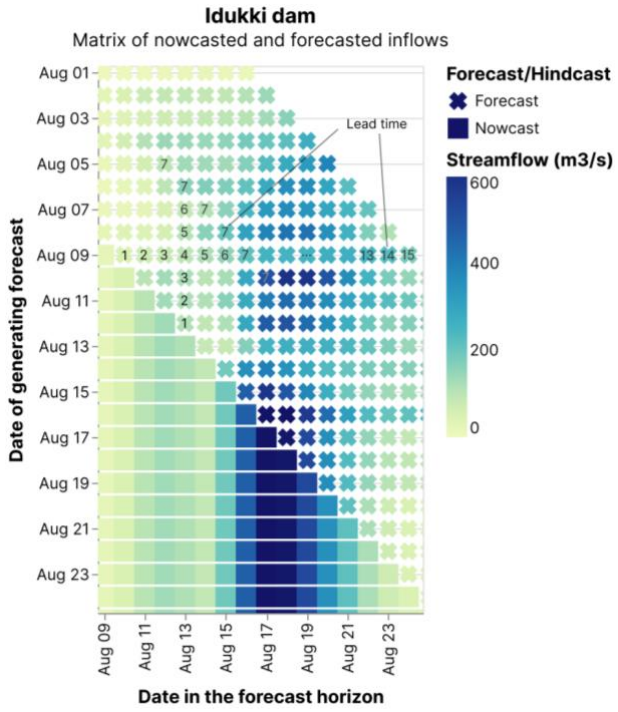

Figure 4.5 Matrix of nowcast (squares) and forecast (crosses) streamflow during the peak of the 2018 flood at the Idukki dam. The y-axis represents the date on which the forecast was generated, and the x-axis represents the date of nowcast/forecast. The lead time of forecast increases moving upwards along the y-axis and rightwards on the x-axis. The lead times associated with the forecasted streamflow generated on August 9^{th,} are annotated along the x-axis, and the forecasted streamflow estimated for August 13th are annotated along the y-axis using numbers. The flood peak of August 17th and 18th can be seen to be forecasted with a lead time of about 7-8 days.

4.3.2 Reservoir operations and outflow forecasting

Forecasting reservoir operations, specifically the storage change, is fundamentally challenging because it is influenced heavily by the decisions taken by reservoir operators that one cannot predict or forecast ahead of time. Thus, any forecasting of reservoir state, such as forecast of end storage, water level or outflow, will have to be based on potential dam operating scenarios. These scenarios can be assumed from an inferred operating rule curve assuming the dam operator will likely follow based on an historical response, see Biswas et al. (2021), analogous to a 'business as usual' scenario. Alternatively, one can assume various dam operating scenarios in reaction to the impending flood that are each physically plausible. Both options are explored here to shed light on the value of forecast-informed reservoir operations.

The scenarios for exploring actionable reservoir operations to mitigate the flood proactively are elaborated as follows.

1. **Target reservoir water level** - The target water level of the reservoir can be specified by the dam operator to simulate the reservoir state in the forecasting horizon, given the forecast of inflow and evaporation. This can be the maximum permissible water level of a reservoir that the dam operator feels should not be exceeded due to dam safety concerns. It can also be a water level lower than the existing water level that the dam operator wants to attain. Thus, if the target level is forecasted to be greater than the current reservoir level, the incoming flow of water is stored until the target level is reached. The stored water is then released if the target water level is estimated to be less than or equal to the current water level. If the target level is lower than the current reservoir level, then the received inflow is released in a temporally constant manner to attain the desired water level.
2. **Fraction of maximum reservoir storage** - The storage change of the reservoir is estimated by considering a range of predefined fractions of maximum reservoir storage capacity that the dam operator deems permissible. For example, a dam operator may try to be conservative and allow little room for reservoir to change storage quickly by selecting a small fraction of maximum reservoir storage the dam is allowed to operate with. On the other hand, a dam operator may wish to prioritize flood mitigation and allow

a larger range for storage change to operate with, thereby allowing more flexibility in outflow and total storage.

3. **Inferred rule curve** - This is operation rule curve-based dam operation where the rule curve is inferred based on historical observations of reservoir operations for the specific time when the flood took place. As mentioned earlier, this is analogous to 'business as usual' scenario. For example, if a certain dam is known to maintain its storage at a certain level during the first week of August based on historical average using past observations, then that is the likely level the dam operator would try to maintain the level at during the flood event. Using historical observations of the storage of the reservoir as a fraction of the maximum storage of reservoir S_t/S_{max} for any time t, the expected storage change in the forecasting horizon (ΔS_{tN}) is obtained as follows -

$$\Delta S_{tN} = (S_{tN}/S_{max} - S_{t0}/S_{max}) \times S_{max}$$

where, t0 is the date when the forecast was generated and tN is the final date of the forecast. If the rule curve dictates a certain storage change during the forecast horizon, and if the net storage change, defined as the difference of rule curve-based storage change and forecasted inflow, is positive, then the inflow received is stored. If the net storage change is negative, then a constant release is made to meet the necessary storage change.

4. **User defined storage change** - The volume of storage change in the forecasting window can also be directly provided to simulate the reservoir state in the forecast horizon. Here, the dam operator may choose to input any custom storage change value (e.g. 15 million m^3 as an example used in this study) to forecast the other reservoir states (outflow and water level). This way, a dam operator can assess the forecast of the reservoir state, including the water level and outflow based on the expected storage change.

The outflow from the reservoir and the corresponding water surface elevation and area are calculated for all the different storage change scenarios. For example, in the first scenario where a target water level is desired, water is accumulated until the target water level is reached. For each time step in the forecast horizon, if the water level of the reservoir is forecasted to be greater than the target water level, the excess volume of water is released as the outflow (O) and the corresponding storage change is calculated as $\Delta S = O - I - E$. Otherwise, water is stored in the reservoir with no outflow and the storage change is calculated as $\Delta S = I - E$. Here, I is the

accumulated inflow, E is the accumulated evaporation and ΔS is the storage change, over the total lead time (T). The change in water elevation is then calculated as ΔH = ΔS/Area. The new water surface elevation of the reservoir is updated using the change in elevation as $H_t = H_{t-1} + \Delta H_t$. The corresponding new surface area is then calculated using the Area-Elevation Curve (AEC). The AEC relates the elevation of the reservoir with the surface area. It can be obtained by surveying the corresponding surface area of a filled reservoir for a given elevation which is usually done before construction of the reservoir. However, in-situ AEC data may not always be available publicly, in which case it can also be obtained using Digital Elevation Models (DEM) (Das et al., 2022). We use AEC derived from the Shuttle Radar Topography Mission (SRTM) DEM in this study.

Similarly, for the other reservoir operation scenarios, the volume of expected storage change during the forecast horizon is first estimated. For instance, in case of the scenario of operating within a pre-defined range of maximum storage change (expressed as a fraction of total storage) or user-defined storage change, the constant outflow rate required within the forecast window is estimated as $O = (I - E - \Delta S)/T$. The water surface elevation and area corresponding to the storage change of the reservoir are then calculated for each time step similar to the methodology described above.

4.4 Results and Discussions

4.4.1 Skill of forecast precipitation

Before analyzing the skill and performance of forecasted flow, it is helpful to first analyze how the precipitation input to the RAT framework performs at forecast time scales. This analysis can help explain the ensuing skill and performance in forecasted flow as the skill of flow forecasting cannot exceed that of skill of forecasted precipitation.

In figure 4.4, we show the precipitation forecasts by CHIRPS-GEFS against in-situ gauge recorded precipitation. Overall, the bias in CHIRPS-GEFS precipitation forecast is within -0.50 mm and 1.5 mm, which can be considered negligible. We also compared the IMERG satellite precipitation estimates against the precipitation at an in-situ gauge-based precipitation data product called GSOD (Global Summary of the Day). This GSOD product is available from the National

Climate Data Center (NCDC) via NOAA at: https://www.ncei.noaa.gov/access/metadata/landing-page/bin/iso?id=gov.noaa.ncdc:C00516.

The specific GSOD station data were extracted for the period of 2015-2024. The average bias in the GPM-IMERG precipitation product over 10 years was negligible at 0.9 mm. This is not to say that multi-sensor precipitation estimation or GEFS has universally low uncertainty in mountainous basins. Both types of precipitation estimation has endemic challenges that are not picked up well due to the paucity and decreasing density of in-situ precipitation gauges as elevation increases. Interested readers can refer to Pradhan et al., (2022).

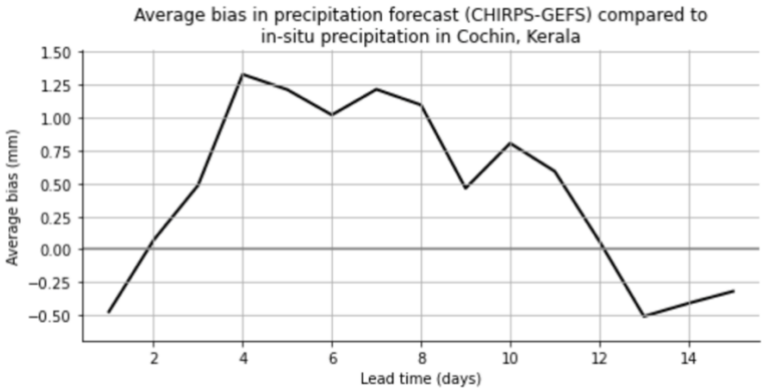

Figure 4.6 Comparison of bias, averaged over 2017-2018 CHIRPS-GEFS precipitation forecast at Cochin, Kerala, compared to in-situ gauge measured precipitation.

We also visually compared the GPM-IMERG in figure 4.7. The precipitation forecasts from CHIRPS-GEFS generally underestimates the intensity of the rainfall when compared to IMERG. The magnitude of the underestimation reduces at shorter lead times, but even at 1 to 3 day lead times, high intensity precipitation is often missed or underrepresented. This underestimation combined with representation of a mountainous terrain in a macroscale gridded model (VIC) is expected to compound the skill of forecasted inflow in the RAT framework for a mountainous and high precipitation region.

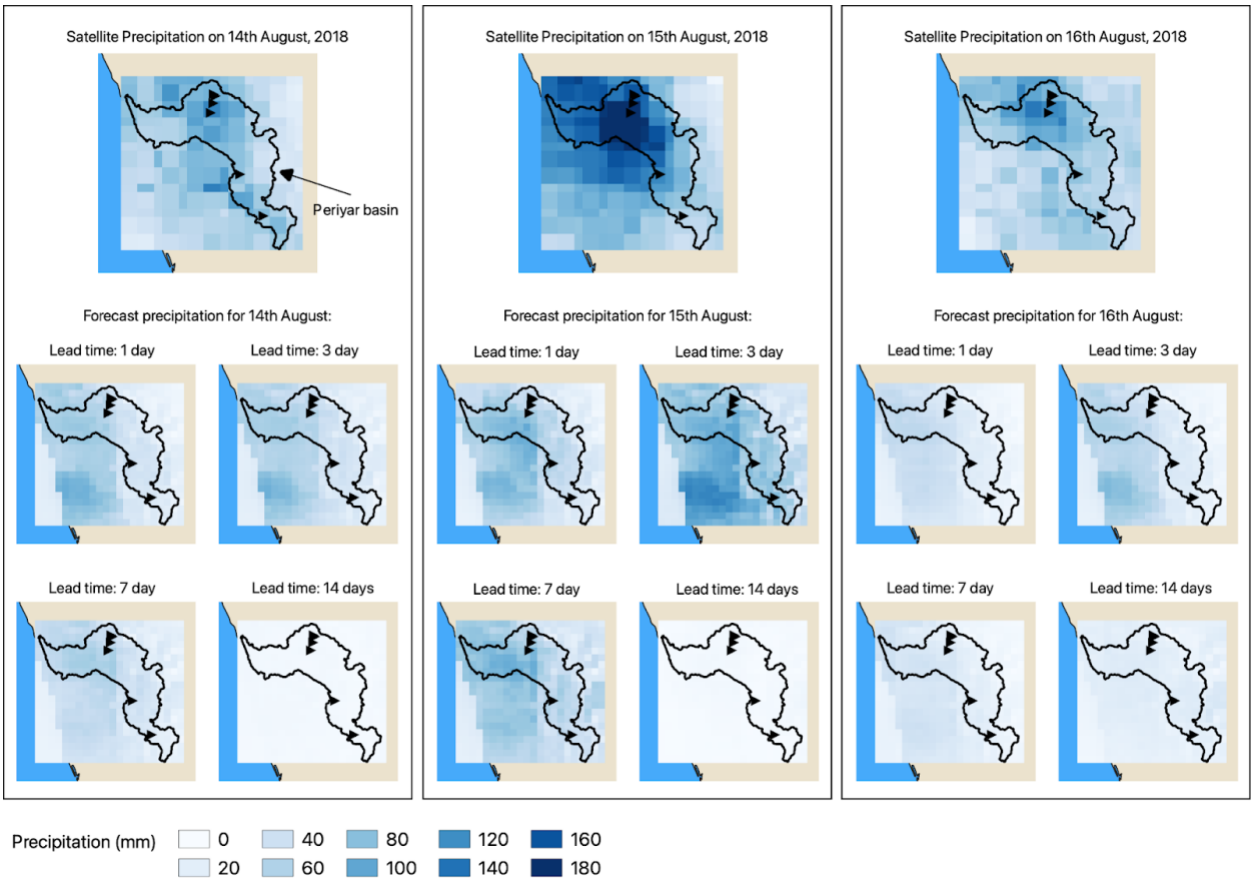

Figure 4.7 Comparison between IMERG satellite precipitation data (which is nowcast) on the three most intense days of rainfall (14, 15 and 16th August, 2018) and precipitation forecasts for the same days by CHIRPS-GEFS at various lead times. This comparison reveals the potential skill of CHIRPS-GEFS forecast precipitation at various lead times as satellite precipitation is a nowcast (or hindcast) product.

Our findings regarding the skill of CHIRPS-GEFS as shown in figure 4.7 is not unexpected given the state of the art of global numerical weather prediction and forecasting of precipitation over highly variable and mountainous terrain. Numerical weather predictions perform well in capturing the small scale orographic effects that are the dominant cause of precipitation in mountainous terrain, especially in South West India. In such cases, dynamic downscaling techniques are necessary for solving the fine scale microphysics from larger scale numerical weather prediction models for skillful predictions.

4.4.2 Optimal lead time for forecasting flood timing

The inflow to all the six reservoirs in the Greater Periyar basin were forecasted during the period when the flood peaked. This period was from August 10 to August 25, 2018. Lead times

ranging from 1 day to 15 days were explored. During the same time period, the inflow was nowcasted using satellite precipitation data. Figure 4.4 compares the forecasted and nowcasted inflow at the Idukki reservoir, where the nowcasted inflow is marked as a black line. The observed inflow is shown as the orange line and forecasted inflows are marked as blue circles, with darker shades representing lower lead times. As the lead time of the forecast decreases, the magnitude of forecasted streamflow matches more closely with the magnitude of nowcast satellite based streamflow estimates from RAT. At a lead time of 1-day to 3-day, both the intensity and timing of the peak flood is well predicted. Compared to the observed streamflow, both the streamflow nowcast and forecast estimates are much lower with a constant bias that could be potentially removed operationally (Figure 4.4). The bias discrepancy can be explained by the extreme nature of the precipitation event (Mishra et al., 2018), which can be challenging for both Numerical Weather Prediction models and satellite based observations to detect and estimate the magnitude over mountainous regions (Harrison et al., 2022). Even with the systematic bias between the satellite-based streamflow estimates and observed streamflow, the timing of the flood and the rate of increase in the magnitude of the streamflow during the flood can be seen to be forecasted very well (figure 4.4).

Figure 4.5 visually represents the forecasted inflow at different lead times as a 2D grid. Forecasts generated on August 4 to August 12 all indicated a peak in the hydrograph with high streamflow around August 16-17, coinciding with the peak of the actual flood event. Within a lead time of 2-3 days, both the magnitude and timing of the streamflow was forecasted with much certainty. Overall, forecasts with lower lead times of up to 7 days were able to better predict the timing and magnitude of the flood event.

The quantitative performance metrics demonstrating the skill of forecast streamflow at different lead times are shown in figure 4.8. To generate this figure, the inflow forecasts were first generated from July 17 to August 30, 2018, for 15 days beyond each date of generating forecast. For each day within the forecast period, forecasts from different lead times were grouped together. These forecasts, made by varying lead times, were treated as individual time-series. These forecast time series at varying lead times were compared against the nowcast inflow considering it as the baseline for the period when the flood peaked, 15th August to 21st August, 2018.

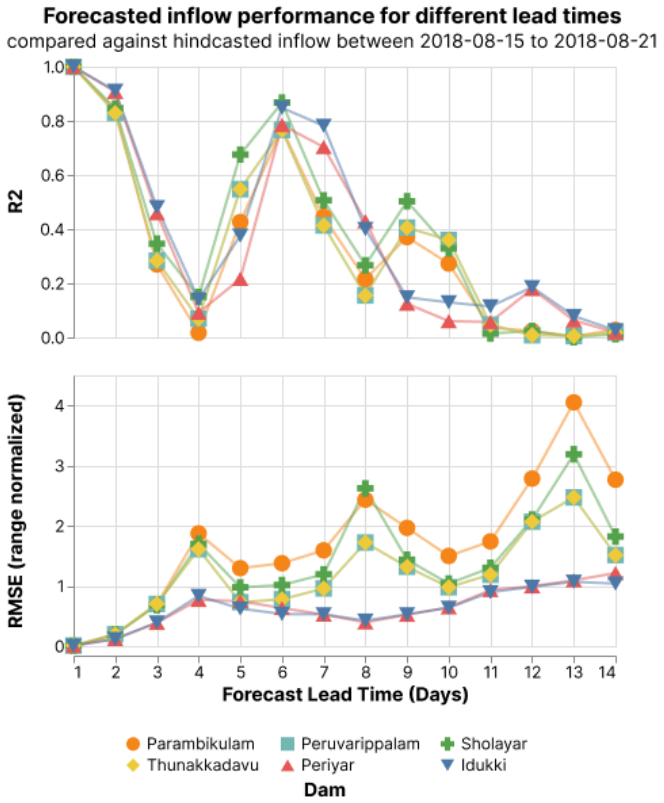

Figure 4.8 Performance metrics, R^2 and RMSE (range normalized), comparing the forecasted streamflow estimates at various lead times against nowcasted streamflow during the peak of the flood, between 15th-21st August 2018.

The R^2 values increase with decreasing lead times. The timing of the peak flood can be quantified at least a week in advance (Figure 4.8). The metrics denote the performance of forecast during the peak of the flood, from August 15 to August 21, across all the dams in the Greater Periyar basin. High R^2 and low RMSE values of the forecast for all dams a week prior to the peak flood underline the ability of CHIRPS-GEFS precipitation forecast to forecast floods in the mountainous regions.

The somewhat oscillating structure of the R^2 in figure 4.8 can be explained to some extent by the precipitation forecast patterns generated at different lead times. For instance, in figure 4.9, we can see that the forecasted precipitation for 15th August generated on 10th August to 12th August suggest that the Idukki basin would receive in excess of 100 mm rainfall, with gradual increase in intensity with decreasing lead time. However, the forecasts generated on August 12 and 14th predict a lower amount of precipitation over the basin as compared to the forecasts on previous days. Such a pattern is expected from Numerical Weather Prediction models as it tries to

solve for an ever changing dynamic system that evolves rapidly over the duration of a storm. Hence the change in forecasted precipitation amount over different lead times results in a similar pattern of modeled inflow to the reservoir.

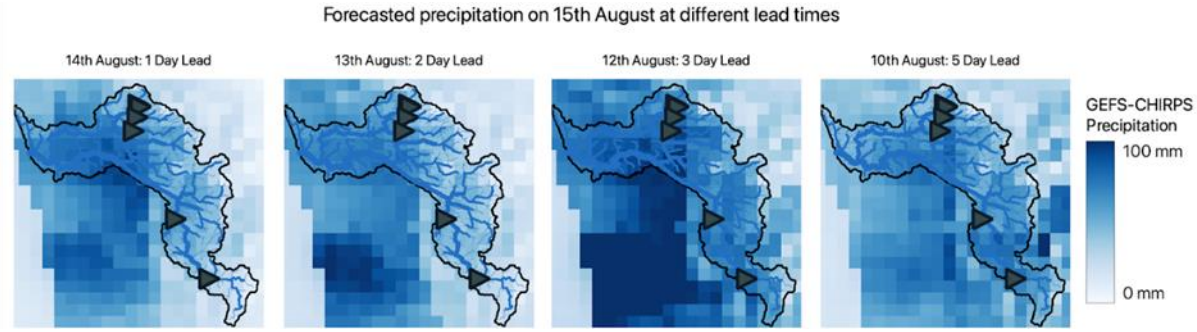

Figure 4.9 Precipitation forecast of 15th August generated at 1, 2, 3, and 5 day lead times.

4.4.3 Exploring actionable reservoir operations based on forecasts and range of scenarios

In this section, we explore the second objective of our study - to explore the range of actionable scenarios for dam operators that could have potentially minimized downstream flood risk of the Kerala 2018 floods with this forecast-informed reservoir operations scheme of RAT. However, before moving into reservoir operation scenarios, let us remind ourselves where the state of the art is in terms of quantitative precipitation forecasting which in turn represents the upper limit of reservoir flow forecasting. For example, the actual outflow from the Idukki reservoir was in the range of 1100-1460 (m3/s) during 15-17 August, 2018 and inflow was in the range of 1440-2000 (m3/s). The actual precipitation on 15th August, 2018 reported by the Indian Meteorological Department (IMD) was in the range of 170-270 mm. Compared to the observed rainfall, the forecasted precipitation over the region was barely above 100mm. The 2018 storm in Kerala was therefore an extreme rainfall event (~200 year return period), an event that the global numerical weather prediction modeling would be limited in capturing its finer physical features without further dynamic downscaling (see section 4.4.1).

Downstream flood risk is defined as the additional risk posed by uncontrolled release of water from a dam when the incoming volume of water during a flood exceeds that of the flood cushion capacity of the dam. In such cases, downstream inhabitants would experience high inflows at times that do not correspond to the natural timing of a flood if the dam was not there, as common intuition would dictate. This makes such floods even more dangerous due to the unpredictability

of the timing of flood for downstream inhabitants, making dissemination of information about dam releases especially important. For this, the reader should refer to the various scenarios defined in section 4.3.2 that a dam operator is likely to operate the dam by. Outflow scenarios are explored to reduce the flood risk by releasing water at a controlled rate, possibly lower than the rate of flow during the peak flood.

To maintain the water level at a target elevation, water is first withheld or stored until the target level is reached, and then released at a rate equal to the peak inflow flow rate of the flood. This scenario lets users simulate the outflow required to maintain a target water level. For instance, a target water level of 801m was simulated for the Sholayar reservoir, which is 10 m below its full water level (FWL) of 811m for dam safety. In this simulated case, water could be stored until August 19th based on the initial storage of the reservoir on August 10th 2018.

In case of storage change experienced by the reservoirs equaling to ±0.5%, ±2.5% and ±4.0% of the maximum storage capacity, the outflow from the reservoir at a constant rate is selected as a range of possible values deemed safe for downstream inhabitants. In all the simulated scenarios plotted in 4.10, the rate of outflow is lower than the peak flow rate of the flood entering the reservoir. The high volume of water incoming to the reservoir is compensated by releasing water proactively before the flood peak. The respective reservoir water levels are plotted alongside the corresponding scenarios in figure 4.10 and 4.11. This range of forecasted outflows and the corresponding water levels provide a range of possible reservoir operation scenarios for the reservoir operators to consider for minimizing the impact of the flood risk downstream.

The outflow from the dam based on inferred rule curve or historical reservoir operations varies on a case-by-case basis for the reservoirs. This is expected, as each dam and reservoir have unique flood routing and spillway capacity along with a unique bathymetry for storage. It simulates a baseline scenario of the forecast of reservoir states if dam operators operated the reservoirs in a 'business as usual' mode continuing the practice of previous years. For instance, if the Sholayar reservoir was operated according to how it had been operated historically, the water level would be higher by about 3 meters on average compared to the other storage change scenarios. Similarly, the reservoir operator can also simulate the corresponding outflow required and the water level using custom storage change values to simulate the reservoir state based on the expected storage change (figure 4.10 and 4.11).

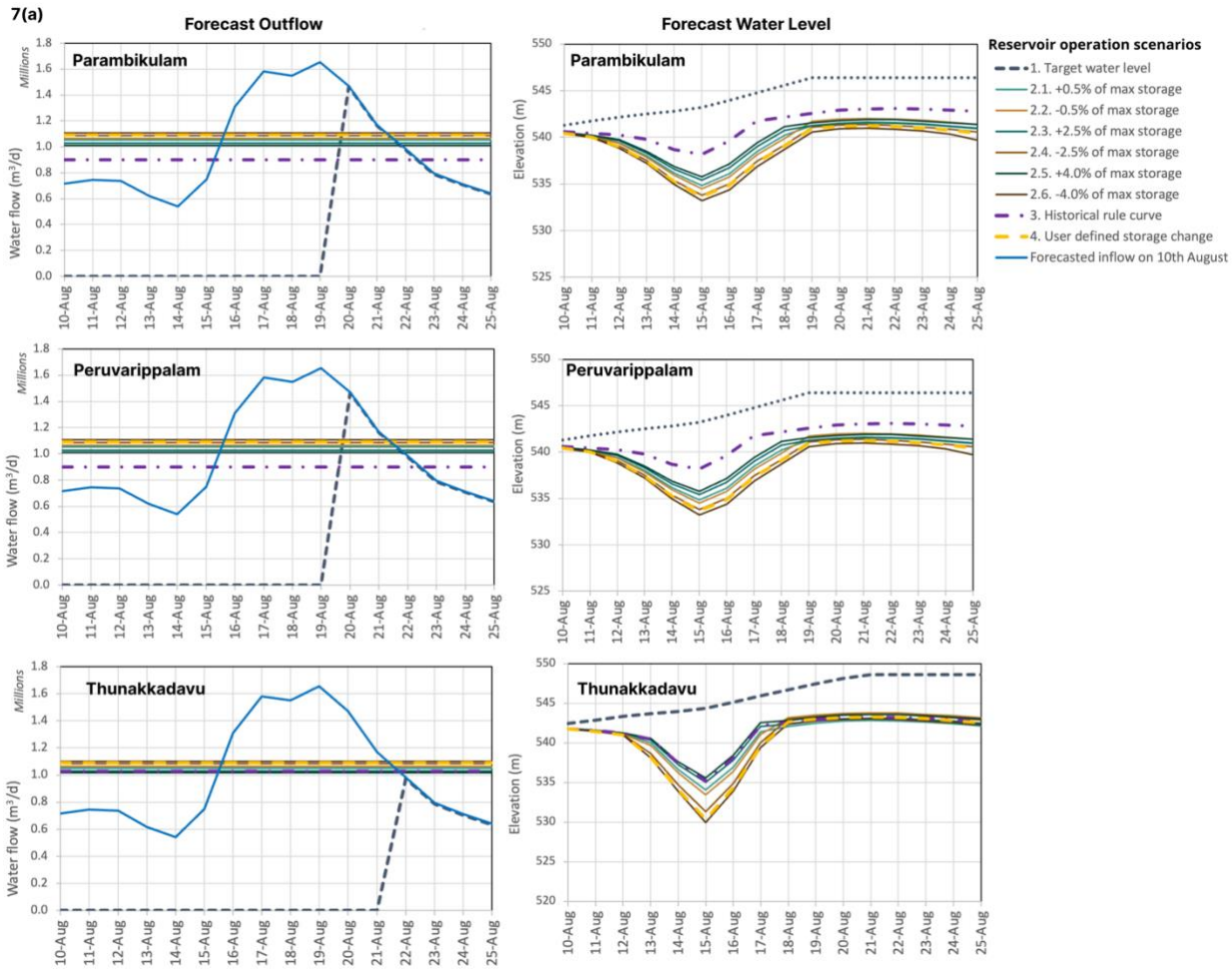

Figure 4.10 Forecasted outflow rates based on different scenarios and their respective forecasted water levels shown for Parambikulam, Peruvarippalam, and Thunakkadavu. Here the blue line on the left panel shows the forecasted inflow generated on day August 10. The idea here is to show how the various dam operator scenarios can potentially mitigate the forecasted inflow (assuming it retained the necessary skill as already seen with up to a 7 day lead time) and attenuate the flood wave with a lower magnitude and more controlled outflow for downstream inhabitants. For dam operating scenarios refer to section 4.3.2.

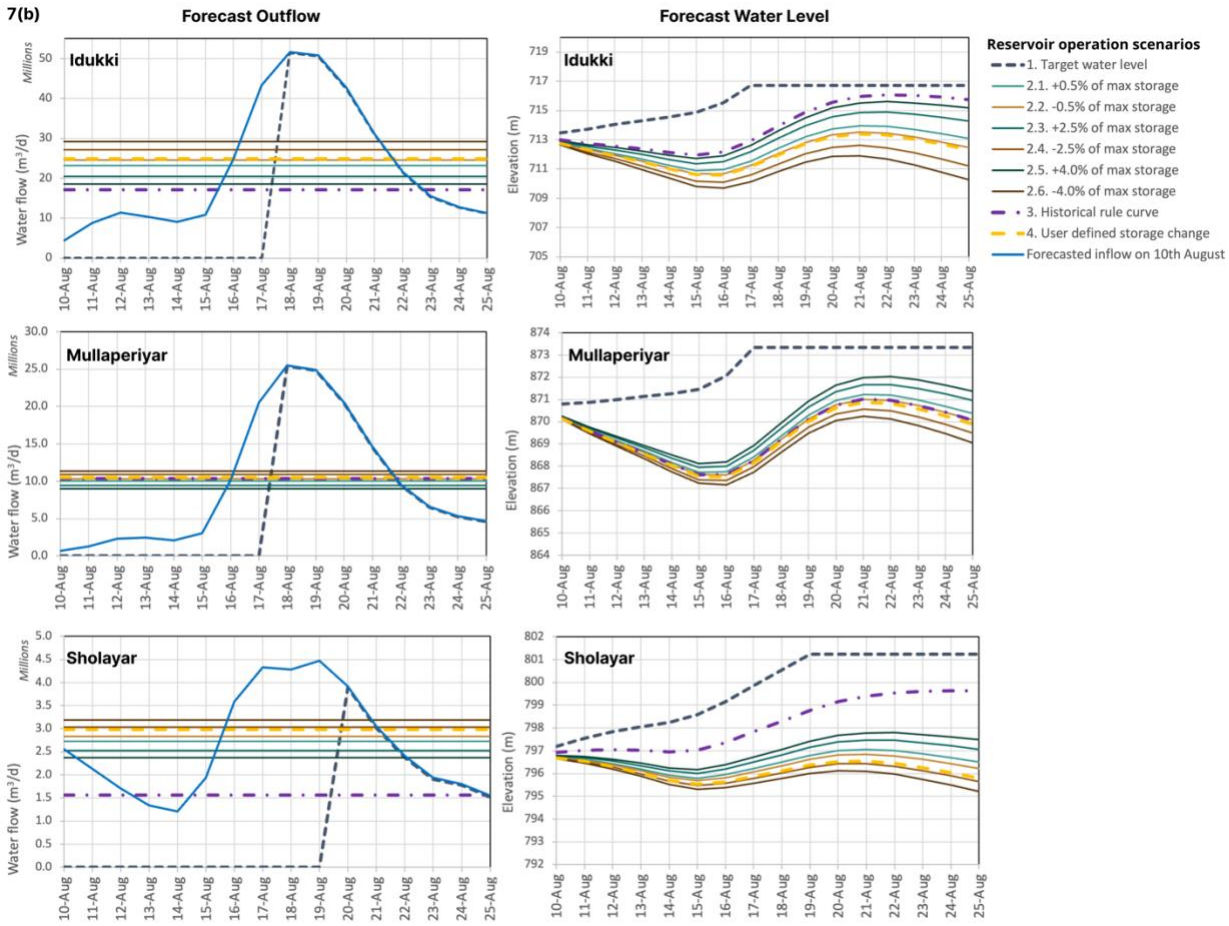

Figure 4.11 Same as figure 4.10 but for reservoirs Idukki, Mullaperiyar and Sholayar.

Based on the different reservoir operation scenarios the forecast of outflow from the reservoirs provide a range of possible forecast-informed reservoir operations scenarios to mitigate or minimize the downstream flood risk. These scenarios can help answer questions such as, (1) how much buffer time can be expected for a target water level to be reached? (2) how would the water level change for different release scenarios given the forecasted inflow? (3) compared to how the reservoirs were operated historically, how would the reservoir state differ based on the release scenarios? (4) could the reservoir operations be adapted to lower the risk posed by the flood?

As discussed in the previous section, the magnitude of the flood was underestimated by both the nowcast and forecasted streamflow but only with a systematic bias that could be removed operationally if needed. Moreover, the timing and the rate of increase in streamflow throughout the week were forecasted very skillfully at a lead time of 7 days (figure 4.4). Hence the outflow

forecasts in 4.10 and 4.11 are representative of the expected outflow for different operation scenarios given the forecasted streamflow, rather than being the "prediction" of the outflow from the reservoirs. Such forecasting of reservation state based solely on satellite observations and publicly available GEFS-CHIRPS data has value for the vast ungauged regions of the world where in-situ data is largely inaccessible.

4.4.4 Scalability of RAT-Forecasting: the recent August 2024 floods of Tripura and Southeastern Bangladesh

We set up a similar example of forecasting reservoir inflow and scenario-based outflow for the Northeastern region of Tripura (India) and Southeastern Bangladesh, wherein the issue of flood preparedness takes an international angle due to transboundary flow (figure 4.12). During August 21-27, 2024, floods that took place first in the upstream region of Tripura (in India) on the Gomti river basin, eventually travelled downstream to Bangladesh. With heavy precipitation, Southeastern Bangladesh was also flooded. The flooding and heavy precipitation in Tripura led to the opening of all gates of the Dumboor dam (India) due to it being at near full reservoir level prior to the flood. Using our RAT framework forced with satellite data and CHIRPS-GEFS, we obtained similar results and inference as we get for the 2018 floods in Kerala (see figure 4.13). Within a 3-day lead time, the intensity and timing of the peak flood is well predicted, and an indication of high inflow is obtained nearly a week prior. Readers can now access the real-time operational system for Tripura/Bangladesh at https://depts.washington.edu/saswe/tripura and for Kerala at https://depts.washington.edu/saswe/kerala.

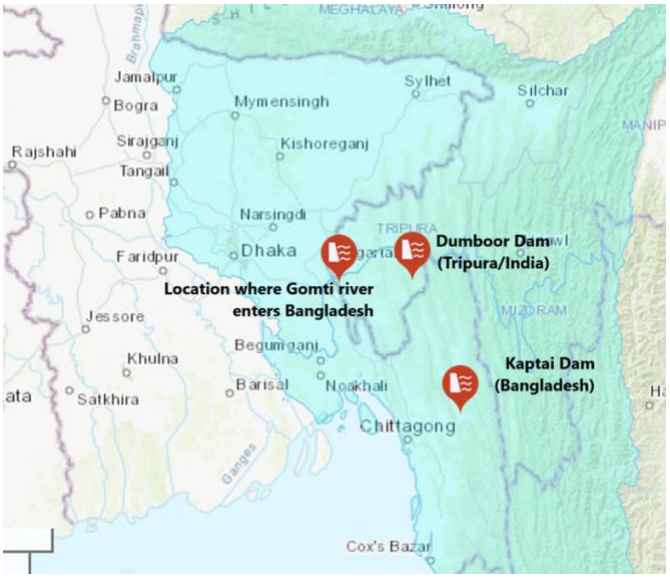

Figure 4.12 Scalability of RAT framework with a recent application in Northeastern state of Tripura and Southeastern Bangladesh to address reservoir operations and transboundary flood preparedness.

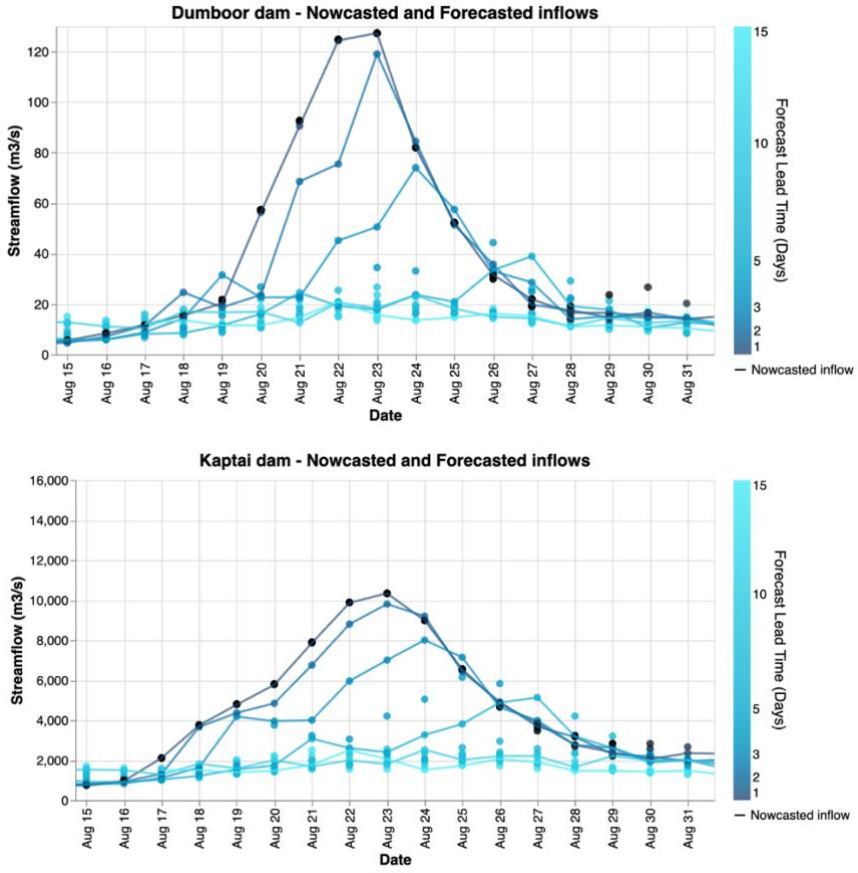

Figure 4.13 Inflow forecast to the Dumboor (Tripura, India) and Kaptai (Chittagong, Bangladesh) dams at various lead times (See previous figure for location of dams).

4.5 Discussion and Conclusions

Dams and reservoirs play an important role in mitigating risk of flooding for downstream inhabitants. However, reservoir operators often must balance the competing goals of hydropower production and flood control. This is especially challenging in mountainous regions where reservoir operations are optimized for hydropower generation but also need to address the mitigation of fast response extreme precipitation events. Reservoir operations based on static rule curves, designed based on seasonal inflow patterns often fail to handle rapidly evolving floods driven by climate-change of extreme precipitation events that occur at low exceedance probabilities. As mentioned earlier, the 2018 floods in Kerala, an out-of-season extreme precipitation event left the reservoir operators with limited options for flood mitigation. Hence, it is crucial that such events are forecast, and the forecasts applied to generate guidance for forecast-informed reservoir operations to mitigate potential damages downstream.

In this study, we investigated the ability of a gauge corrected precipitation forecast product, the CHIRPS-GEFS, in forecasting the inflow during the extreme precipitation event of 2018 in Kerala. We explored a range of actionable scenarios for dam operators that could potentially minimize downstream flood risk with this forecast-informed reservoir operations scheme of RAT. For the extreme flood experienced by Kerala in August 2018, the magnitude of the flood peak was not captured with sufficient accuracy. However, the timing of the flood peak and the rate of increasing flow was forecasted quite well with a week's notice using forecasted precipitation from GEFS-CHIRPS. Moreover, the performance in forecasting the timeliness of the flood increased at shorter lead times, although the performance was found to vary from each reservoir. Our exploration of the range of actionable scenarios of reservoir operations based on inflow forecasts within the satellite-based RAT framework revealed that for most cases, the reservoir operator could have made proactive decisions related to reservoir operations to potentially mitigate the flood.

The forecasting module developed for RAT and investigated in this study using the Kerala 2018 floods as a case study (and also for Northeastern region of Tripura, India and Southeastern Bangladesh) demonstrates its promise for application in similar regions and extreme precipitation environments around the world. In that spirit of empowering dam operators and managers of regulated river basins of the world, we have made the forecast module an integral part of the RAT

3.0 software package. Interested readers should visit www.satellitedams.net and https://github.com/UW-SASWE/RAT to access this version of RAT along with its documentation on http://ratdocs.io for implementing RAT 3.0 in forecast mode using GEFS-CHIRPS at a river basin of their interest. Given that RAT is a publicly available, open-source and open-science reservoir tracking software package (Minocha et al. 2023), it is our hope that forecast-informed reservoir operations within a satellite-based tracking framework will improve flood management in regulated river basins where in-situ data or public access to information is scarce.

In closing, the key innovation to the body of knowledge in our opinion is the advancement on the use of weather forecasting for reservoir operations in developing regions of the world that are mountainous with high precipitation (shown in figure 4.14). These are the regions where satellite data are often the only viable alternative (and hence the use of RAT as the reservoir tracking tool; Minocha et al. 2023), as demonstrated through a scalable application in the Indian region of Tripura and Southeastern Bangladesh.

In this chapter, we added the capability to forecast reservoir inflow and outflows in the RAT framework. In the next chapter, we continue to assess the accuracy of reservoir storage change estimation in the hindcast timeframe using the recently launched SWOT satellite.

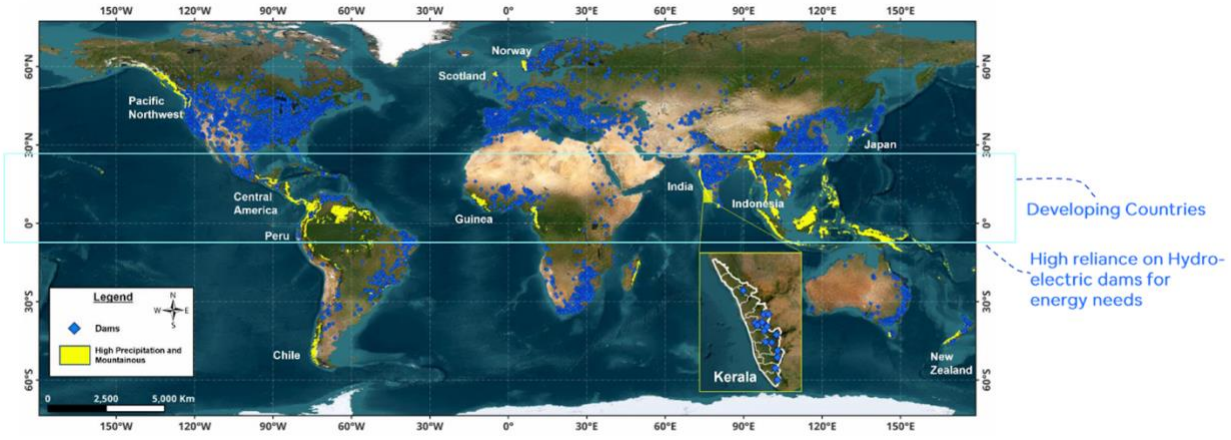

Figure 4.14 Map showing high precipitation and mountainous regions around the world where this study will be applicable.

Chapter 5. Multi-satellite Tracking of Surface Water Storage Change in the Era of Surface Water and Ocean Topography (SWOT) Satellite Mission

***Note**: This chapter has been adapted from an article submitted to the special edition of the Earth and Space Science journal: Science from the Surface Water and Ocean Topography Mission.*

Das, P., and Hossain, F. (2025). Multi-satellite Tracking of Surface Water Storage Change in the Era of Surface Water and Ocean Topography (SWOT) Satellite Mission. *Earth and Space Science: Science from the Surface Water and Ocean Topography Mission*.

Key Points:

- SWOT is very skillful in measuring water surface elevation of reservoirs as validated by in-situ observations from over 100 reservoirs around the world.
- The accuracy of storage estimates by SWOT elevation data is highly dependent on the accuracy of the Area-Elevation-Volume curve of reservoir.
- Integrating SWOT with other satellite data to improve frequency of reservoir storage estimation currently presents challenges and requires further development.

Abstract: The Surface Water and Ocean Topography (SWOT) satellite, launched in December 2022, represents a significant advancement in the remote sensing of global water bodies, providing simultaneous measurements of water surface elevation and extent in all-weather conditions. This study evaluates SWOT's capability to estimate reservoir storage dynamics in comparison to pre-SWOT methods. SWOT demonstrates high accuracy in measuring water surface elevation, achieving a median R2 close to 1 and root mean square errors (RMSE) nearly an order of magnitude lower compared to earlier non-SWOT approaches. SWOT offers substantial improvement over single-sensor and multi-sensor methods, due to spatial averaging of distributed elevation measurements, which was further validated by similar measurements of the ICESat-2 satellite. The key limiting factor in estimating storage from elevation measuring sensors was found to be the accuracy of Area-Elevation-Volume (AEV) curve. Furthermore, preliminary applications of machine learning to integrate SWOT with non-SWOT datasets show promise, although constrained by limited data availability of SWOT as of late 2024.

5.1 INTRODUCTION

The previous three chapters dealt with building a framework for estimating reservoir operations in the past and short-term future, as well as estimating the resulting regulation of streamflow. The key variable that dictates the accuracy of all the estimates is the storage change of reservoirs. While estimating storage change using traditional satellite sensors have their limitations that have been studied extensively, the recently launched SWOT satellite, with its simultaneous area and elevation measuring sensor promises to drastically improve the accuracy of estimation of surface water dynamics. In this chapter, we test the accuracy with which SWOT is able to estimate the storage change of reservoirs.

Freshwater lakes and reservoirs are an important store of water for human use. These water bodies store nearly 9% of all the freshwater on the surface of the planet (Abbott et al., 2019). There are over a million natural lakes, and over 62,000 reservoirs globally (ICOLD CIGB, 2023). Even though human-managed reservoirs account for only a tenth of the total water stored within lakes and reservoirs, they contribute to a staggering 57% of the seasonal storage variability (Cooley et al., 2021). These fully human-operated reservoirs play a very important role in the overall hydrological system of a basin, including downstream water availability, water quality and flood safety (Darkwah et al., 2024; Suresh et al., 2024). It is hence crucial to monitor how these surface water bodies, both artificial and natural lakes, evolve over time. However, in practice, the sheer number of these water bodies spread across the world makes this task very challenging (Figure

5.1).

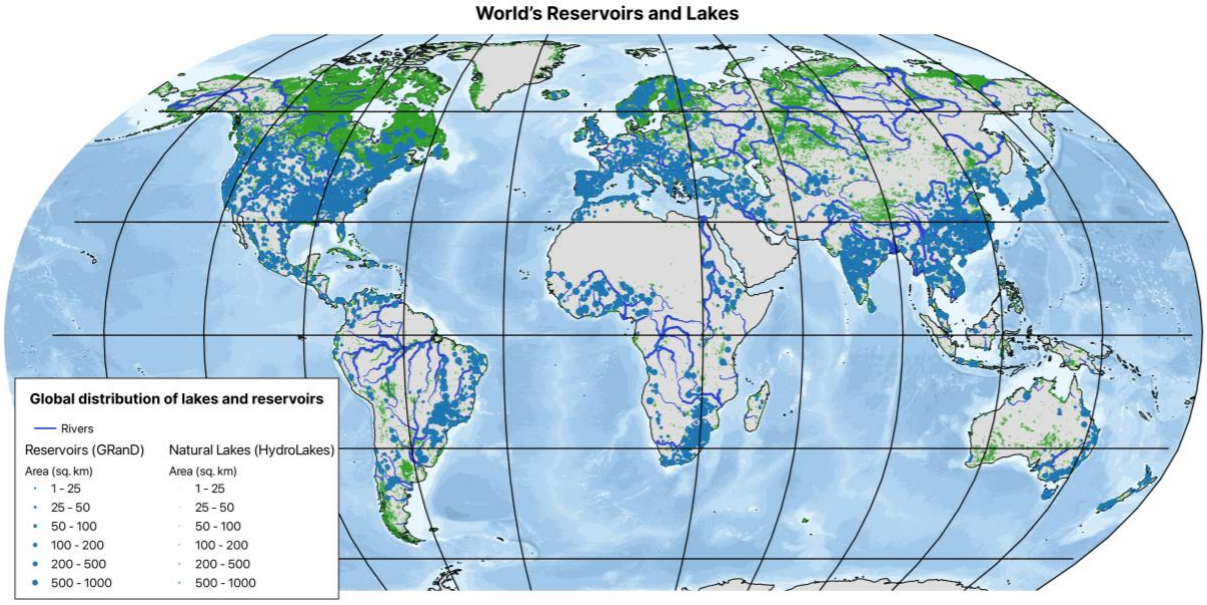

Figure 5.1 Global map of lakes (green) and reservoirs (blue) and current estimates of storage trends over the last three decades. Spatial distribution of 7320 reservoirs (Lehner et al., 2011) and nearly 183,300 natural lakes (Messager et al., 2016) represented as points.

Due to the sheer number of lakes and reservoirs around the world, remote sensing-based Earth Observation (EO) from space has been the only viable way to study these inland surface water bodies extensively. For instance, Pekel et al., (2016) used multi-decadal Landsat observations to identify inland water bodies at a global scale from 1980s to 2015. The resulting dataset has seen many uses across and has been instrumental in improving our understanding of inland surface water, such as an increase in flood risk and rapid changes in river morphology (Tellman et al., 2021; Wu et al., 2011). Yao et al. (2023) have reported a significant decline in the storage of more than half of all the natural lakes observed using satellites, over a period of three decades.

In contrast to natural lakes, reservoirs are formed by man-made inundation of previously dry land when a dam is constructed on a river. Reservoirs are of special importance because they are completely managed by humans. In the 21st century, reservoirs in the hydrological cycle cannot be ignored while accounting for the hydrological budget of a basin (Abbott et al., 2019; Das et al., 2024). Hence, their impact on the environment warrants more scrutiny so that we can manage them more sustainably and equitably, especially in a changing climate. Specifically, the

amount of water stored and its change over time is critical for understanding the key role played by reservoirs in the global water budget, ecosystem, and regional water management.

For storage change estimation of reservoirs using remote sensing-based EO, either the change in water surface area or the elevation of the reservoir needs to be estimated. Altimetry satellites are equipped with a radar or LiDAR sensor that can measure the elevation change of the reservoir water surface down to a few centimeters (Abdalla et al., 2021). On the other hand, Optical and Synthetic Aperture Radar (SAR) sensor based satellites can measure the area of the reservoir by mapping the lake extent, usually up to a typical pixel size of 30m×30m for Landsat (optical) or 10m×10m for Sentinel-1 (SAR) missions (Torres et al., 2012). Due to the higher measurement precision of the altimeter sensors, even small changes in water surface elevation can be detected at centimeter-scale, while for area measuring sensors, the change in surface area needs to be relatively larger in magnitude in order to be detected with sufficient skill. Especially for mountainous reservoirs with steep bathymetry, where the area of the reservoir does not change as significantly with storage change, it is more challenging to accurately estimate the storage change using area-measuring sensors. Hence, estimates of reservoir storage change by altimetry satellites are usually more accurate as compared to the area measuring satellites (Biswas et al., 2019; Okeowo et al., 2017)

However, the higher vertical resolution comes at the cost of lower spatial coverage and temporal frequency for satellite radar altimeters. Most reservoirs are not observed by these elevation measuring sensors. Satellites with optical sensors on the other hand have more spatial coverage of the world's water bodies. For these sensors, the presence of clouds can severely limit its ability to make a valid observation of the water surface. Moreover, the ability to resolve storage change of reservoirs is limited by how much the area or elevation changes as a result. Thus, it is challenging for optical sensors to resolve small amounts of storage change accurately in mountainous terrain and in presence of clouds. Even with these limitations, the value of optically sensed reservoir observations lies in global spatial coverage afforded by multiple satellite missions. These satellite missions also have a long history such as the Landsat mission with an observational record since the 1980s. MODIS and VIIRS take daily observations, and have been utilized for tracking reservoir storage change of large reservoirs at a weekly frequency (Y. Li et al., 2021; Shah et al., 2024).

Similarly, SAR satellite sensors can also be used to track the change in the area of the reservoir. SAR uses microwave energy and hence is unaffected by the presence of clouds. However, partially inundated vegetation and wind driven surface waves can increase the surface roughness and make it difficult to distinguish the water surface from its surroundings. Moreover, terrain shadows can also result in lower accuracy of water classification in SAR images. Even with these above-mentioned limitations of estimating reservoir storage change using satellite observations, they have been successfully utilized, especially since SAR estimates the trends in storage change of reservoirs more accurately owing to their cloud-penetrating ability (Chang et al., 2023; Das et al., 2022).

It is widely recognized that the utility of remote sensing observations increases many folds when multiple independent sources are combined (Huffman et al., 2007, 2020; Jones, J. W. and Shiroma, G. H. X., 2023; Jung, J., 2023). The cloud-penetrating nature of SAR sensors and the long heritage of optical imagery naturally complement each other. By combining both these sources of data using a tiered set of logical operations, the Tiered Multi-Sensor – Optical/SAR (TMS-OS) algorithm was first introduced by Das et al., (2022). Using this TMS-OS in the backend of the open-source Reservoir Assessment Tool (RAT) framework (Biswas et al., 2019; Das et al., 2022; Minocha et al., 2023), a more robust and frequent record of reservoir storage change has been obtained for river basins across the world, such as the Columbia, Nile, Tigris-Euphrates, Mekong, Indus and Kerala (Darkwah et al., 2024; Das et al., 2022; Eldardiry and Hossain, 2019; Hossain et al., 2023; Suresh et al., 2024).

Prior to 2022, the available record of satellite remote sensing observations for reservoir storage change tracking were from satellites that either measure the surface area, or the elevation of the reservoir, and at disparate times of sampling. Optical or SAR sensor based satellites measure only the area, while altimetry satellites measure elevation, but the observations rarely coincide in time. However, the recently launched Surface Water and Ocean Topography Mission (SWOT) satellite mission can measure both the area and water surface elevation of the reservoir simultaneously (Alsdorf et al., 2007; Biancamaria et al., 2016). Similar to SAR sensors, SWOT is able to take measurements in all-weather conditions. Due to its simultaneous ability to measure water surface extent and elevation, and its near global coverage, SWOT is expected to significantly improve the state-of-the-art of tracking of storage change of inland water bodies in this new era. Prior to the launch of the SWOT mission, the scientific community has had to work around the

lack of simultaneous measurements of water extent and elevation by combining various non-SWOT sensors that can estimate water extent (e.g., Landsat, MODIS and Sentinel 2, SAR Sentinel-1) with sensors that can estimate water elevation (e.g. altimeters of the Jason series) or apply remotely-sensed bathymetry of reservoirs (e.g. using digital elevation data from Shuttle Radar Topography Mission – SRTM) to derive storage changes (Bonnema et al., 2016). Naturally the results that have been reported on storage change in this "jury-rigged" fashion during the pre-SWOT era is subject to high uncertainty and the representativeness in capturing the human regulation of our Earth's surface water has remained questionable. Now that SWOT has been acquiring observations for almost two years, we ask the following overarching research question: *How well is the SWOT satellite able to estimate reservoir storage, compared to the pre-existing methods of satellite-based storage change estimation?*

The specific research questions we aimed to answer are as follows: (1) How accurate are SWOT based estimates of reservoir storage dynamics? (2) How does SWOT compare to existing established methods that use non-SWOT satellites? (3) What are the factors that affect the ability of SWOT to accurately capture reservoir storage dynamics? And finally, (4) can non-SWOT satellites be calibrated to SWOT to develop a SWOT-charged multi-sensor technique for estimating reservoir storage?

5.2 Study Area and Data

5.2.1 Study area and in-situ data

Given the wide range of variability, it is important to have a dataset of in-situ observations that is widely representative of a diverse range of reservoir characteristics for validation of any global reservoir storage change algorithm or remote sensing sensor. In this study, we therefore built a quality controlled dataset of in-situ reservoir dynamics and static characteristics of 245 reservoirs (Figure 5.2). The reservoir data, comprising water level and storage were obtained from the Royal Irrigation Department, Thailand (RID, 2024), the US Bureau of Reclamation (Bureau of Reclamation, n.d.), Steyaert et al., (2022), and Donchyts et al., (2022). Observations were obtained during the period of observation by the SWOT satellite – post July 2023 to October 2024. The static characteristics, including the reservoir capacity, geometry, location, and primary use, were obtained from the Global Reservoir and Dam Database (GRanD) (Lehner et al., 2011).

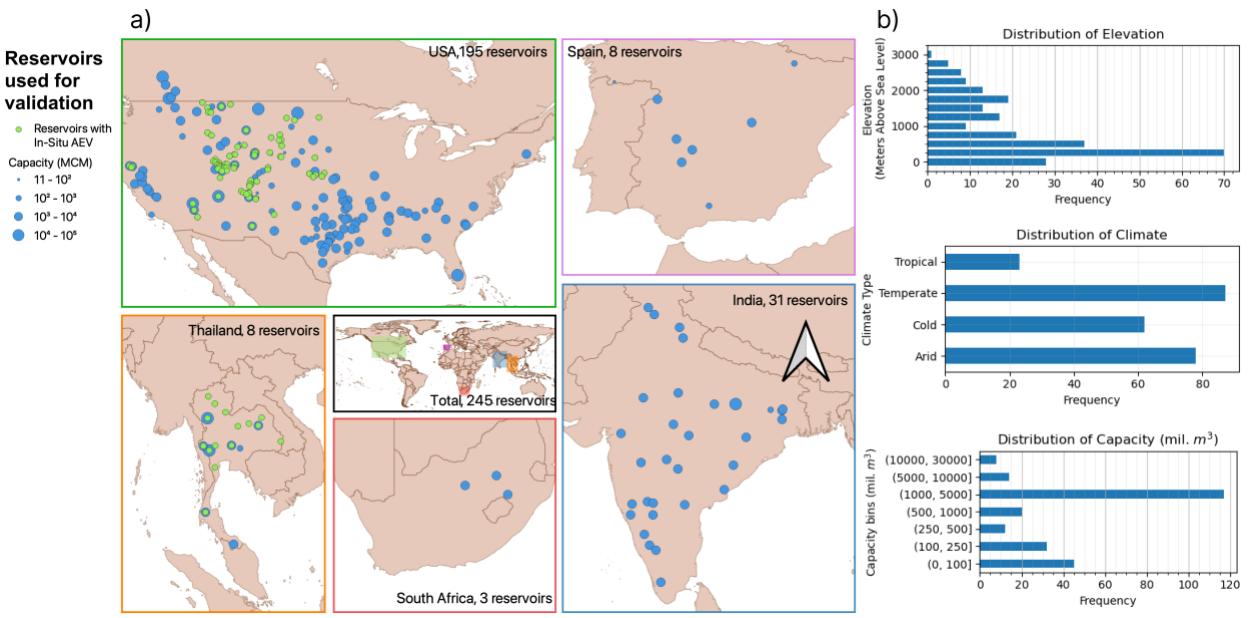

Figure 5.2 (a) Map of reservoirs with in-situ data used for validating the satellite-based storage estimates. In-situ data from 5 different regions across the world were obtained – United States, Spain, India, South Africa and Thailand. (b) Distribution of capacity, major climate and bottom elevation of reservoirs used for validation.

The 245 reservoirs were sampled across five distinct regions with varying ecological, climatological and physical characteristics (Figure 5.2(b)). Capacities of the reservoirs varied from 11 million m^3 to above 30,000 million m^3 (or 30 km^3). The reservoirs are mostly situated in arid and cold climatic conditions, which stretch across the central and northern parts of the United States. On the other hand, the reservoirs in Thailand experience a tropical climate, with hot temperatures and high humidity all year round. The reservoirs are also situated at varied elevations, with most reservoirs clustered around 200 m and 1800 m above mean sea level. Reservoirs at higher elevations would likely also be surrounded by steep mountains and hence are more challenging for area estimating satellites to consistently measure surface area changes.

5.2.2 Establishing the baseline of non-SWOT reservoir storage estimation

The idea of a baseline is to reference the performance of SWOT based methods relative to the pre-existing methods (see research questions 1 and 2 of section 5.1) and quantify the benefit SWOT brings to the table. To define an acceptable baseline a non-SWOT (or pre-SWOT) method, the following three non-SWOT methods were first compared to each other– TMS-OS (Das et al., 2022), Global Reservoir Storage (GRS; Li et al., (2023)) and Global Lake Water Storage (GLWS;

Yao et al., (2023a)). The GLWS dataset consists of lake surface area, storage, and water level time-series for large lakes and reservoirs from 1992 to 2020 at a monthly frequency. Similarly, the GRS dataset also estimates reservoir storage globally from 1999 to 2018 at a monthly frequency. Globally, these datasets map 1972 and 7245 reservoirs respectively. The TMS-OS method is a globally scalable and open-source algorithm to obtain reservoir area and storage using a constellation of satellites as opposed to relying on a single sensor. It leverages SAR sensor's better ability to estimate trends in change of water surface area over time, and the higher accuracy of optical sensors during clear conditions to obtain a combined time-series that is more accurate than its parts. Using four satellites at once, TMS-OS is able to estimate reservoir storage dynamics at a frequency of 1-5 days.

The estimated area by the three satellite based reservoir storage methods were used to estimate the storage of reservoirs and compared against in-situ observations at a monthly frequency. The estimates by TMS-OS were also resampled to a monthly frequency for comparison with GLWS and GRS storage estimates. The availability of range of time for which data is available in these datasets is shown in Figure 5.3. While GLWS and GRS timeseries have a longer period of data availability, they end by 2020 and 2018, respectively. The SWOT satellite started taking observations in its "science orbit" phase in July of 2023. Since neither GLWS, nor GRS had any corresponding data, they could not be directly compared with SWOT. TMS-OS had estimates since 2019 – a 6 year long record of reservoir storage dynamics, which is sufficiently long for establishing a performance benchmark for the pre-SWOT era. We compared SWOT with TMS-OS with overlapping samples during the period of operation of SWOT since July 2023. The results of this comparison are provided in section 5.4.2.

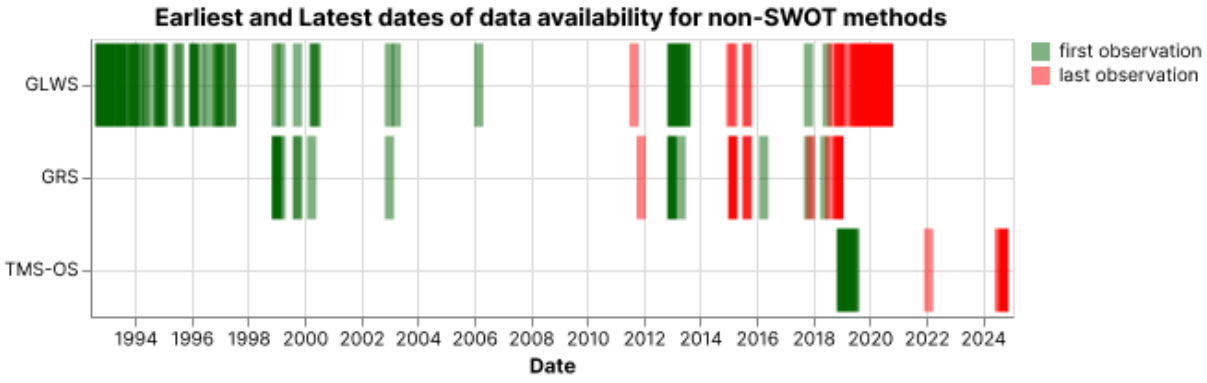

Figure 5.3 Range of dates for which data is available for various non-SWOT based methods. GRS ends in December of 2018, while GLWS usually contains records until December of 2020. The

start date of TMS-OS record corresponds to the beginning of Sentinel-2's observational record, from 2019.

5.2.3 TMS-OS – Multi-sensor water area estimating method

We used the ortho-rectified and ground range detected C-band SAR observations from Sentinel-1, which provides radar returns at a 12-day frequency. Additionally, we use surface reflectance observations by the Landsat 8, Landsat 9 and Sentinel-2 A/B satellites. Combined, these four satellites with optical sensors can take repeat observations every 5 days or less, providing temporally dense observations at a relevant time-scale of reservoir operations (within a week). For more information on how TMS-OS works, the reader is referred to Das et al., (2022). The strengths and weaknesses of each sensor type are discussed in detail in the introduction section. The datasets and satellite sensors used in this study are summarized in Table 1.

5.2.4 Estimating Water Surface Elevation and Storage from SWOT

We used the SWOT Level 2 Water Mask Raster (SWOT, 2024b) image product at a 100m spatial resolution which measures both the elevation and extent of a water body. It is generated by the Ka-band Radar Interferometer (KaRIn) sensor. The KaRIn sensor works on the principle of SAR interferometry, and hence is unaffected by cloud cover. It operates in a region of 10-60 km on either side of nadir, with a combined swath of 100km. The repeat period of the satellite is 21 days near the equator and reduces pole-wards. The KaRIn sensor's wide-swath allows it to measure water surface elevation over a surface, instead of point measurements taken by previous altimeters. This drastically increases the number of Earth's water bodies whose water elevation can be observed from space, unlike previous altimeters which had to pass directly over a water body to make a valid observation (Biancamaria et al., 2016).

We also use the SWOT Level 2 Nadir Altimeter (SWOT, 2024a) Geophysical Data Record (GDR) processed from SWOT's Poseidon-3 Nadir altimeter. This Jason-class altimeter is similar to the nadir altimeters aboard the Jason-3 and Sentinel-6 satellites, which have a long history of measuring water surface elevation at cm-scale accuracy (Abdalla et al., 2021). While all of these sensors can only measure the elevation of the water surface directly under the satellite, they have a proven record of measuring water surface elevation reliably for inland water bodies (Okeowo et al., 2017). The data processing methodology is discussed in-depth in section 5.3.2.

Table 5.1 Summary of satellite data products used in the study.

Satellite Data Product	Temporal and Spatial Resolution	Sensor type
SWOT L2 Water Mask Raster Image (v2.0)	21 days; 100m	SAR Interferometry (KaRIn)
SWOT L2 Nadir Altimeter GDR	21 days; minimum 300m intersection with water body	Radar altimetry (Poseidon-3C nadir Altimeter)
Sentinel-1 C-band SAR GRD	12 days; 10m	Synthetic Aperture Radar (SAR)
Landsat 8 Surface Reflectance	16 days; 30m	Optical (Operational Land Imager, OLI)
Landsat 9 Surface Reflectance	16 days; 30m	Optical (Operational Land Imager-2, OLI-2)
Sentinel 2 A/B Surface Reflectance	5 days; 20m	Optical (Multispectral Instrument, MSI)

5.3 METHODS

5.3.1 Area Elevation Volume Curve and Reservoir Storage

The storage, or the volume of the water in a reservoir was estimated using the Area-Elevation-Volume (AEV) curve as illustrated in Figure 5.4. The AEV curves were generated by extending the Area-Elevation Curve (AEC) generation method by Das et al., (2022). The AEC was derived from the Shuttle Radar Topography Mission (SRTM) DEM by calculating the area corresponding to elevations at each 1 m interval within a small region surrounding the reservoir. The resulting curve represents the relationship between area and elevation of the portion of the reservoir bathymetry that was exposed during February 2001, when the SRTM observations were taken. For reservoirs built after February 2001, SRTM can capture the full bathymetry from the reservoir bottom to yield a complete AEV. For reservoirs built prior to 2001, the AEC generation method was extended by adding the lower limit of the AEC, corresponding to zero storage.

The lower limit of the AEC corresponds to the lowest elevation in the reservoir which was estimated as the elevation of the riverbank immediately downstream of the reservoir. The Global River Width from Landsat (GRWL) (Allen and Pavelsky, 2018) river centerlines and the Merit dem (Yamazaki et al., 2017) were used to obtain the elevation along the river at the downstream river. For some smaller reservoirs in the upper reaches of their basins where GRWL river centerlines may be missing, the 1st percentile value within a 500m region around the dam location was considered as the elevation of the reservoir bottom.

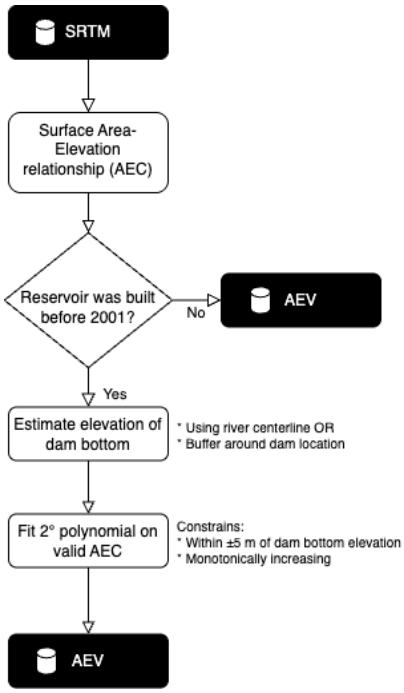

Figure 5.4 Flowchart showing methodology for generating the Area-Elevation-Volume (AEV) from SRTM DEM.

A second-degree polynomial, constrained to an intercept near the estimated bottom elevation, was then fitted to the SRTM-derived AEC. To refine the fit, the AEC was truncated above the observed SRTM water level and below the maximum possible water level, calculated as the dam height plus the estimated bottom elevation. The rest of the AEV was generated by integrating the AEC at 1m intervals. Using the AEV curve, the storage was obtained using the area and elevation estimates from the methods tested in the study. The accuracy of the AEV was assessed using available in-situ observations which are presented in section 5.4.1.

5.3.2 Reservoir Storage Estimation using SWOT

First, the water surface elevation is estimated from SWOT observations as illustrated in Figure 5.5. The Ka-band Radar Interferometer (KaRIn) estimates the elevation over a surface as a point-cloud. The level 2 (version 2.0) water raster elevation product aggregates these point-cloud measurements to estimate the elevation at a resolution of 100m by 100m. However, currently, the water classification algorithm of the new KaRIN sensor misclassifies water pixels often, resulting in high uncertainty estimates of water elevation. Hence, further processing was required to obtain reliable elevations. The water elevations with high uncertainty (>100 cm) are masked out, based on the nominal accuracy of altimeters. If the interquartile range (IQR) of the elevation values of the remaining pixels is high (>50 cm), the observation is discarded. The rationale being that a high IQR suggests that the particular overpass had high uncertainty. Such a condition may occur due to bad viewing geometry over a reservoir such as at the edge of a reservoir and partial coverage of the reservoir. In such cases the observation may not be useful and has to be discarded. The water surface elevation was estimated as the median value of the pixels remaining after the filtering steps.

Observations from the Jason-class Poseidon sensor – the other altimeter aboard SWOT – were processed using the Okeowo et al., (2017) method which uses unsupervised learning to estimate water surface elevation very accurately. However, this sensor may have sparse samples over in-land reservoirs, as it is designed primarily for applications over oceans. Hence, whenever available, the water surface elevation estimated using the Poseidon sensor was also used in tandem.

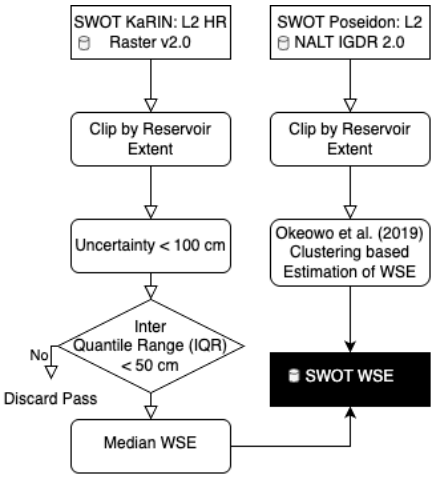

Figure 5.5 Flowchart for obtaining Water Surface Elevation (WSE) from SWOT.

5.3.3 Integration of SWOT in a Multi-satellite Sensor framework for estimating Storage

To fully leverage the ability of SWOT to better estimate the water surface elevation, we explored integration of observations from other satellites. An integrated fleet of satellites for reservoir storage tracking can have many benefits. The higher fidelity of the SWOT satellite can guide the lower-fidelity higher frequency observations by non-SWOT satellites just as we have experienced in the case of multi-sensor precipitation estimation, such as the IMERG data product (Huffman et al., 2020). If one satellite fails to take a valid observation, say due to cloud cover, it could be corrected using other temporally proximate observations. Overall, by using a teamwork of satellites, the combined ability of the sensors to resolve reservoir operation dynamics can become more accurate and frequent.

To integrate SWOT with non-SWOT satellites, we employed two methods. First, using Machine Learning (ML) techniques to transfer the skill of the SWOT satellite to non-SWOT satellites. ML methods have been used skillfully to improve the signal to noise ratio in time-series data (Basu and Meckesheimer, 2007). We employed a Random Forest (RF) model to calibrate non-SWOT observations to SWOT-based storages. We used non-SWOT satellite data, reservoir specific variables such as climate, irregularity (Area/Perimeter) and surrounding topographical slope to train against SWOT based reservoir storage estimates. Using this model, non-SWOT data could be calibrated to SWOT-like storage estimates.

Second, we used a TMS approach (from TMS-OS) with SWOT as the calibration sensor. We used observations by the SWOT satellite to filter and correct the trends of non-SWOT satellite observations. Similar to the filtering and trend correction done by the SAR sensor in the TMS-OS algorithm. In both approaches, observations by several non-SWOT satellites were taken - Sentinel-2, Landsat-8, Landsat-9 (optical sensors) and Sentinel-1 (SAR). The lessons learned from attempts at integrating non-SWOT observations with SWOT observations are presented in section 5.4.5.

5.4 Results and Discussion

5.4.1 Reliability of Satellite-based Area-Elevation Volume (AEV) curve

The performance of satellite-derived AEV using the method described in section 5.3.1 was compared with in-situ derived AEV to establish reliability of the AEV generation method in terms

of global scalability to the 245 reservoirs. Based on the availability of in-situ elevation and storage values of 98 reservoirs, the in-situ AEV was generated and compared in figure 5.6. The location of these reservoirs is shown as green circles in the map of validation sites in figure 5.2.

The derived Elevation-Storage relationship of these reservoirs yielded a median R^2 value of 0.9 and RMSE of 31.18 million m^3. This suggests that the satellite based method to obtain the AEV, using method to estimate reservoir bottom and complete the AEC, captures the trends of the Elevation-Storage relationship well. While the RMSE can occasionally rise above 500 million m3, seen as outliers in Figure 5.6, for the vast majority of cases, about 75%, the estimated storage is accurate to within 100 mil. m^3. Hence, these AEV curves were used throughout this study to estimate and compare storage of reservoirs, where previously only storage change could be compared due to a lack of information on the lower limit of the AEV.

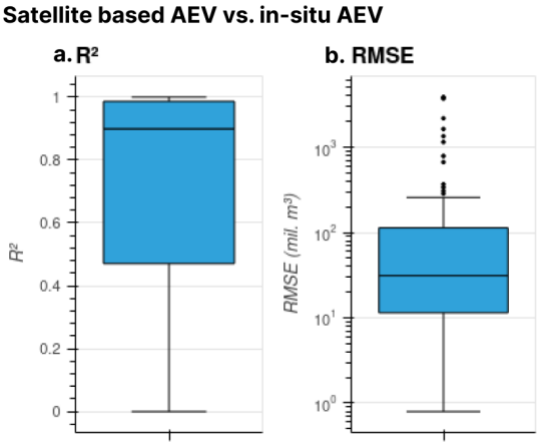

Figure 5.6 Performance of satellite-based Area-Elevation-Volume (AEV) curve compared to in-situ AEV.

5.4.2 Baseline performance of non-SWOT satellite-based reservoir storage tracking

The performance of estimation of monthly reservoir storage in the pre-SWOT era are represented by the R^2 and RMSE in Figure 5.7. R^2 is a measure of how well the method is able to explain the variance in the observed storage, while the RMSE represents the overall error in the estimated and observed values. Although GLWS is able to explain the trends in storage, the actual estimated storage has the highest error among all the three potential baseline methods, at 600 mil. m^3. On the other hand, TMS-OS and GRS have RMSE of around 40 and 50 mil. m^3, respectively.

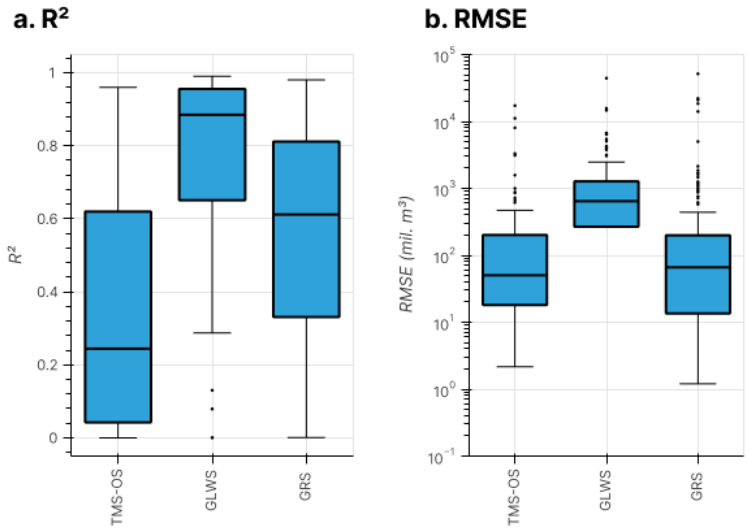

Figure 5.7 Baseline performance of three non-SWOT (pre-SWOT) techniques for estimating reservoir storage. The edges of the box show the 25th and 75th percentiles of the distribution. The horizontal line inside the box represents the median and the vertical line capped by horizontal lines represents the 1.5X the interquartile range. Outliers are represented as individual circles. Panels (a) and (b) plot the performance metrics - coefficient of determination and the root mean squared error (RMSE).

GLWS shows high precision with a strong R^2 and tight RMSE spread, however it consistently overestimates, as reflected in its higher median RMSE. GRS performs well in consistency but faces challenges due to limited historical data and low temporal resolution. TMS-OS performs similarly or better than the other two methods, with a lower RMSE and more frequent data. Additionally, TMS-OS is an open-source methodology applicable to any reservoir in the world to obtain reservoir storage estimates using latest satellite observations, unlike the static number of reservoirs mapped in GRS and GLWS which are also limited to a set date in the past (Figure 5.3). Another distinct feature of TMS-OS is the ease with which sensors can be added or removed as well as sensor calibration methods altered. Hence, because of TMS-OS's versatility, comparable accuracy, and observations available during SWOT's observational period, it is used hereafter as an acceptable baseline of non-SWOT methods to compare against SWOT estimates.

5.4.3 Impact of SWOT relative to non-SWOT baseline

Reservoir storage estimates from SWOT observations were compared against non-SWOT baseline (TMS-OS). SWOT has a median R^2 value exceeding 0.8 and relatively compact interquartile ranges, indicating consistently good performance, irrespective of the AEV used

(Figure 5.8a). The in-situ E-S variants of SWOT perform only marginally better than its counterpart, with the same median R^2 and a slightly tighter inter-quartile range (IQR). Comparatively, TMS-OS has a poorer R^2, suggesting that SWOT is able to capture the trends of storage dynamics far better, irrespective of the AEV used.

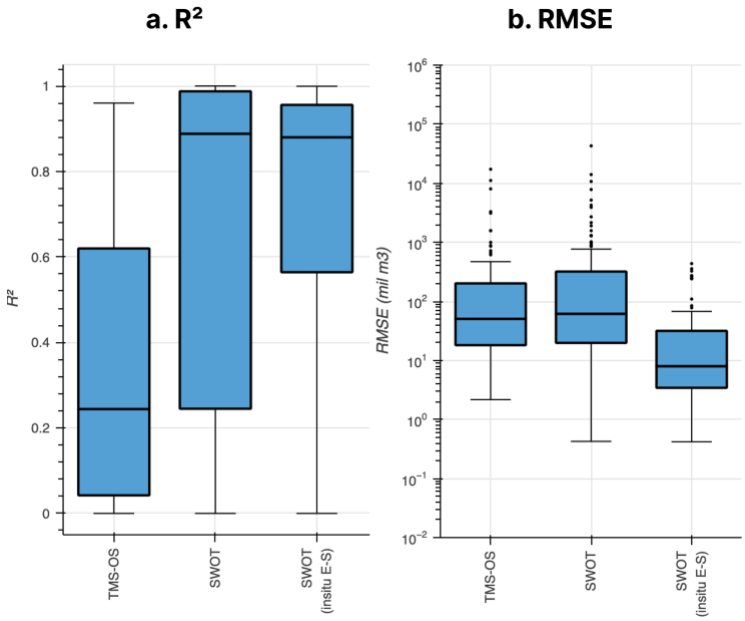

Figure 5.8 Comparison of performance of SWOT and TMS-OS in estimating the storage dynamics of reservoirs between July 2023 and October 2024. Storage from SWOT is first obtained using satellite derived AEV, referred to as satellite E-S in the figure, and in-situ observations derived AEV (insitu E-S).

Counterintuitively, the performance in estimating the absolute values of storage, as indicated by the RMSE, was similar for SWOT and TMS-OS (Figure 5.8b) using satellite derived AEV. Common sense would dictate that with more accurate water surface elevation would result in more accurate estimated storage. This discrepancy in high skill in estimating trends, but lower skill in estimating absolute values, can be explained by a poor Elevation-Storage relationship. The performance of storage estimated using these in-situ AEV curves are also shown in Figure 5.8. The RMSE improved by nearly an order for SWOT (see Figure 5.8b), without an alteration in the R^2. This means that with an improved AEV relationship, the absolute values of estimated storage improved significantly as well, while the performance of estimating the trends in storage remained nearly the same. The uncertainty in estimated storage values was largely due to the uncertainty in the AEV curve. Similarly, the uncertainty in the storage estimated using TMS-OS is largely due

to the uncertainty in the water surface area time-series by the teamwork of non-SWOT satellite sensors.

Figure 5.9 illustrates the spatial distribution of the performance. The higher end of RMSE observed with SWOT remains confined to a range of 100–1000 million m^3, while TMS-OS exhibits significantly higher errors, ranging from 1000–10,000 million m^3. This disparity highlights the considerable advantage offered by SWOT. Nearly all reservoirs demonstrate an order of magnitude improvement in performance when using SWOT compared to the non-SWOT baseline, showcasing SWOT's ability to enhance accuracy across diverse locations. In monsoon-prone regions like Thailand, a higher proportion of reservoirs perform poorly with TMS-OS due to structural limitations; however, these same reservoirs show marked improvement with SWOT, benefiting from its all-weather capabilities and superior fidelity in water surface elevation estimation.

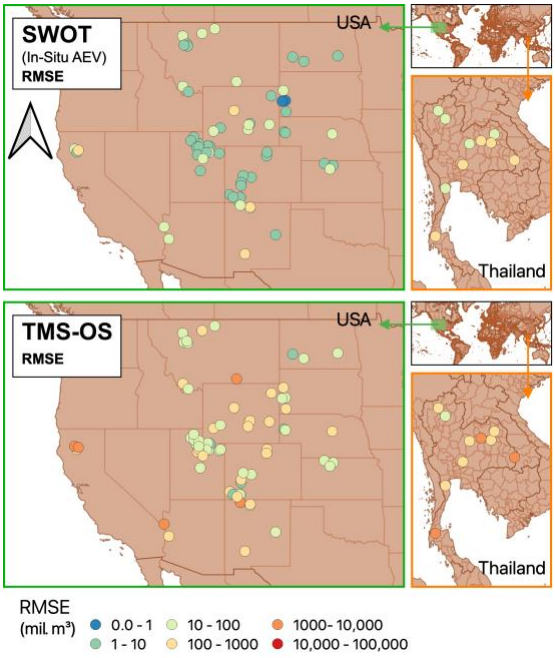

Figure 5.9 Spatial distribution of performance of SWOT and TMS-OS compared against in-situ reservoir storage observations.

Comparison of storage time-series of six selected reservoirs in Figure 5.10 highlight the difference in storage estimation ability of SWOT relative to TMS-OS, the non-SWOT baseline. The results clearly show that SWOT is significantly more accurate than TMS-OS, effectively capturing not only the trends but also the absolute storage as a time-series. In contrast, TMS-OS provides relatively less accurate estimates, which, while in the general ballpark, can deviate

considerably from in-situ observations. Occasionally SWOT may produce outliers, as seen in the Lam Pao Dam (top-left panel of Figure 5.10), such instances are rare based on our manual inspection of performance over remaining reservoirs. For most reservoirs, SWOT's storage estimates align closely with in-situ observations. Overall, SWOT represents a substantial improvement in the ability to estimate reservoir storage compared to previous satellite-based methods.

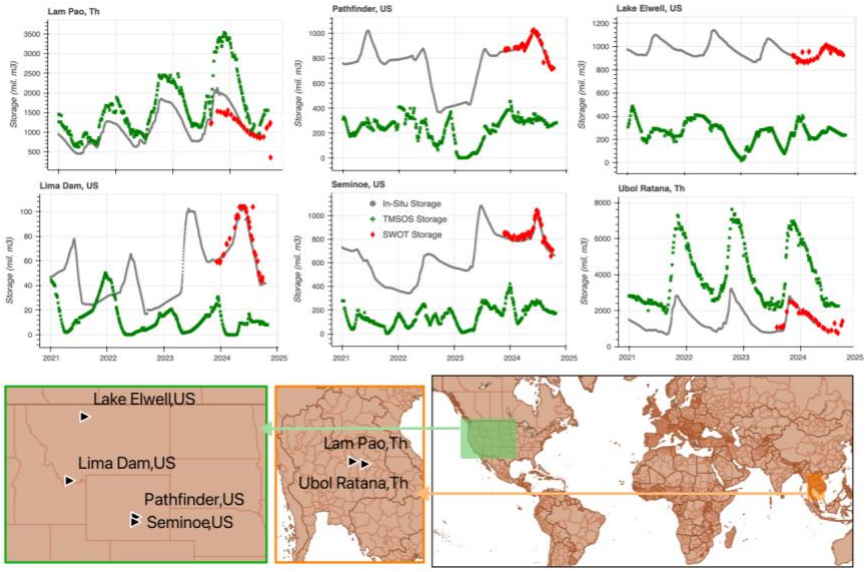

Figure 5.10 Selected time-series of six dams comparing TMS-OS and SWOT based storage estimates against in-situ observations.

5.4.4 Multi-point sampling of water surface elevation results in improved reservoir storage dynamics

While the previous section demonstrates the higher accuracy of SWOT, this section focuses on exploring the key factor yielding better performance from SWOT. We hypothesize here that the multiple elevations over a reservoir, resulting in a spatially distributed 'water terrain' leads to a more robust mean elevation for the reservoir than sensors that produce single or limited elevations such as the non-SWOT sensors of TMS-OS. To test this hypothesis, water surface elevation of over 100 reservoirs were obtained from the ICESat-2 sensor that can also produce a 'water terrain.' ICESat-2 has a laser altimeter onboard that takes measurements at 10kHz, pinging the water surface multiple times during a single overpass and producing numerous elevation returns. SWOT and ICESat-2 are similar in the sense that they estimate the water surface elevation over multiple different points on the reservoir water surface. Hence, even if a single measurement

is erroneous, we believe the central tendency of all the measurements during an overpass tends to closely represent the actual mean water surface elevation at that time. Comparatively, area measuring sensors, such as Sentinel-1 and Landsat-8 capture just a single snapshots in time.

The effect of multi-point averaging can be clearly seen translated into performance metrics in Figure 5.11 (a) and (b). The median coefficients of determination (R^2) are 0.91 and 0.98 respectively for SWOT and ICESat-2. Similarly, the median Root Mean Squared Error (RMSE) is 0.92 m and 0.98 m, respectively. While ICESat-2 altimetry satellites offer superior overall performance, their ability to repeatedly observe a reservoir is significantly lower compared to area-measuring satellites. Figure 5.11 proves the hypothesis that "Multi-point sampling of water surface elevation results in improved reservoir storage dynamics."

For this comparison, ICESat-2 managed to observe reservoirs an average of four times, while SWOT observed reservoirs an average of thirty times, and TMS-OS could obtain an impressive 140 observations during the same period. It is clear that SWOT can offer an optimal balance between accuracy and sampling frequency. The performance and number of observations together highlight that SWOT provides high accuracy estimates of the water surface elevation at a higher frequency than ICESat-2 and higher accuracy than TMS-OS.

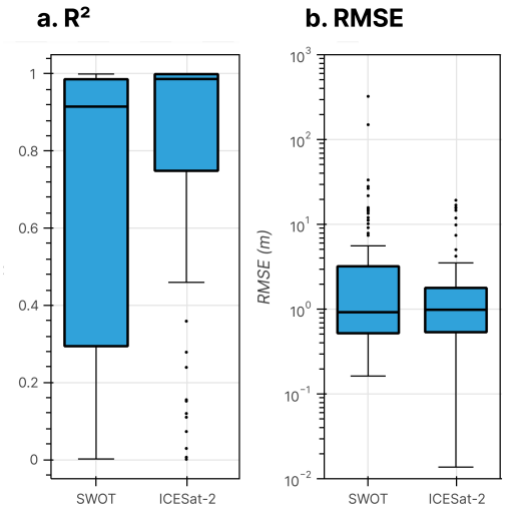

Figure 5.11 Inter-comparison of performance of SWOT and ICESat-2 for estimating the water surface elevation of reservoirs against in-situ data obtained between 2023-24.

5.4.5 Lessons Learned from Multi-Sensor Integration

SWOT's KaRIN sensor is designed to estimate both the area and elevation of the water surface. However, in the current version of processed L2 data, the L2-HR-Water Mask Raster v2.0, water pixels are often misclassified. The area estimates, hence, can be quite noisy. While misclassification of water pixels can also result in higher uncertainties in water surface elevation estimates if any additional processing is not conducted. The approach in Figure 5.4 alleviates this problem by filtering out individual pixels based on their uncertainties, and entire passes if required, so that the estimated water surface elevation is accurate over time. Using this approach, and SWOT's observations, the water surface elevation of nearly any water surface on Earth can be obtained. Unlike previous altimeter missions which missed vast portions of the Earth, the ability of SWOT as a global altimeter can be leveraged independent of its area estimating ability.

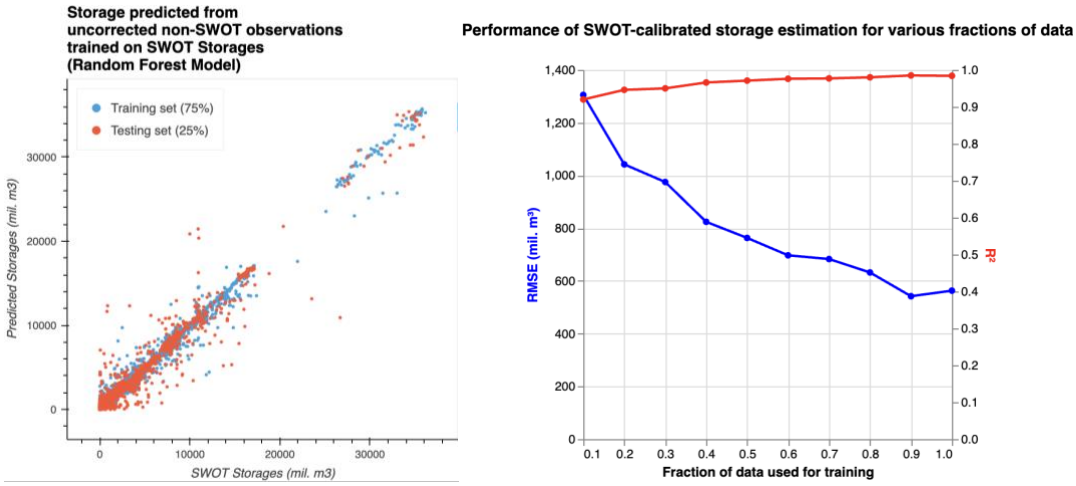

Figure 5.12 (a) Performance of a Random Forest Machine Learning model trained on uncorrected areas from non-SWOT sensors and other relevant features, with SWOT-storages as the target. (b) To establish a relationship between data availability and model performance, different fractions of data were used for training and the RMSE and R^2 of predicted storages were compared against the target values (SWOT storages). For instance, at 0.1 data fraction, only 10% of the entire dataset was used.

We trained a Random Forest (RF) model to quantify the performance of the model trained on currently available SWOT observations and gauge the requirement of further data. Figure 5.12(a) illustrates the performance of predicted storage by the RF model, compared against the target – SWOT based storages. The scatterplot visually shows a generally good agreement between model predictions and the target values, illustrating that training a ML model to estimate SWOT-like storages from observations by non-SWOT sensors are possible.

To assess the role of data availability, the model was trained on limited data. The available record of SWOT observations used for training were limited to various fractions, from 0.1 (10% values used) to 1.0 (all values used). Figure 5.12(b) quantifies the performance of the model in terms of RMSE and R^2. The resulting performance of these models shows the trend with which increasing data availability improves the predictive performance of the model. Using all the available data (~14,000 records), the RMSE is about 600 mil. m^3, which gradually increases as data available for model training reduces. The R^2 doesn't improve as drastically with more data and stays relatively stagnant. However, the trend of decrease in RMSE with increasing data availability is promising, indicating that the model's predictive capability increases with more data. While currently the performance of models leaves much to be desired for, the poor performance of the ML model is probably best explained by the short observation record of SWOT so far – only 1.5 years. With a more extensive record of observations in future, ML models trained for predicting reservoir storage calibrated to SWOT is expected to perform much better as seen in Figure 5.12 (b). Continuing from the trends, with about 1.5 years more data (double the current available), the RMSE may potentially reduce to under 100 million m^3.

On the second approach for integrating SWOT with non-SWOT sensors using the TMS approach, we conclude two findings. First, SWOT's elevation estimates at a global scale are usable by themselves if the observational frequency or timeliness is not a concern. The area-averaging nature of observations by SWOT (as validated with the use of ICESat-2 elevation data) allows these sensors to estimate the elevation of water surface more accurately. Second, the area estimated by Optical and SAR sensors cannot be trivially grouped together for applying the TMS algorithm. Figure 5.13 shows the difference in estimated area by different sensors. Sentinel-1, when compared to any other optical sensor tends to have a larger difference in estimated area (bias at reservoir-level). On the other hand, optical satellites irrespective of the mission, tend to have more agreement amongst themselves, as indicated by the larger peak centered around 0 and tighter spread. Hence, when SAR and Optical are used together as area-estimating sensors, it results in high apparent noise due to the difference in the area estimated by the two sensors (Figure 5.13). Furthermore, for using SWOT observations for filtering and trend correction, the elevations first have to be converted to area values using the satellite derived AEC. This adds additional uncertainty, because of the relatively high vertical uncertainty of SRTM DEM which can be a few meters (Chai et al., 2022).

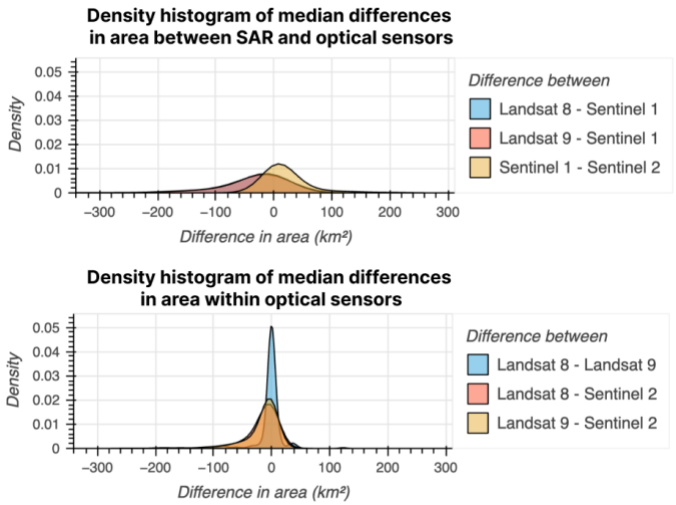

Figure 5.13 Distribution of the difference in median area of reservoirs estimated by optical and SAR sensors. The first panel shows differences between optical and SAR sensors, while the second panel shows the difference within optical sensors. Optical sensors tend to agree more amongst themselves, indicated by the higher magnitude peak centered around 0. Comparatively, the SAR sensor tends to disagree with optical sensors more, indicated by larger tails of the distribution.

Due to these limitations, integration of multiple satellites observations still requires further development to improve the accuracy of estimated storage than what is afforded by SWOT alone. However, with further improvements in the algorithm for classifying water pixels in SWOT's KaRIN sensor, and a longer observational record, accurate multi-satellite estimation of reservoir storage at a higher frequency using ML techniques should be possible.

5.5 Conclusion

This research paper examined the ability of the recently launched Surface Water and Ocean Topography (SWOT) mission to estimate reservoir storage around the world. It examined the performance of recently launched SWOT satellites in estimating reservoir storage dynamics, comparing it to pre-existing multi-sensor and single-sensor non-SWOT methods. SWOT's all-weather SAR Interferometry based sensor, KaRIN, was found able to estimate both water surface extent and elevation simultaneously with superior accuracy. The water surface elevations were estimated accurately at 245 reservoirs making SWOT a one-of-its-kind global sensor. This global coverage distinguishes SWOT from previous altimeter missions, which do not observe vast portions of the planet.

Two key findings emerged from this study – (1) SWOT is able to capture the trends and absolute values of reservoir storage well using its elevation measurements. (2) The error of storage estimates (RMSE) reduced drastically when in-situ AEV was used. R^2 stayed relatively consistent for SWOT, suggesting that the limiting factor for accurately estimate reservoir storage using SWOT is the accuracy of AEV. Both these findings were further validated using the ICESat-2 satellite – to validate the reason for superior performance of SWOT elevations in estimating storage to the pre-SWOT baseline, and the role of AEV in determining the accuracy.

Another no less important finding that emerged is that the integration of SWOT data in non-SWOT methods, whether it is using machine learning or calibration techniques, needs further development. The paucity of SWOT record (< 2. 0 years) is likely the reason and a longer data record from SWOT should be able to make the sensor ready to 'run the show' of multi-sensor storage estimation akin to how the Global Precipitation Measurement (GPM) sensor for multi-sensor precipitation product development.

Acknowledgments

This study was supported from the NASA grant 80NSSC24K1644 (Quantifying the net impact of the SWOT mission in improving our Understanding of Human Regulation of Surface Water around the World) of NASA Physical Oceanography program. Generous support from another NASA grant - 80NSSC22K0918 (Improved Reservoir Management with Simultaneous Monitoring of Water Quantity and Quality using Multiple Satellites, SWOT and RAT-WQ2) of the NASA Earth Science to Action program to the first author is also acknowledged.

Open Research

SWOT data was obtained from PODAAC at https://podaac.jpl.nasa.gov/dataset/SWOT_L2_HR_Raster_2.0 and Earthdata at https://search.earthdata.nasa.gov/search. ICESat-2 data was also obtained from Earthdata. Google Earth Engine (https://earthengine.google.com/) was used to obtain observations from Landsat 8, Landsat 9, Sentinel 2, and Sentinel 1 satellites for the multi-sensor TMS-OS approach. The code for the study is available at https://github.com/UW-SASWE/tmspp**.**

Chapter 6. Conclusions and Future Recommendations

6.1 CONCLUSIONS

Rivers around the world today are increasingly regulated by dams and reservoirs. The true scale of the impacts on the ecosystem, downstream water availability, is not fully understood due to a lack of data and publicly available tools that can help monitor reservoirs and the resulting regulation. This dissertation builds the foundation for an open-source toolset for independently estimating reservoir operations using multi-sensor remote sensing and hydrological monitoring. In Chapter 2, the second version of the RAT framework is developed. A decision support system, RAT-Mekong, is also implemented on the Mekong River Basin that operationally estimates reservoir operations in the basin. Chapter 2 introduced a scalable river regulation estimation model, ResORR, that improves the regulated streamflow estimates in the heavily regulated Cumberland River basin. Chapter 3 extended the temporal domain of RAT to the short-term future by integrating gauge-corrected precipitation and meteorological forecasts from numerical weather prediction models. It is tested on the Periyar River basin in Kerala which experienced massive scale damage due to floods in 2018 exacerbated by the failure of regulatory structures to effectively contain the flood. Finally, in chapter 4, the accuracy with which storage change of reservoirs can be estimated by the recently launched SWOT satellite is assessed. The key takeaways from each chapter are summarized below.

6.1.1 Stakeholder-Driven Improvements to Satellite Remote Sensing Based Reservoir Monitoring

First, the frequency and accuracy of reservoir area estimation is improved by developing the Tiered Multi-Satellite - Optical and SAR (TMS-OS) algorithm. It combines observations from optical and SAR sensors to estimate the water surface area at a higher frequency and accuracy than any individual sensor. This allows RAT to operationally estimate reservoir dynamics at a frequency of 1-5 days and in all-weather conditions. Strides are also made in the computational efficiency of the model. Parallel computation mode of the Variable Infiltration Capacity (VIC) hydrological model is introduced for higher computational efficiency along with parallelizing the routing scheme using the dask python package.

While the performance of the model estimates is obtained by comparing against in-situ observations for reservoirs in Thailand, the framework has been designed as an open-source tool that can be scaled to any river basin of the world.

6.1.2 Integration of Reservoirs in Modeling Streamflow of Heavily Regulated Rivers

The important gap of representation of reservoirs within a river basin was addressed in Chapter 3. Taking reservoir operations into account improved the streamflow estimates in a heavily regulated basin, underscoring the importance of inclusion of reservoirs in modeling the streamflow of a heavily regulated basin. A novel method for partitioning the regulated inflow into its constituent natural and regulated parts was developed.

The numerical robustness of the ResORR model was first established using a toy example of a regulated basin. Then the model was applied over the heavily regulated Cumberland basin in a set of consecutive experiments. In initial experiments, observed reservoir dynamics and inflow were used to establish the ability of the model to use "best" estimates of reservoir operations within a basin to estimate regulated streamflow. In the later experiments, additional uncertainty was added by replacing in-situ data with modeled data. In all cases the regulated streamflow was estimated with a higher accuracy than not considering reservoirs, establishing the added value of the model. Finally, using satellite-based reservoir operations estimates, the accuracy of regulated streamflow estimates was improved for three quarters of the cases. As expected, the largest improvement in performance was experienced by reservoirs that were preceded by large reservoirs. The key limitation on which the performance of the model is dependent is the accuracy of storage change estimates and the modeled streamflow at the upstream most reservoirs. Overall, ResORR demonstrates the ability to improve streamflow estimates within a regulated basin using satellite derived reservoir storage dynamics.

6.1.3 Value of Forecasting Reservoir Operations during Extreme Precipitation-driven Floods

In this chapter, the value of forecasting reservoir operations during extreme precipitation induced flooding is assessed in the mountainous region of Kerala. While currently the accuracy of numerical weather prediction models in accurately estimating the intensity of precipitation events limit the ability to estimate the peak of floods accurately, the timing of the peak and trend of increasing streamflow is estimated accurately within a period of 2-3 days. Reservoir operations

are also forecasted based on a range of likely operating scenarios. The tool is also integrated within the RAT framework and is designed to be scalable, especially in the mountainous developing regions of the world. In addition to Kerala, it is also applied over the case of flooding of the state of Tripura, India, and Southeastern Bangladesh in 2024.

6.1.4 Multi-Sensor Integration of SWOT

Storage change is the most crucial factor in estimating river regulation. The SWOT satellite offers an opportunity to enhance the accuracy of reservoir storage change estimation. The value added by SWOT was assessed by pursuing integration of non-SWOT sensors with SWOT. Although machine learning-based integration was limited by the data record of SWOT, it alone can accurately estimate reservoir storage globally using its all-weather Ka-band SAR interferometry sensor, KaRIn. This sensor enables better estimation of both trends and absolute values of reservoir storage through its global elevation measurements. The primary limitation in estimating storage and storage changes of reservoirs using SWOT is the accuracy of the AEV relationship.

6.2 Future Recommendations

The SWOT satellite will be key in the future of remote sensing-based understanding of the terrestrial water surface. With the availability of a little less than two years of observations, SWOT is already improving the global picture of the terrestrial surface water storage and dynamics. This will pay dividends in improving our ability to incorporate reservoirs within hydrological models based on observations instead of parameterization, which is often inaccurate and difficult to perform due to the human aspect of reservoir operations. Our recommendations are as follows:

(1) Towards a Global Surface Water mission: SWOT's unique capability to estimate water surface elevation at an accuracy and scale surpasses that of any existing non-SWOT satellite. While this ability of SWOT as a global altimeter is a breakthrough for applications in terrestrial water surface studies, the future of terrestrial water storage dynamics studies lies in multi-sensor methods that leverage the wide array of Earth Observing satellites. There exists a wide ranging, long history and temporally dense record of non-SWOT data that could be used together with SWOT to get a complete, more frequent, and more accurate picture of the global terrestrial water dynamics. Analogous to how the Global Precipitation Mission (GPM) satellite

played a key role in multi-sensor precipitation estimation (Integrated Multi-satellitE Retrievals for GPM, IMERG), SWOT is poised to play a similar role in better understanding terrestrial surface water resources. Machine Learning based methods have shown extensive use and success in other fields, including time-series anomaly detection (Blázquez-García et al., 2022; Munir et al., 2019) and multi sensor remote sensing data fusion (Schmitt and Zhu, 2016), which should be explored in the future for fusing SWOT and non-SWOT data with availability of longer record of SWOT observations.

(2) Reservoirs within Hydrological Models: Parameterized methods of incorporating reservoirs within hydrological models often fail to accurately represent the "human aspect" of reservoir operations. They can truly be incorporated within models only based on observations, since reservoir operators regularly must deviate from ideal operating conditions operationally for optimizing for hydropower, flood control, and dynamic operation based on forecasts. Future studies should focus on better representing reservoirs within hydrological models using improved satellite observational record of reservoir dynamics.

Bibliography

Abbott, B. W., Bishop, K., Zarnetske, J. P., Minaudo, C., Chapin, F. S., Krause, S., Hannah, D. M., Conner, L., Ellison, D., Godsey, S. E., Plont, S., Marçais, J., Kolbe, T., Huebner, A., Frei, R. J., Hampton, T., Gu, S., Buhman, M., Sara Sayedi, S., … Pinay, G. (2019). Human domination of the global water cycle absent from depictions and perceptions. *Nature Geoscience*, *12*(7), 533–540. https://doi.org/10.1038/s41561-019-0374-y

Abdalla, S., Abdeh Kolahchi, A., Ablain, M., Adusumilli, S., Aich Bhowmick, S., Alou-Font, E., Amarouche, L., Andersen, O. B., Antich, H., Aouf, L., Arbic, B., Armitage, T., Arnault, S., Artana, C., Aulicino, G., Ayoub, N., Badulin, S., Baker, S., Banks, C., … Zlotnicki, V. (2021). Altimetry for the future: Building on 25 years of progress. *Advances in Space Research*, *68*(2), 319–363. https://doi.org/10.1016/j.asr.2021.01.022

Ahmad, S. K., & Hossain, F. (2020a). Maximizing energy production from hydropower dams using short-term weather forecasts. *Renewable Energy*, *146*, 1560–1577. https://doi.org/10.1016/j.renene.2019.07.126

Ahmad, S. K., & Hossain, F. (2020b). Maximizing energy production from hydropower dams using short-term weather forecasts. *Renewable Energy*, *146*, 1560–1577. https://doi.org/10.1016/j.renene.2019.07.126

Ahmad, S. K., Hossain, F., Eldardiry, H., & Pavelsky, T. M. (2020). A Fusion Approach for Water Area Classification Using Visible, Near Infrared and Synthetic Aperture Radar for South Asian Conditions. *IEEE Transactions on Geoscience and Remote Sensing*, *58*(4), 2471–2480. IEEE Transactions on Geoscience and Remote Sensing. https://doi.org/10.1109/TGRS.2019.2950705

Ahmad, S. K., Hossain, F., Holtgrieve, G. W., Pavelsky, T., & Galelli, S. (2021). Predicting the Likely Thermal Impact of Current and Future Dams Around the World. *Earth's Future*, *9*(10), e2020EF001916. https://doi.org/10.1029/2020EF001916

Ahmad, S. K., Hossain, F., Pavelsky, T., Parkins, G. M., Yelton, S., Rodgers, M., Little, S., Haldar, D., Ghafoor, S., Khan, R. H., Shawn, N. A., Haque, A., & Biswas, R. K. (2020). Understanding Volumetric Water Storage in Monsoonal Wetlands of Northeastern Bangladesh. *Water Resources Research*, *56*(12). https://doi.org/10.1029/2020WR027989

Alcamo, J., Döll, P., Henrichs, T., Kaspar, F., Lehner, B., Rösch, T., & Siebert, S. (2003). Development and testing of the WaterGAP 2 global model of water use and availability. *Hydrological Sciences Journal*, *48*(3), 317–337. https://doi.org/10.1623/hysj.48.3.317.45290

Allen, G. H., & Pavelsky, T. M. (2018). Global extent of rivers and streams. *Science*, *361*(6402), 585–588. https://doi.org/10.1126/science.aat0636

Alsdorf, D. E., Rodríguez, E., & Lettenmaier, D. P. (2007). Measuring surface water from space. *Reviews of Geophysics*, *45*(2). https://doi.org/10.1029/2006RG000197

Anghileri, D., Voisin, N., Castelletti, A., Pianosi, F., Nijssen, B., & Lettenmaier, D. P. (2016). Value of long-term streamflow forecasts to reservoir operations for water supply in snow-dominated river catchments. *Water Resources Research*, *52*(6), 4209–4225. https://doi.org/10.1002/2015WR017864

Arias, M. E., Cochrane, T. A., Piman, T., Kummu, M., Caruso, B. S., & Killeen, T. J. (2012). Quantifying changes in flooding and habitats in the Tonle Sap Lake (Cambodia) caused by

water infrastructure development and climate change in the Mekong Basin. *Journal of Environmental Management*, *112*, 53–66. https://doi.org/10.1016/j.jenvman.2012.07.003

Bakker, M. H. N. (2009). Transboundary River Floods and Institutional Capacity. *JAWRA Journal of the American Water Resources Association*, *45*(3), 553–566. https://doi.org/10.1111/j.1752-1688.2009.00325.x

Balthrop, C., & Hossain, F. (2010). Short note: A review of state of the art on treaties in relation to management of transboundary flooding in international river basins and the Global Precipitation Measurement mission. *Water Policy*, *12*(5), 635–640. https://doi.org/10.2166/wp.2009.117

Barbarossa, V., Schmitt, R. J. P., Huijbregts, M. A. J., Zarfl, C., King, H., & Schipper, A. M. (2020). Impacts of current and future large dams on the geographic range connectivity of freshwater fish worldwide. *Proceedings of the National Academy of Sciences*, *117*(7), 3648–3655. https://doi.org/10.1073/pnas.1912776117

Basu, S., & Meckesheimer, M. (2007). Automatic outlier detection for time series: An application to sensor data. *Knowledge and Information Systems*, *11*(2), 137–154. https://doi.org/10.1007/s10115-006-0026-6

Bennett, A., Hamman, J., & Nijssen, B. (2020). MetSim: A Python package for estimation and disaggregation of meteorological data. *Journal of Open Source Software*, *5*(47), 2042. https://doi.org/10.21105/joss.02042

Bernauer, T., & Böhmelt, T. (2020). International conflict and cooperation over freshwater resources. *Nature Sustainability*, *3*(5), 350–356. https://doi.org/10.1038/s41893-020-0479-8

Biancamaria, S., Lettenmaier, D. P., & Pavelsky, T. M. (2016). The SWOT Mission and Its Capabilities for Land Hydrology. *Surveys in Geophysics*, *37*(2), 307–337. https://doi.org/10.1007/s10712-015-9346-y

Biemans, H., Haddeland, I., Kabat, P., Ludwig, F., Hutjes, R. W. A., Heinke, J., von Bloh, W., & Gerten, D. (2011). Impact of reservoirs on river discharge and irrigation water supply during the 20th century. *Water Resources Research*, *47*(3). https://doi.org/10.1029/2009WR008929

Birkett, C. M., Reynolds, C. A., Deeb, E. J., Ricko, M., Beckley, B. D., & Yang, X. (2018, December 14). *G-REALM: A Lake/Reservoir Monitoring tool for Water Resources and Regional Security assessment*. AGU Fall Meeting 2018. https://agu.confex.com/agu/fm18/meetingapp.cgi/Paper/374138

Biswas, N. K., & Hossain, F. (2022). A Multidecadal Analysis of Reservoir Storage Change in Developing Regions. *Journal of Hydrometeorology*, *23*(1), 71–85. https://doi.org/10.1175/JHM-D-21-0053.1

Biswas, N. K., Hossain, F., Bonnema, M., Lee, H., & Chishtie, F. (2021). Towards a global Reservoir Assessment Tool for predicting hydrologic impacts and operating patterns of existing and planned reservoirs. *Environmental Modelling & Software*, *140*, 105043. https://doi.org/10.1016/j.envsoft.2021.105043

Biswas, N. K., Hossain, F., Bonnema, M., Okeowo, M. A., & Lee, H. (2019). An altimeter height extraction technique for dynamically changing rivers of South and South-East Asia. *Remote Sensing of Environment*, *221*, 24–37. https://doi.org/10.1016/j.rse.2018.10.033

Blázquez-García, A., Conde, A., Mori, U., & Lozano, J. A. (2022). A Review on Outlier/Anomaly Detection in Time Series Data. *ACM Computing Surveys*, *54*(3), 1–33. https://doi.org/10.1145/3444690

Bonnema, M., & Hossain, F. (2017). Inferring reservoir operating patterns across the Mekong Basin using only space observations. *Water Resources Research*, *53*(5), 3791–3810. https://doi.org/10.1002/2016WR019978

Bonnema, M., Sikder, S., Miao, Y., Chen, X., Hossain, F., Ara Pervin, I., Mahbubur Rahman, S. M., & Lee, H. (2016). Understanding satellite-based monthly-to-seasonal reservoir outflow estimation as a function of hydrologic controls: Satellite-Based Reservoir Outflow. *Water Resources Research*, *52*(5), 4095–4115. https://doi.org/10.1002/2015WR017830

Bonnet, M., Witt, A., Steart, K., Hadjerioua, B., & Mobley, M. (2015). *The Economic Benefits of Multipurpose Reservoirs in the United States-Federal Hydropower Fleet*. https://doi.org/10.13140/RG.2.2.15894.14400

Boulange, J., Hanasaki, N., Yamazaki, D., & Pokhrel, Y. (2021). Role of dams in reducing global flood exposure under climate change. *Nature Communications*, *12*(1), Article 1. https://doi.org/10.1038/s41467-020-20704-0

Bureau of Reclamation. (n.d.). *RISE | Bureau of Reclamation*. Retrieved December 7, 2022, from https://data.usbr.gov/time-series/search?order=&page=2&search=&v=1

Caissie, D. (2006). The thermal regime of rivers: A review. *Freshwater Biology*, *51*(8), 1389–1406. https://doi.org/10.1111/j.1365-2427.2006.01597.x

Calinski, T., & Harabasz, J. (1974). A dendrite method for cluster analysis. *Communications in Statistics - Theory and Methods*, *3*(1), 1–27. https://doi.org/10.1080/03610927408827101

Central Water Commission. (2018). *Kerala Floods of August 2018*. Hydrology (S) Directorate, Hydrological Sciences Division, Central Water Commission.

Chai, L. T., Wong, C. J., James, D., Loh, H. Y., Liew, J. J. F., Wong, W. V. C., & Phua, M. H. (2022). Vertical accuracy comparison of multi-source Digital Elevation Model (DEM) with Airborne Light Detection and Ranging (LiDAR). *IOP Conference Series: Earth and Environmental Science*, *1053*(1), 012025. https://doi.org/10.1088/1755-1315/1053/1/012025

Chang, C.-H., Lee, H., Do, S. K., Du, T. L. T., Markert, K., Hossain, F., Ahmad, S. K., Piman, T., Meechaiya, C., Bui, D. D., Bolten, J. D., Hwang, E., & Jung, H. C. (2023). Operational forecasting inundation extents using REOF analysis (FIER) over lower Mekong and its potential economic impact on agriculture. *Environmental Modelling & Software*, *162*, 105643. https://doi.org/10.1016/j.envsoft.2023.105643

Cheng, Y., Nijssen, B., Holtgrieve, G. W., & Olden, J. D. (2022). Modeling the freshwater ecological response to changes in flow and thermal regimes influenced by reservoir dynamics. *Journal of Hydrology*, *608*, 127591. https://doi.org/10.1016/j.jhydrol.2022.127591

Cheng, Y., Voisin, N., Yearsley, J. R., & Nijssen, B. (2020). Reservoirs Modify River Thermal Regime Sensitivity to Climate Change: A Case Study in the Southeastern United States. *Water Resources Research*, *56*(6), e2019WR025784. https://doi.org/10.1029/2019WR025784

Columbia River Basin Dams. (n.d.). Retrieved January 30, 2025, from https://www.nwd.usace.army.mil/crwm/cr-dams/

Cooley, S. W., Ryan, J. C., & Smith, L. C. (2021). Human alteration of global surface water storage variability. *Nature*, *591*(7848), Article 7848. https://doi.org/10.1038/s41586-021-03262-3

Cordeiro, M. C. R., Martinez, J.-M., & Peña-Luque, S. (2021). Automatic water detection from multidimensional hierarchical clustering for Sentinel-2 images and a comparison with Level 2A processors. *Remote Sensing of Environment*, *253*, 112209. https://doi.org/10.1016/j.rse.2020.112209

Dac Tran, D., Thi Nguyen, V., Thi My To, H., Trung Nguyen, T., & Minh Dinh, Q. (2020). Species composition and biodiversity index of gobiid assemblage in estuarine areas of the Mekong Delta, Vietnam. *Egyptian Journal of Aquatic Biology and Fisheries*, *24*(7-Special issue), 931–941. https://doi.org/10.21608/ejabf.2020.131385

Dams in ganga basin—INDIA WRIS WIKI. (2021). https://indiawris.gov.in/wiki/doku.php?id=dams_in_ganga_basin

Darkwah, G. K., Hossain, F., Tchervenski, V., Holtgrieve, G., Graves, D., Seaton, C., Minocha, S., Das, P., Khan, S., & Suresh, S. (2024). Reconstruction of the Hydro-Thermal Behavior of Regulated River Networks of the Columbia River Basin Using Satellite Remote Sensing and Data-Driven Techniques. *Earth's Future*, *12*(10), e2024EF004815. https://doi.org/10.1029/2024EF004815

Das, P., Hossain, F., Khan, S., Biswas, N. K., Lee, H., Piman, T., Meechaiya, C., Ghimire, U., & Hosen, K. (2022). Reservoir Assessment Tool 2.0: Stakeholder driven improvements to satellite remote sensing based reservoir monitoring. *Environmental Modelling & Software*, *157*(105533). https://doi.org/10.1016/j.envsoft.2022.105533

Das, P., Hossain, F., Minocha, S., Suresh, S., Darkwah, G. K., Lee, H., Andreadis, K., Laverde-Barajas, M., & Oddo, P. (2024). ResORR: A globally scalable and satellite data-driven algorithm for river flow regulation due to reservoir operations. *Environmental Modelling & Software*, *176*, 106026. https://doi.org/10.1016/j.envsoft.2024.106026

Das, P., Suresh, S., Hossain, F., Balakrishnan, V., Jainet, P. J., Lee, H., Laverde, M., Hosen, K., Meechaiya, C., & Towashiraporn, P. (2025). Forecast-Informed Reservoir Operations within a Satellite-Based Framework for Mountainous and High-Precipitation Regions: Case of the 2018 Kerala Floods. *Journal of Hydrologic Engineering*, *30*(2), 05025003. https://doi.org/10.1061/JHYEFF.HEENG-6276

Dingman, S. L. (2015). *Physical hydrology* (Third edition). Waveland Press, Inc.

Donchyts, G., Winsemius, H., Baart, F., Dahm, R., Schellekens, J., Gorelick, N., Iceland, C., & Schmeier, S. (2022a). High-resolution surface water dynamics in Earth's small and medium-sized reservoirs. *Scientific Reports*, *12*(1), 13776. https://doi.org/10.1038/s41598-022-17074-6

Donchyts, G., Winsemius, H., Baart, F., Dahm, R., Schellekens, J., Gorelick, N., Iceland, C., & Schmeier, S. (2022b). *Supplementary materials for the High-resolution surface water dynamics in Earth's small and medium-sized reservoirs*. https://doi.org/10.6084/m9.figshare.20359860.v1

Dong, N., Yang, M., Wei, J., Arnault, J., Laux, P., Xu, S., Wang, H., Yu, Z., & Kunstmann, H. (2023). Toward Improved Parameterizations of Reservoir Operation in Ungauged Basins: A Synergistic Framework Coupling Satellite Remote Sensing, Hydrologic Modeling, and

Conceptual Operation Schemes. *Water Resources Research*, *59*(3), e2022WR033026. https://doi.org/10.1029/2022WR033026

Dunn, F. E., Darby, S. E., Nicholls, R. J., Cohen, S., Zarfl, C., & Fekete, B. M. (2019). Projections of declining fluvial sediment delivery to major deltas worldwide in response to climate change and anthropogenic stress. *Environmental Research Letters*, *14*(8), 084034. https://doi.org/10.1088/1748-9326/ab304e

Dunn, R. J. H., Alexander, L. V., Donat, M. G., Zhang, X., Bador, M., Herold, N., Lippmann, T., Allan, R., Aguilar, E., Barry, A. A., Brunet, M., Caesar, J., Chagnaud, G., Cheng, V., Cinco, T., Durre, I., De Guzman, R., Htay, T. M., Wan Ibadullah, W. M., … Bin Hj Yussof, M. N. (2020). Development of an Updated Global Land In Situ-Based Data Set of Temperature and Precipitation Extremes: HadEX3. *Journal of Geophysical Research: Atmospheres*, *125*(16), e2019JD032263. https://doi.org/10.1029/2019JD032263

Earth Resources Observation And Science (EROS) Center. (2017). *Shuttle Radar Topography Mission (SRTM) 1 Arc-Second Global* [Tiff]. U.S. Geological Survey. https://doi.org/10.5066/F7PR7TFT

EGAT. (2019). *The Study of Probable Maximum Flood and Spillway Operation for Dam Safety of EGAT's Dam*. Electricity Generating Authority of Thailand, Ministry of Energy.

Eldardiry, H., & Hossain, F. (2019). Understanding Reservoir Operating Rules in the Transboundary Nile River Basin Using Macroscale Hydrologic Modeling with Satellite Measurements. *Journal of Hydrometeorology*, *20*(11), 2253–2269. https://doi.org/10.1175/JHM-D-19-0058.1

Eldardiry, H., & Hossain, F. (2021). A blueprint for adapting high Aswan dam operation in Egypt to challenges of filling and operation of the Grand Ethiopian Renaissance dam. *Journal of Hydrology, 598*, 125708. https://doi.org/10.1016/j.jhydrol.2020.125708

Fernandes, M. R., Aguiar, F. C., Martins, M. J., Rivaes, R., & Ferreira, M. T. (2020). Long-term human-generated alterations of Tagus River: Effects of hydrological regulation and land-use changes in distinct river zones. *CATENA*, *188*, 104466. https://doi.org/10.1016/j.catena.2020.104466

Fischer, A. M., Keller, D. E., Liniger, M. A., Rajczak, J., Schär, C., & Appenzeller, C. (2015). Projected changes in precipitation intensity and frequency in Switzerland: A multi-model perspective. *International Journal of Climatology*, *35*(11), 3204–3219. https://doi.org/10.1002/joc.4162

Freeman, M. C., Bestgen, K. R., Carlisle, D., Frimpong, E. A., Franssen, N. R., Gido, K. B., Irwin, E., Kanno, Y., Luce, C., Kyle McKay, S., Mims, M. C., Olden, J. D., LeRoy Poff, N., Propst, D. L., Rack, L., Roy, A. H., Stowe, E. S., Walters, A., & Wenger, S. J. (2022). Toward Improved Understanding of Streamflow Effects on Freshwater Fishes. *Fisheries*, *47*(7), 290–298. https://doi.org/10.1002/fsh.10731

Funk, C., Peterson, P., Landsfeld, M., Pedreros, D., Verdin, J., Shukla, S., Husak, G., Rowland, J., Harrison, L., Hoell, A., & Michaelsen, J. (2015). The climate hazards infrared precipitation with stations—A new environmental record for monitoring extremes. *Scientific Data, 2*(1), 150066. https://doi.org/10.1038/sdata.2015.66

Gao, H., Birkett, C., & Lettenmaier, D. P. (2012). Global monitoring of large reservoir storage from satellite remote sensing. *Water Resources Research*, *48*(9), 2012WR012063. https://doi.org/10.1029/2012WR012063

Google. (2022, March 10). *Ee.Clusterer.wekaCascadeKMeans | Google Earth Engine*. Google Developers. https://developers.google.com/earth-engine/apidocs/ee-clusterer-wekacascadekmeans

Grill, G., Lehner, B., Lumsdon, A. E., MacDonald, G. K., Zarfl, C., & Reidy Liermann, C. (2015). An index-based framework for assessing patterns and trends in river fragmentation and flow regulation by global dams at multiple scales. *Environmental Research Letters*, *10*(1), 015001. https://doi.org/10.1088/1748-9326/10/1/015001

Grill, G., Lehner, B., Thieme, M., Geenen, B., Tickner, D., Antonelli, F., Babu, S., Borrelli, P., Cheng, L., Crochetiere, H., Ehalt Macedo, H., Filgueiras, R., Goichot, M., Higgins, J., Hogan, Z., Lip, B., McClain, M. E., Meng, J., Mulligan, M., … Zarfl, C. (2019). Mapping the world's free-flowing rivers. *Nature*, *569*(7755), 215–221. https://doi.org/10.1038/s41586-019-1111-9

Gupta, H. V., Kling, H., Yilmaz, K. K., & Martinez, G. F. (2009). Decomposition of the mean squared error and NSE performance criteria: Implications for improving hydrological modelling. *Journal of Hydrology*, *377*(1–2), 80–91. https://doi.org/10.1016/j.jhydrol.2009.08.003

Haddeland, I., Skaugen, T., & Lettenmaier, D. P. (2006). Anthropogenic impacts on continental surface water fluxes. *Geophysical Research Letters*, *33*(8), L08406. https://doi.org/10.1029/2006GL026047

Hamman, J. J., Nijssen, B., Bohn, T. J., Gergel, D. R., & Mao, Y. (2018). The Variable Infiltration Capacity model version 5 (VIC-5): Infrastructure improvements for new applications and reproducibility. *Geoscientific Model Development*, *11*(8), 3481–3496. https://doi.org/10.5194/gmd-11-3481-2018

Hamman, J., & Nijssen, B. (2016). *Vic: Vic 4.2.D* [Computer software]. Zenodo. https://doi.org/10.5281/ZENODO.56057

Hamman, J., Nijssen, B., Bohn, T., Gergel, D., Franssen, W., Yixin Mao, Homefc, Hordur Helgason, Suzuki, K., RK, M., Badger, T. G., Craig, T., Zwart, J., Kiritokun07, & Peng, B. (2021). *UW-Hydro/VIC: VIC 5.1.0* (Version 5.1.0) [Computer software]. Zenodo. https://doi.org/10.5281/ZENODO.5781377

Han, Z., Long, D., Huang, Q., Li, X., Zhao, F., & Wang, J. (2020). Improving Reservoir Outflow Estimation for Ungauged Basins Using Satellite Observations and a Hydrological Model. *Water Resources Research*, *56*(9), e2020WR027590. https://doi.org/10.1029/2020WR027590

Hanasaki, N., Kanae, S., & Oki, T. (2006). A reservoir operation scheme for global river routing models. *Journal of Hydrology*, *327*(1–2), 22–41. https://doi.org/10.1016/j.jhydrol.2005.11.011

Hanasaki, N., Yoshikawa, S., Pokhrel, Y., & Kanae, S. (2018). A global hydrological simulation to specify the sources of water used by humans. *Hydrology and Earth System Sciences*, *22*(1), 789–817. https://doi.org/10.5194/hess-22-789-2018

Harbeck, G. E. (1962). *A practical field technique for measuring Reservoir Evaporation utilizing mass-transfer theory* (Studies of Evaporation) [Geological Survey Professional Paper 272-E]. U.S. Department of the Interior.

Harrison, L., Landsfeld, M., Husak, G., Davenport, F., Shukla, S., Turner, W., Peterson, P., & Funk, C. (2022). Advancing early warning capabilities with CHIRPS-compatible NCEP GEFS precipitation forecasts. *Scientific Data*, *9*(1), Article 1. https://doi.org/10.1038/s41597-022-01468-2

Hersbach, H., Bell, B., Berrisford, P., Hirahara, S., Horányi, A., Muñoz-Sabater, J., Nicolas, J., Peubey, C., Radu, R., Schepers, D., Simmons, A., Soci, C., Abdalla, S., Abellan, X., Balsamo, G., Bechtold, P., Biavati, G., Bidlot, J., Bonavita, M., … Thépaut, J. (2020). The ERA5 global reanalysis. *Quarterly Journal of the Royal Meteorological Society*, *146*(730), 1999–2049. https://doi.org/10.1002/qj.3803

Hossain, F., Alwash, A., Minocha, S., & Eldardiry, H. (2023). Restoring the Mesopotamian Rivers for Future Generations: A Practical Approach. *Water Resources Research*, *59*(5), e2023WR034514. https://doi.org/10.1029/2023WR034514

Hossain, F., Sikder, S., Biswas, N., Bonnema, M., Lee, H., Luong, N. D., Hiep, N. H., Du Duong, B., & Long, D. (2017). Predicting Water Availability of the Regulated Mekong River Basin Using Satellite Observations and a Physical Model. *Asian Journal of Water, Environment and Pollution*, *14*(3), 39–48. https://doi.org/10.3233/AJW-170024

Huffman, G. J., Adler, R. F., Bolvin, D. T., Gu, G., Nelkin, E. J., Bowman, K. P., Hong, Y., Stocker, E. F., & Wolff, D. B. (2007). The TRMM Multisatellite Precipitation Analysis

(TMPA): Quasi-Global, Multiyear, Combined-Sensor Precipitation Estimates at Fine Scales. *Journal of Hydrometeorology*, *8*(1), 38–55.

Huffman, G. J., Bolvin, D. T., Braithwaite, D., Hsu, K.-L., Joyce, R. J., Kidd, C., Nelkin, E. J., Sorooshian, S., Stocker, E. F., Tan, J., Wolff, D. B., & Xie, P. (2020). Integrated Multi-satellite Retrievals for the Global Precipitation Measurement (GPM) Mission (IMERG). In V. Levizzani, C. Kidd, D. B. Kirschbaum, C. D. Kummerow, K. Nakamura, & F. J. Turk (Eds.), *Satellite Precipitation Measurement: Volume 1* (pp. 343–353). Springer International Publishing. https://doi.org/10.1007/978-3-030-24568-9_19

ICOLD CIGB. (2023). *World Register of Dams / Registre Mondial des Barrages* [Dataset]. https://www.icold-cigb.org/GB/publications/world_register_of_dams.asp

India-WRIS. (n.d.). Retrieved December 30, 2022, from https://indiawris.gov.in/wris/#/Reservoirs

Intergovernmental Panel On Climate Change (Ed.). (2014). Long-term Climate Change: Projections, Commitments and Irreversibility Pages 1029 to 1076. In *Climate Change 2013 – The Physical Science Basis* (1st ed., pp. 1029–1136). Cambridge University Press. https://doi.org/10.1017/CBO9781107415324.024

Jones, J. W. & Shiroma, G. H. X. (2023, January 20). *OPERA Level-3 Dynamic Surface Water Extent from Harmonized Landsat-8 and Sentinel-2A/B Product Specification*. NASA. https://d2pn8kiwq2w21t.cloudfront.net/documents/ProductSpec_DSWX_URS309746.pdf

Jung, J. (2023, October 5). *OPERA Level-3 Dynamic Surface Water Extent from Sentinel-1A/B Product Specification*. NASA JPL. https://d2pn8kiwq2w21t.cloudfront.net/documents/ProductSpec_DSWX_S1.pdf

Khandekar, N., & Srinivasan, V. (2021). Dispute Resolution in the Cauvery Basin, India. In R. Ferrier & A. Jenkins (Eds.), *Handbook of Catchment Management 2e* (1st ed., pp. 549–577). Wiley. https://doi.org/10.1002/9781119531241.ch22

Kharin, V. V., Flato, G. M., Zhang, X., Gillett, N. P., Zwiers, F., & Anderson, K. J. (2018). Risks from Climate Extremes Change Differently from 1.5°C to 2.0°C Depending on Rarity. *Earth's Future*, *6*(5), 704–715. https://doi.org/10.1002/2018EF000813

Knoben, W. J. M., Freer, J. E., & Woods, R. A. (2019). *Technical note: Inherent benchmark or not? Comparing Nash-Sutcliffe and Kling-Gupta efficiency scores* [Preprint]. Catchment hydrology/Modelling approaches. https://doi.org/10.5194/hess-2019-327

Kondolf, G. M., Schmitt, R. J. P., Carling, P., Darby, S., Arias, M., Bizzi, S., Castelletti, A., Cochrane, T. A., Gibson, S., Kummu, M., Oeurng, C., Rubin, Z., & Wild, T. (2018). Changing sediment budget of the Mekong: Cumulative threats and management strategies for a large river basin. *Science of The Total Environment*, *625*, 114–134. https://doi.org/10.1016/j.scitotenv.2017.11.361

Kumar, S., Imen, S., Sridharan, V. K., Gupta, A., McDonald, W., Ramirez-Avila, J. J., Abdul-Aziz, O. I., Talchabhadel, R., Gao, H., Quinn, N. W. T., Weiss, W. J., Poulose, T., Palmate, S. S., Lee, C. M., & Baskaran, L. (2024). Perceived barriers and advances in integrating earth observations with water resources modeling. *Remote Sensing Applications: Society and Environment*, *33*, 101119. https://doi.org/10.1016/j.rsase.2023.101119

Lee, H., Durand, M., Jung, H. C., Alsdorf, D., Shum, C. K., & Sheng, Y. (2010). Characterization of surface water storage changes in Arctic lakes using simulated SWOT measurements.

International Journal of Remote Sensing, *31*(14), 3931–3953. https://doi.org/10.1080/01431161.2010.483494

Lehner, B., Liermann, C. R., Revenga, C., Vörösmarty, C., Fekete, B., Crouzet, P., Döll, P., Endejan, M., Frenken, K., Magome, J., Nilsson, C., Robertson, J. C., Rödel, R., Sindorf, N., & Wisser, D. (2011). High-resolution mapping of the world's reservoirs and dams for sustainable river-flow management. *Frontiers in Ecology and the Environment*, *9*(9), 494–502. https://doi.org/10.1890/100125

Li, C., Zwiers, F., Zhang, X., Li, G., Sun, Y., & Wehner, M. (2021). Changes in Annual Extremes of Daily Temperature and Precipitation in CMIP6 Models. *Journal of Climate*, *34*(9), 3441–3460. https://doi.org/10.1175/JCLI-D-19-1013.1

Li, S., Xu, Y. J., & Ni, M. (2021). Changes in sediment, nutrients and major ions in the world largest reservoir: Effects of damming and reservoir operation. *Journal of Cleaner Production*, *318*, 128601. https://doi.org/10.1016/j.jclepro.2021.128601

Li, Y., Zhao, G., Allen, G. H., & Gao, H. (2023). Diminishing storage returns of reservoir construction. *Nature Communications*, *14*(1), Article 1. https://doi.org/10.1038/s41467-023-38843-5

Li, Y., Zhao, G., Shah, D., Zhao, M., Sarkar, S., Devadiga, S., Zhao, B., Zhang, S., & Gao, H. (2021). NASA's MODIS/VIIRS Global Water Reservoir Product Suite from Moderate Resolution Remote Sensing Data. *Remote Sensing*, *13*(4), Article 4. https://doi.org/10.3390/rs13040565

Liang, X., Lettenmaier, D. P., Wood, E. F., & Burges, S. J. (1994). A simple hydrologically based model of land surface water and energy fluxes for general circulation models. *Journal of*

Geophysical Research: Atmospheres, *99*(D7), 14415–14428. https://doi.org/10.1029/94JD00483

Lohmann, D., Nolte-Holube, R., & Raschke, E. (1996). A large-scale horizontal routing model to be coupled to land surface parametrization schemes. *Tellus A: Dynamic Meteorology and Oceanography*, *48*(5), 708–721. https://doi.org/10.3402/tellusa.v48i5.12200

Lohmann, D., Raschke, E., Nijssen, B., & Lettenmaier, D. P. (1998). Regional scale hydrology: I. Formulation of the VIC-2L model coupled to a routing model. *Hydrological Sciences Journal*, *43*(1), 131–141. https://doi.org/10.1080/02626669809492107

Marcaida, M., Farhat, Y., Muth, E.-N., Cheythyrith, C., Hok, L., Holtgrieve, G., Hossain, F., Neumann, R., & Kim, S.-H. (2021). A spatio-temporal analysis of rice production in Tonle Sap floodplains in response to changing hydrology and climate. *Agricultural Water Management*, *258*, 107183. https://doi.org/10.1016/j.agwat.2021.107183

Mekong River Commission. (2019). *State of the Basin Report 2018*. Mekong River Commission. https://www.mrcmekong.org/assets/Publications/SOBR-v8_Final-for-web.pdf

Mekong River Commission. (2021). *The integrated water resources management–based Basin Development Strategy for the Lower Mekong Basin 2021–2030 and the MRC Strategic Plan 2021–2025*. https://www.mrcmekong.org/assets/Publications/BDS-2021-2030-and-MRC-SP-2021-2025.pdf

Messager, M. L., Lehner, B., Grill, G., Nedeva, I., & Schmitt, O. (2016). Estimating the volume and age of water stored in global lakes using a geo-statistical approach. *Nature Communications*, *7*(1), 13603. https://doi.org/10.1038/ncomms13603

Minocha, S., Hossain, F., Das, P., Suresh, S., Khan, S., Darkwah, G., Lee, H., Galelli, S., Andreadis, K., & Oddo, P. (2023). Reservoir Assessment Tool Version 3.0: A Scalable and User-Friendly Software Platform to Mobilize the Global Water Management Community. *Geoscientific Model Development Discussions*, *2023*, 1–23. https://doi.org/10.5194/gmd-2023-130

Mishra, V., Aaadhar, S., Shah, H., Kumar, R., Pattanaik, D. R., & Tiwari, A. D. (2018). The Kerala flood of 2018: Combined impact of extreme rainfall and reservoir storage. *Hydrology and Earth System Sciences Discussions*, 1–13. https://doi.org/10.5194/hess-2018-480

Mulligan, M., van Soesbergen, A., & Sáenz, L. (2020). GOODD, a global dataset of more than 38,000 georeferenced dams. *Scientific Data*, *7*(1), 31. https://doi.org/10.1038/s41597-020-0362-5

Munir, M., Siddiqui, S. A., Dengel, A., & Ahmed, S. (2019). DeepAnT: A Deep Learning Approach for Unsupervised Anomaly Detection in Time Series. *IEEE Access*, *7*, 1991–2005. https://doi.org/10.1109/ACCESS.2018.2886457

Nash, J. E., & Sutcliffe, J. V. (1970). River flow forecasting through conceptual models part I — A discussion of principles. *Journal of Hydrology*, *10*(3), 282–290. https://doi.org/10.1016/0022-1694(70)90255-6

National Centers For Environmental Prediction/National Weather Service/NOAA/U.S. Department Of Commerce. (2015). *NCEP GFS 0.25 Degree Global Forecast Grids Historical Archive* (p. 109.074 TB) [WMO_GRIB2,WMO_GRIB2]. UCAR/NCAR - Research Data Archive. https://doi.org/10.5065/D65D8PWK

Neel, J. K., & Allen, W. R. (1964). The mussel fauna of the upper Cumberland Basin before its impoundment. *Malacologia*, *1*(3), 427–459.

Nilsson, C., Reidy, C. A., Dynesius, M., & Revenga, C. (2005). Fragmentation and Flow Regulation of the World's Large River Systems. *Science*, *308*(5720), 405–408. https://doi.org/10.1126/science.1107887

Okeowo, M. A., Lee, H., Hossain, F., & Getirana, A. (2017). Automated Generation of Lakes and Reservoirs Water Elevation Changes From Satellite Radar Altimetry. *IEEE Journal of Selected Topics in Applied Earth Observations and Remote Sensing*, *10*(8), 3465–3481. https://doi.org/10.1109/JSTARS.2017.2684081

Pekel, J.-F., Cottam, A., Gorelick, N., & Belward, A. S. (2016). High-resolution mapping of global surface water and its long-term changes. *Nature*, *540*(7633), 418–422. https://doi.org/10.1038/nature20584

Penman, H. L. (1948). Natural evaporation from open water, bare soil and grass. *Proceedings of the Royal Society of London. Series A. Mathematical and Physical Sciences*, *193*(1032), 120–145. https://doi.org/10.1098/rspa.1948.0037

Plengsaeng, B., Wehn, U., & van der Zaag, P. (2014). Data-sharing bottlenecks in transboundary integrated water resources management: A case study of the Mekong River Commission's procedures for data sharing in the Thai context. *Water International*, *39*(7), 933–951. https://doi.org/10.1080/02508060.2015.981783

Pokhrel, Y., Shin, S., Lin, Z., Yamazaki, D., & Qi, J. (2018). Potential Disruption of Flood Dynamics in the Lower Mekong River Basin Due to Upstream Flow Regulation. *Scientific Reports*, *8*(1), Article 1. https://doi.org/10.1038/s41598-018-35823-4

Pradhan, R. K., Markonis, Y., Vargas Godoy, M. R., Villalba-Pradas, A., Andreadis, K. M., Nikolopoulos, E. I., Papalexiou, S. M., Rahim, A., Tapiador, F. J., & Hanel, M. (2022). Review of GPM IMERG performance: A global perspective. *Remote Sensing of Environment*, *268*, 112754. https://doi.org/10.1016/j.rse.2021.112754

Pramanick, N., Acharyya, R., Mukherjee, S., Mukherjee, S., Pal, I., Mitra, D., & Mukhopadhyay, A. (2022). SAR based flood risk analysis: A case study Kerala flood 2018. *Advances in Space Research*, *69*(4), 1915–1929. https://doi.org/10.1016/j.asr.2021.07.003

Precipitation Processing System (PPS). (2022). *Version 7 Late 24-Hour IMERG_GIS* (Version 7) [Dataset]. National Aeronautics and Space Administration. https://doi.org/10.25966/ZP54-TB85

Rentschler, J., Salhab, M., & Jafino, B. A. (2022). Flood exposure and poverty in 188 countries. *Nature Communications*, *13*(1), Article 1. https://doi.org/10.1038/s41467-022-30727-4

RID. (n.d.). *Reservoir monitoring system for Thailand*. Retrieved March 31, 2022, from http://app.rid.go.th:88/reservoir/

RID. (2024). *Reservoir monitoring system for Thailand*. http://app.rid.go.th:88/reservoir/

Robinson, J. A. (2019). *Estimated use of water in the Cumberland River watershed in 2010 and projections of public-supply water use to 2040* (Report 2018–5130; Scientific Investigations Report, p. 74). USGS Publications Warehouse. https://doi.org/10.3133/sir20185130

Ryan, J. C., Smith, L. C., Cooley, S. W., Pitcher, L. H., & Pavelsky, T. M. (2020). Global Characterization of Inland Water Reservoirs Using ICESat-2 Altimetry and Climate

Reanalysis. *Geophysical Research Letters*, *47*(17), e2020GL088543. https://doi.org/10.1029/2020GL088543

Saavedra Valeriano, O. C., Koike, T., Yang, K., Graf, T., Li, X., Wang, L., & Han, X. (2010). Decision support for dam release during floods using a distributed biosphere hydrological model driven by quantitative precipitation forecasts. *Water Resources Research*, *46*(10). https://doi.org/10.1029/2010WR009502

Schmitt, M., & Zhu, X. X. (2016). Data Fusion and Remote Sensing: An ever-growing relationship. *IEEE Geoscience and Remote Sensing Magazine*, *4*(4), 6–23. IEEE Geoscience and Remote Sensing Magazine. https://doi.org/10.1109/MGRS.2016.2561021

Shah, D., Zhang, S., Sarkar, S., Davidson, C., Zhang, R., Zhao, M., Devadiga, S., Noojipady, P., Román, M. O., & Gao, H. (2024). Transitioning from MODIS to VIIRS Global Water Reservoir Product. *Scientific Data*, *11*(1), 209. https://doi.org/10.1038/s41597-024-03028-2

Shin, H. (2023, July 17). South Korea flood death toll rises to 40, Yoon blames botched responses. *Reuters*. https://www.reuters.com/world/asia-pacific/south-korea-flood-death-toll-rises-39-yoon-orders-all-out-effort-2023-07-17/

Simon, A., & Mohankumar, K. (2004). Spatial variability and rainfall characteristics of Kerala. *Journal of Earth System Science*, *113*(2), 211–221. https://doi.org/10.1007/BF02709788

Siqueira, V. A., Fan, F. M., Paiva, R. C. D. D., Ramos, M.-H., & Collischonn, W. (2020). Potential skill of continental-scale, medium-range ensemble streamflow forecasts for flood prediction in South America. *Journal of Hydrology*, *590*, 125430. https://doi.org/10.1016/j.jhydrol.2020.125430

Steyaert, J. C., Condon, L. E., W. D. Turner, S., & Voisin, N. (2022). ResOpsUS, a dataset of historical reservoir operations in the contiguous United States. *Scientific Data*, *9*(1), Article 1. https://doi.org/10.1038/s41597-022-01134-7

Sudheer, K. P., Murty Bhallamudi, S., Narasimhan, B., Thomas, J., Bindhu, V. M., Vema, V., & Kurian, C. (2019). Role of Dams on the Floods of August 2018 in Periyar River Basin, Kerala. *Current Science*, *116*(5), 780. https://doi.org/10.18520/cs/v116/i5/780-794

Sun, Q., Zhang, X., Zwiers, F., Westra, S., & Alexander, L. V. (2021). A Global, Continental, and Regional Analysis of Changes in Extreme Precipitation. *Journal of Climate*, *34*(1), 243–258. https://doi.org/10.1175/JCLI-D-19-0892.1

Suresh, S., Hossain, F., Minocha, S., Das, P., Khan, S., Lee, H., Andreadis, K., & Oddo, P. (2024). Satellite-based tracking of reservoir operations for flood management during the 2018 extreme weather event in Kerala, India. *Remote Sensing of Environment*, *307*, 114149. https://doi.org/10.1016/j.rse.2024.114149

SWOT. (2024a). *SWOT Level 2 Nadir Altimeter Geophysical Data Record with Waveforms Version 2.0* [Dataset]. NASA Physical Oceanography Distributed Active Archive Center. https://doi.org/10.5067/SWOT-NALT-GDR-2.0

SWOT. (2024b). *SWOT Level 2 Water Mask Raster Image Data Product* [Dataset]. NASA Physical Oceanography Distributed Active Archive Center. https://doi.org/10.5067/SWOT-RASTER-2.0

Tellman, B., Sullivan, J. A., Kuhn, C., Kettner, A. J., Doyle, C. S., Brakenridge, G. R., Erickson, T. A., & Slayback, D. A. (2021). Satellite imaging reveals increased proportion of

population exposed to floods. *Nature*, *596*(7870), 80–86. https://doi.org/10.1038/s41586-021-03695-w

Thomas, J., & Prasannakumar, V. (2016). Temporal analysis of rainfall (1871–2012) and drought characteristics over a tropical monsoon-dominated State (Kerala) of India. *Journal of Hydrology*, *534*, 266–280. https://doi.org/10.1016/j.jhydrol.2016.01.013

Tippit, R. N., Brown, J. K., Sharber, J. F., & Miller, A. C. (1995). Modifying Cumberland River system reservoir operations to improve mussel habitat. *Conservation and Management of Freshwater Mussels II: Initiatives for the Future. Proceedings of a UMRCC Symposium*, 229–235.

Torres, R., Snoeij, P., Geudtner, D., Bibby, D., Davidson, M., Attema, E., Potin, P., Rommen, B., Floury, N., Brown, M., Traver, I. N., Deghaye, P., Duesmann, B., Rosich, B., Miranda, N., Bruno, C., L'Abbate, M., Croci, R., Pietropaolo, A., … Rostan, F. (2012). GMES Sentinel-1 mission. *Remote Sensing of Environment*, *120*, 9–24. https://doi.org/10.1016/j.rse.2011.05.028

USACE. (n.d.). *WM Data Dissemination*. Retrieved October 15, 2023, from https://water.usace.army.mil/a2w/f?p=100:1::::::#

Valbo-Jørgensen, J., Coates, D., & Hortle, K. (2009). Fish Diversity in the Mekong River Basin. In *The Mekong* (pp. 161–196). Elsevier. https://doi.org/10.1016/B978-0-12-374026-7.00008-5

Van Bavel, C. H. M. (1966). Potential evaporation: The combination concept and its experimental verification. *Water Resources Research*, *2*(3), 455–467. https://doi.org/10.1029/WR002i003p00455

Van Der Knijff, J. M., Younis, J., & De Roo, A. P. J. (2010). LISFLOOD: A GIS-based distributed model for river basin scale water balance and flood simulation. *International Journal of Geographical Information Science*, *24*(2), 189–212. https://doi.org/10.1080/13658810802549154

Vanderkelen, I., Gharari, S., Mizukami, N., Clark, M. P., Lawrence, D. M., Swenson, S., Pokhrel, Y., Hanasaki, N., van Griensven, A., & Thiery, W. (2022). Evaluating a reservoir parametrization in the vector-based global routing model mizuRoute (v2.0.1) for Earth system model coupling. *Geoscientific Model Development*, *15*(10), 4163–4192. https://doi.org/10.5194/gmd-15-4163-2022

Vijaykumar, P., Abhilash, S., Sreenath, A. V., Athira, U. N., Mohanakumar, K., Mapes, B. E., Chakrapani, B., Sahai, A. K., Niyas, T. N., & Sreejith, O. P. (2021). Kerala floods in consecutive years—Its association with mesoscale cloudburst and structural changes in monsoon clouds over the west coast of India. *Weather and Climate Extremes*, *33*, 100339. https://doi.org/10.1016/j.wace.2021.100339

Vu, D. T., Dang, T. D., Galelli, S., & Hossain, F. (2021). *Satellite observations reveal thirteen years of reservoir filling strategies, operating rules, and hydrological alterations in the Upper Mekong River Basin* [Preprint]. Hydrology. https://doi.org/10.1002/essoar.10507302.1

Wada, Y., Bierkens, M. F. P., de Roo, A., Dirmeyer, P. A., Famiglietti, J. S., Hanasaki, N., Konar, M., Liu, J., Müller Schmied, H., Oki, T., Pokhrel, Y., Sivapalan, M., Troy, T. J., van Dijk, A. I. J. M., van Emmerik, T., Van Huijgevoort, M. H. J., Van Lanen, H. A. J., Vörösmarty, C. J., Wanders, N., & Wheater, H. (2017). Human–water interface in hydrological

modelling: Current status and future directions. *Hydrology and Earth System Sciences*, *21*(8), 4169–4193. https://doi.org/10.5194/hess-21-4169-2017

Wang, F., Wang, L., Zhou, H., Saavedra Valeriano, O. C., Koike, T., & Li, W. (2012). Ensemble hydrological prediction-based real-time optimization of a multiobjective reservoir during flood season in a semiarid basin with global numerical weather predictions. *Water Resources Research*, *48*(7). https://doi.org/10.1029/2011WR011366

Wang, X., Xie, S., Zhang, X., Chen, C., Guo, H., Du, J., & Duan, Z. (2018). A robust Multi-Band Water Index (MBWI) for automated extraction of surface water from Landsat 8 OLI imagery. *International Journal of Applied Earth Observation and Geoinformation*, *68*, 73–91. https://doi.org/10.1016/j.jag.2018.01.018

Wilson, C. B., & Clark, H. W. (1914). *The mussels of the Cumberland River and its tributaries* (Issue 781). US Government Printing Office.

Wisser, D., & Fekete, B. M. (2009). *Reconstructing 20th century global hydrography*.

Wu, H., Adler, R. F., Hong, Y., Tian, Y., & Policelli, F. (2012). Evaluation of Global Flood Detection Using Satellite-Based Rainfall and a Hydrologic Model. *Journal of Hydrometeorology*, *13*(4), 1268–1284. https://doi.org/10.1175/JHM-D-11-087.1

Wu, H., Kimball, J. S., Mantua, N., & Stanford, J. (2011). Automated upscaling of river networks for macroscale hydrological modeling: UPSCALING OF GLOBAL RIVER NETWORKS. *Water Resources Research*, *47*(3). https://doi.org/10.1029/2009WR008871

Yamazaki, D., Ikeshima, D., Tawatari, R., Yamaguchi, T., O'Loughlin, F., Neal, J. C., Sampson, C. C., Kanae, S., & Bates, P. D. (2017). A high-accuracy map of global terrain elevations:

Accurate Global Terrain Elevation map. *Geophysical Research Letters*, *44*(11), 5844–5853. https://doi.org/10.1002/2017GL072874

Yao, F., Livneh, B., Rajagopalan, B., Wang, J., Crétaux, J.-F., Wada, Y., & Berge-Nguyen, M. (2023a). Global database of lake water storage (GLWS) v1.1. *Science*. https://doi.org/10.1126/science.abo2812

Yao, F., Livneh, B., Rajagopalan, B., Wang, J., Crétaux, J.-F., Wada, Y., & Berge-Nguyen, M. (2023b). Satellites reveal widespread decline in global lake water storage. *Science*, *380*(6646), 743–749. https://doi.org/10.1126/science.abo2812

Yoon, Y., & Beighley, E. (2015). Simulating streamflow on regulated rivers using characteristic reservoir storage patterns derived from synthetic remote sensing data. *Hydrological Processes*, *29*(8), 2014–2026. https://doi.org/10.1002/hyp.10342

Yoon, Y., Beighley, E., Lee, H., Pavelsky, T., & Allen, G. (2016). Estimating Flood Discharges in Reservoir-Regulated River Basins by Integrating Synthetic SWOT Satellite Observations and Hydrologic Modeling. *Journal of Hydrologic Engineering*, *21*(4), 05015030. https://doi.org/10.1061/(ASCE)HE.1943-5584.0001320

Zhao, G., & Gao, H. (2018). Automatic Correction of Contaminated Images for Assessment of Reservoir Surface Area Dynamics. *Geophysical Research Letters*. https://doi.org/10.1029/2018GL078343

Zhao, G., Li, Y., Zhou, L., & Gao, H. (2022). Evaporative water loss of 1.42 million global lakes. *Nature Communications*, *13*(1), 3686. https://doi.org/10.1038/s41467-022-31125-6

Zhou, T., Nijssen, B., Gao, H., & Lettenmaier, D. P. (2016). The Contribution of Reservoirs to Global Land Surface Water Storage Variations. *Journal of Hydrometeorology*, *17*(1), 309–325. https://doi.org/10.1175/JHM-D-15-0002.1

Zhou, X., Zhu, Y., Hou, D., Fu, B., Li, W., Guan, H., Sinsky, E., Kolczynski, W., Xue, X., Luo, Y., Peng, J., Yang, B., Tallapragada, V., & Pegion, P. (2022). The Development of the NCEP Global Ensemble Forecast System Version 12. *Weather and Forecasting*, *37*(6), 1069–1084. https://doi.org/10.1175/WAF-D-21-0112.1

Ziv, G., Baran, E., Nam, S., Rodríguez-Iturbe, I., & Levin, S. A. (2012). Trading-off fish biodiversity, food security, and hydropower in the Mekong River Basin. *Proceedings of the National Academy of Sciences*, *109*(15), 5609–5614. https://doi.org/10.1073/pnas.1201423109

Appendix A

The choice of threshold for filtering optical data points based on normalized deviations from SAR sensor data is shown in Figure A.1. The threshold is chosen as a percent of the nominal surface area of the reservoir. So, if the nominal surface area of a reservoir is 200 km^2, the 1% threshold would correspond to 2km^2 and data points that deviate by this much will be filtered out. The panels in the figure below correspond to a range of percent values chosen to show the effect of deviation thresholds.

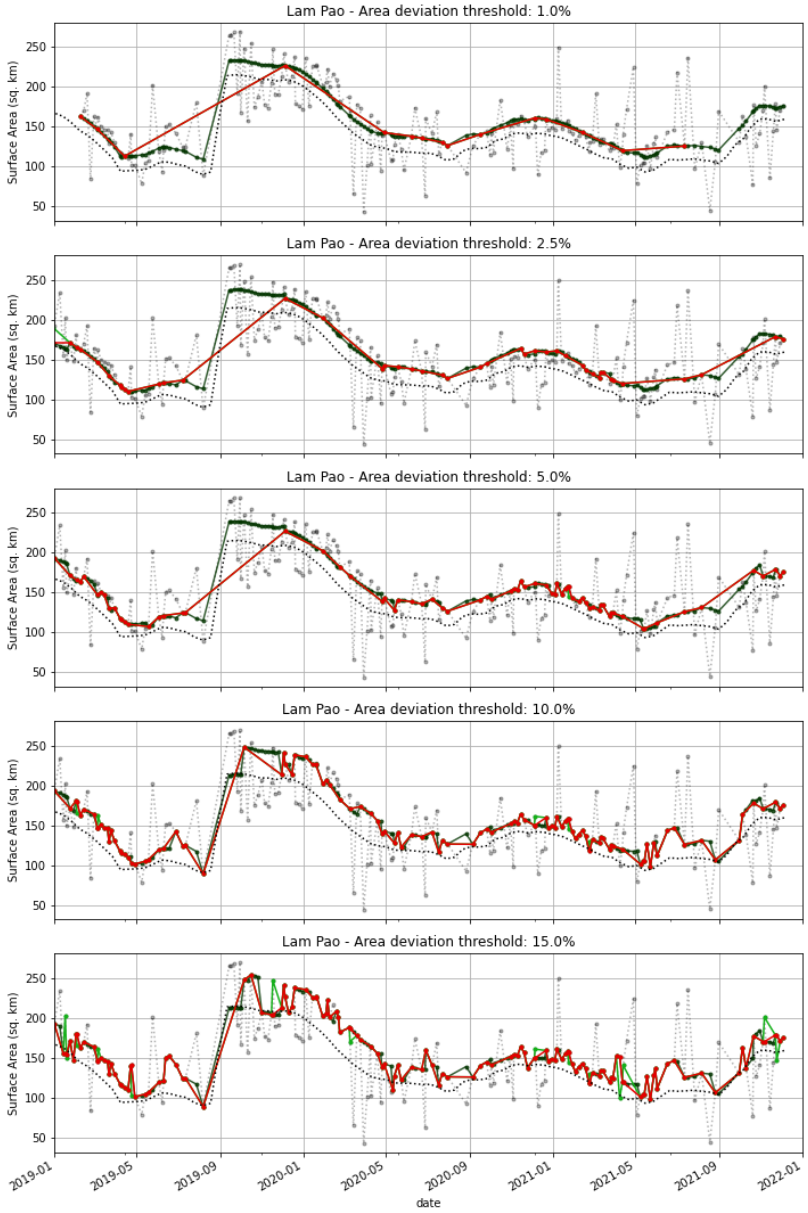

Figure A.1. Effect of the choice of filtering 1 threshold on the surface area time-series – Lam Pao.

The figure below compares the storage change of two reservoirs estimated by satellites in the Mun River, a tributary of the Mekong River, against in-situ storage change estimates.

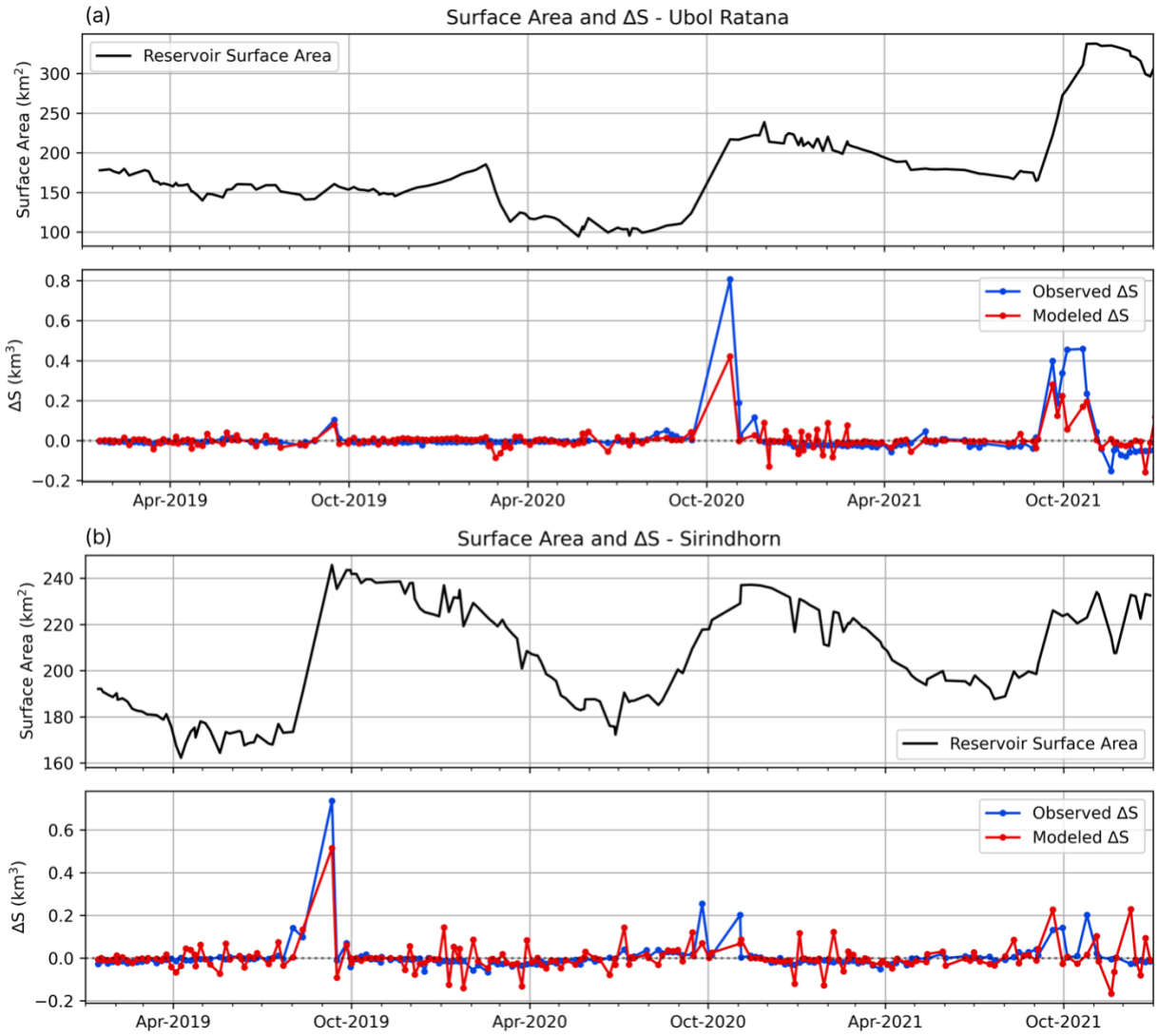

Figure A.2. Comparison of modeled storage change with observed storage change for the three validation reservoirs. (a) ΔS for Sirindhorn, (b) ΔS for Ubol Ratana.

The figure below compares the storage change estimated using observations of the Jason-3 altimeter over the Sirindhorn reservoir in Thailand against in-situ storage change.

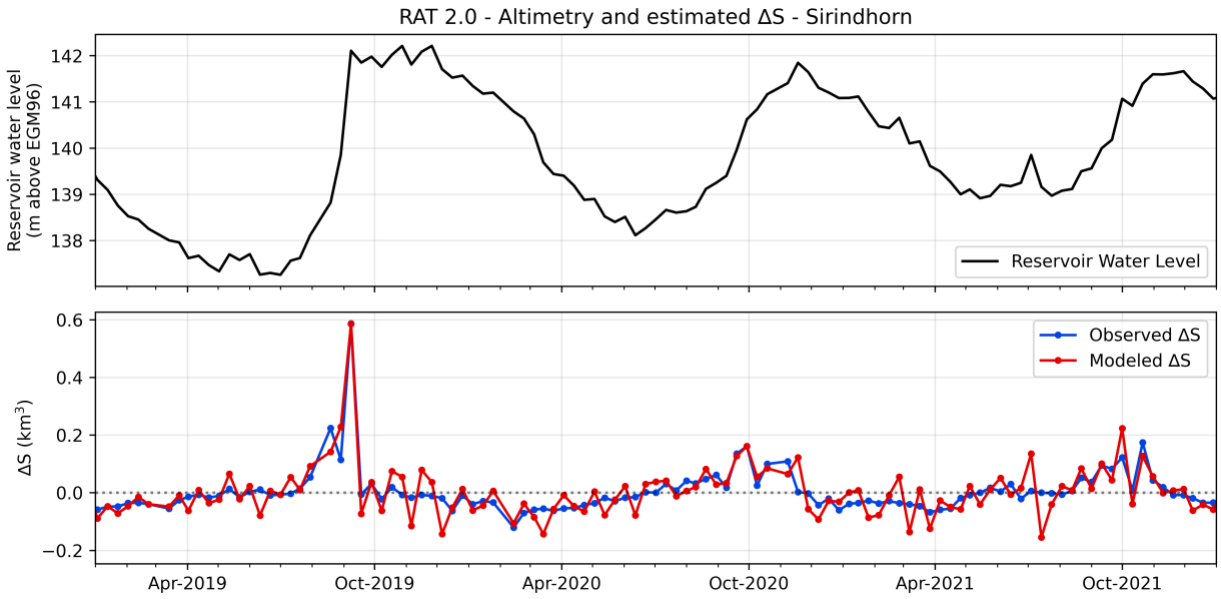

Figure A.3. Comparison of modeled storage change using altimeter measurement of reservoir water level with observed storage change for Sirindhorn, Thailand.

Appendix B

B.1. River-regulation algorithm ResORR tested in a theoretical two-reservoir system using synthetic data

A theoretical two inter-connected linear reservoir system with artificially generated headwater flow inputs was used to test the theoretical robustness of the mass conserving and numerical stability of the ResORR algorithm. This classic problem (**Error! Reference source not found.**) also helped visualize the outputs of ResORR algorithm and verify if mass balance is maintained.

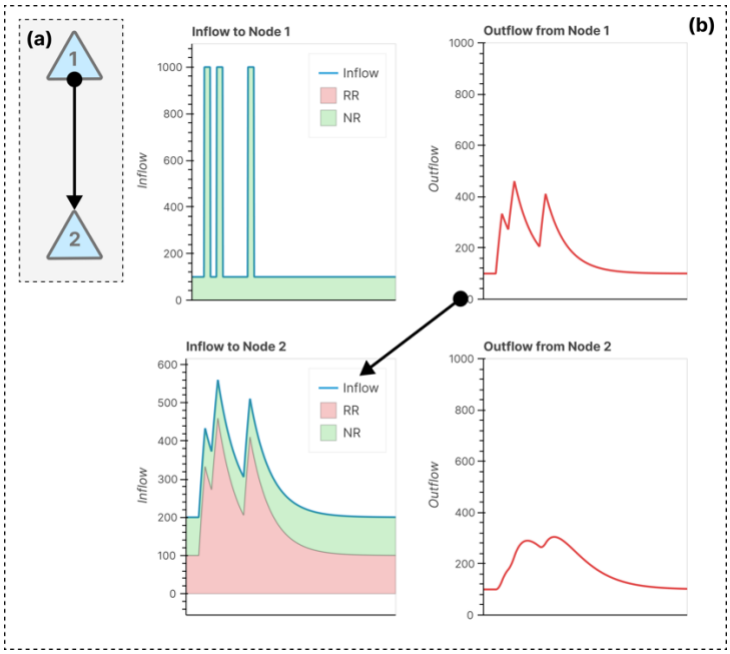

Figure B.1: (a) Schematic showing the two-reservoir system setup. The black arrow denotes the direction of flow of water. (b) Hydrographs showing inflow and outflow from nodes 1 and 2. In this case, three input pulses of 1000 L^3/T units were fed into node 1, and its outflow was treated as the inflow to the downstream node 2. The inflow and outflow at node 2 represent the 'theoretical' answer for the ResORR algorithm to be theoretically valid.

A system of two interconnected linear reservoirs were set up, like the schematic shown in **Error! Reference source not found.**. To understand how the outflow from an upstream reservoir would affect the inflow to the downstream reservoir, we first generated a synthetic headwater inflow hydrograph for reservoir 1and then applied ResORR to predict the regulated inflow to the downstream reservoir at node 2. Both the reservoirs were provided with a constant water influx of 100 L^3/T units in the form of natural runoff, NR. Additionally, the upstream reservoir, at node 1,

was provided with three pulses of high inflow volumes of 1000 L^3/T units. The reservoirs were treated as linear reservoirs, where the outflow from a reservoir at any given time as a linear function of the instantaneous storage, and can be defined as follows –

$$O = K \times S$$

Where, K $[T^{-1}]$ is the reaction factor, which determines how quickly the reservoir drains ($K = 0.01$ in this experiment). The outflow from the upstream reservoir at node 1 was then treated as the regulated runoff, RR for the downstream reservoir, node 2. Using the inflows and outflows obtained at both the reservoirs, the storage change was obtained using (5). The theoretical natural runoff, TNR, was also obtained using (3). The ResORR was then run using this simulated storage change and TNR information as inputs, to model the inflow at both the reservoirs. The modeled inflow of ResORR was then compared with the synthetically generated inflow at the downstream node 2, with a perfect match between them. The closure of water balance was also tested by comparing the total inflow volumes in the modeled and synthetic inflow.

B.2. Performance metrics used for assessing ResORR

The following five commonly used performance metrics were used in this study to quantify the skill of the river regulation model –

Table B.1: Table of performance metrics used.

Metric	Equation	Description
Nash-Sutcliffe Efficiency (NSE) (Nash and Sutcliffe, 1970)	$1 - \frac{\sum_{t=1}^{T}(Q_O^t - Q_M^t)^2}{\sum_{t=1}^{T}(Q_O^t - \overline{Q_O})^2}$ Where, Q_O^t and Q_M^t are observed and modeled streamflow respectively. $\overline{Q_O}$ is the mean observed streamflow.	The NSE can vary between $-\infty$ and 1. A value of 1 indicates a perfect match between observed and modeled values. A value of 0 indicates that the model predictions are as performant as using the mean of the observed values as a predictor. Higher values are better.
Kling-Gupta Efficiency (KGE) (Gupta et al., 2009)	$1 - \sqrt{(r-1)^2 + (\alpha-1)^2 + (\beta-1)^2}$ Where, r is the linear correlation between modeled and observed values, $\alpha = \left(\frac{\sigma_M}{\sigma_O} - 1\right)^2$, σ_M and σ_O are the standard deviations of the modeled and	The KGE varies between $-\infty$ and 1. A value of -0.41 indicates model performance equal to using the mean of the observed values as a predictor (Knoben et al., 2019). Higher values are better.

	observed values, $\beta = \left(\frac{\mu_M}{\mu_O} - 1\right)^2$, μ_M and μ_O are mean modeled and observed values.	
Pearson's R	$\frac{cov(Q_O, Q_M)}{\sigma_O \sigma_M}$ Where, $cov(Q_O, Q_M)$ is the covariance of the observed and modeled values. σ_M and σ_O are the standard deviations of the modeled and observed values	The Pearson's R can vary from -1 to 1, where 1 indicates a perfect positive linear correlation. A value of 0 indicates no correlation.
Normalized Root-Mean Squared Error (NRMSE)	$\frac{\sqrt{\frac{\sum_{i=1}^{N}(Q_O - Q_M)^2}{N}}}{\max(Q_O) - \min(Q_O)}$ Where, $\max(Q_O)$ and $\min(Q_O)$ are the maximum and minimum observed streamflow values.	The NRMSE represents the standard deviation of the residuals as a fraction of the range of the observed values. Lower values are better.
Normalized Mean Absolute Error (NMAE)	$\frac{\frac{\sum_{i=1}^{N}\lvert Q_M - Q_O\rvert}{N}}{\max(Q_O) - \min(Q_O)}$ Where, N is the number of observations, $\lvert Q_M - Q_O\rvert$ is the absolute difference of modeled and observed values	The NMAE represents the average absolute difference between observed and modeled values as a fraction of the range of observed values. Lower values are better.

B.3. HANDLING MISSING IN-SITU STORAGE DATA

Two dams in the basin, Old Hickory and Laurel, had missing in-situ storage data after April 2015, due to which storage change could not be calculated using observed (in-situ) storage. This missing data was filled by assuming water mass-balance owing to inflow and outflow from the reservoirs, $\Delta S = I - O$.

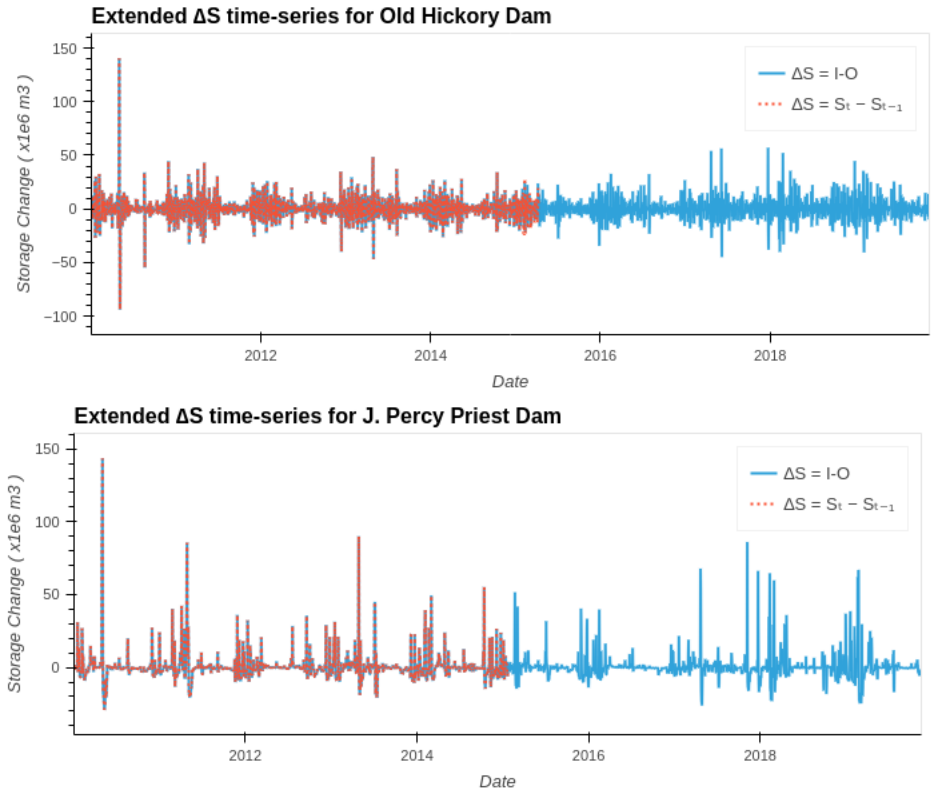

Figure B.2: Handling of missing in-situ data for comparison of observed and modeled regulated streamflow.